Study of cosmic-ray interactions in candidate sources. Applications to the interpretation of the energy spectrum and mass composition data of the Pierre Auger Observatory

Candidate: Antonio Condorelli

Supervisor: Sergio Petrera
(GSSI)

Co-supervisor: Denise Boncioli
(University of L'Aquila)

Outline

- Introduction: UHECRs
- The Pierre Auger Observatory
- Combined fit of the energy spectrum and mass composition above the “ankle”
- Extended combined fit
- Source-propagation model
- Conclusions and future perspectives

Cosmic Ray Spectrum

- It spans over several order of magnitude in energy and flux;
- Several detection techniques are needed;
- Power law: it reflects acceleration mechanism;
- Features can be addressed to propagation and/or acceleration processes.

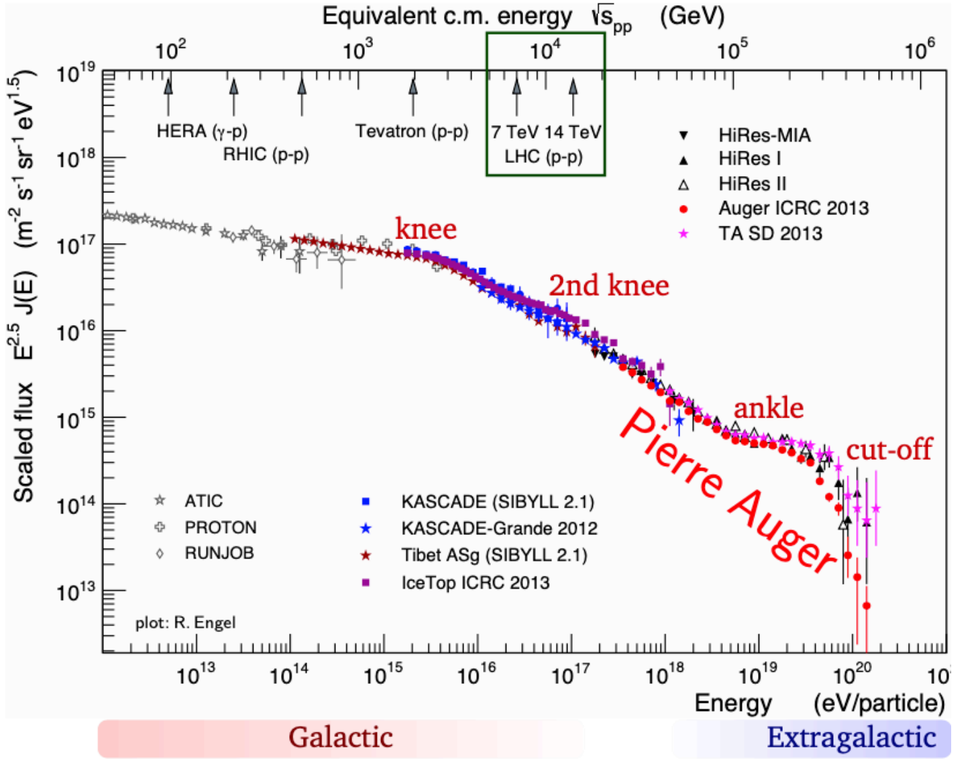

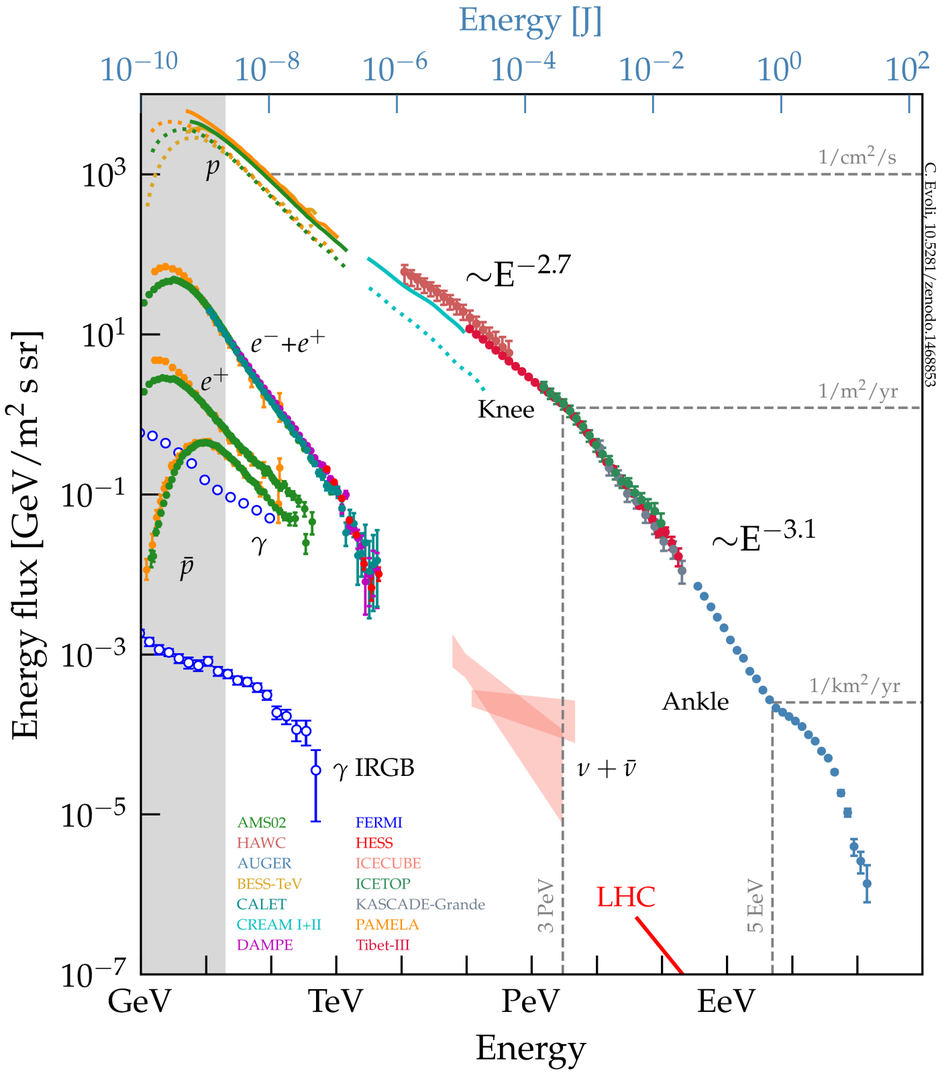

Where do the UHECRs come from?

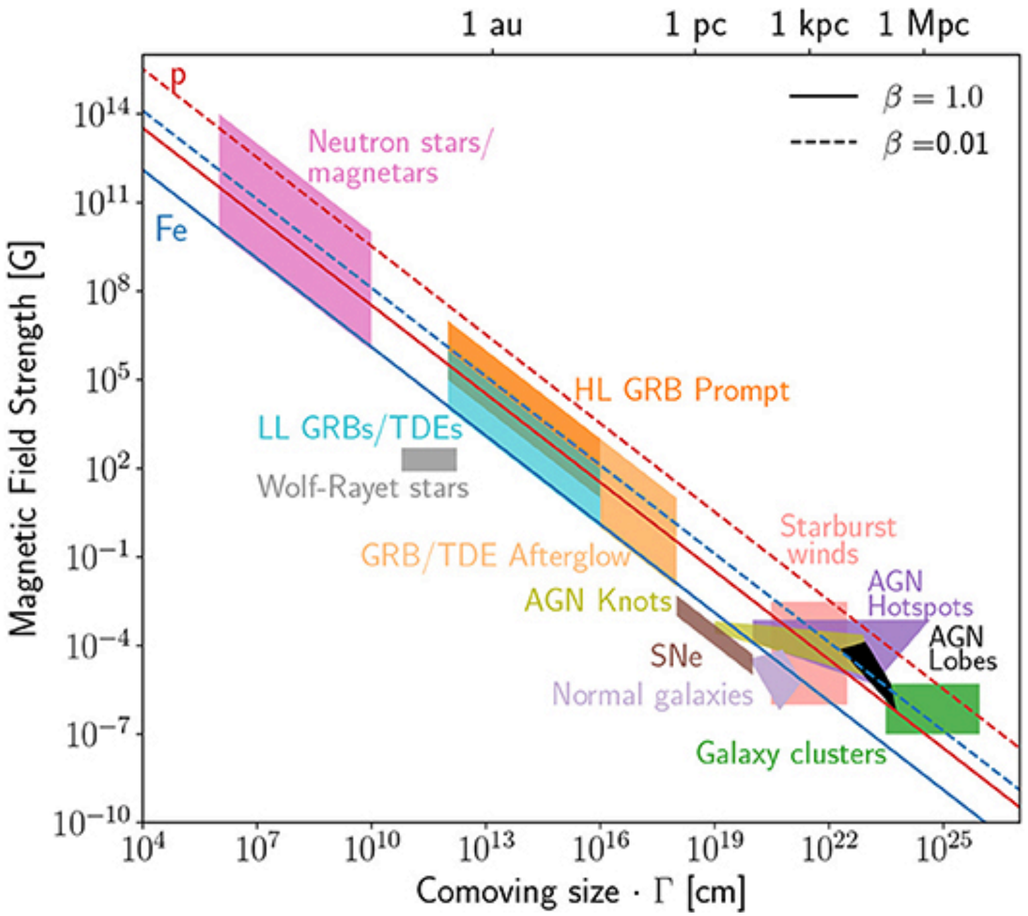

Looking at the size and at the magnetic field it is possible to have an estimation of possible maximum energy

$$E_{\max} \propto \beta \cdot Z \cdot L \cdot B$$

Below the knee ($\simeq 10^{15}$ eV) possible source candidates are the Supernovae.

Propagation of UHECRs

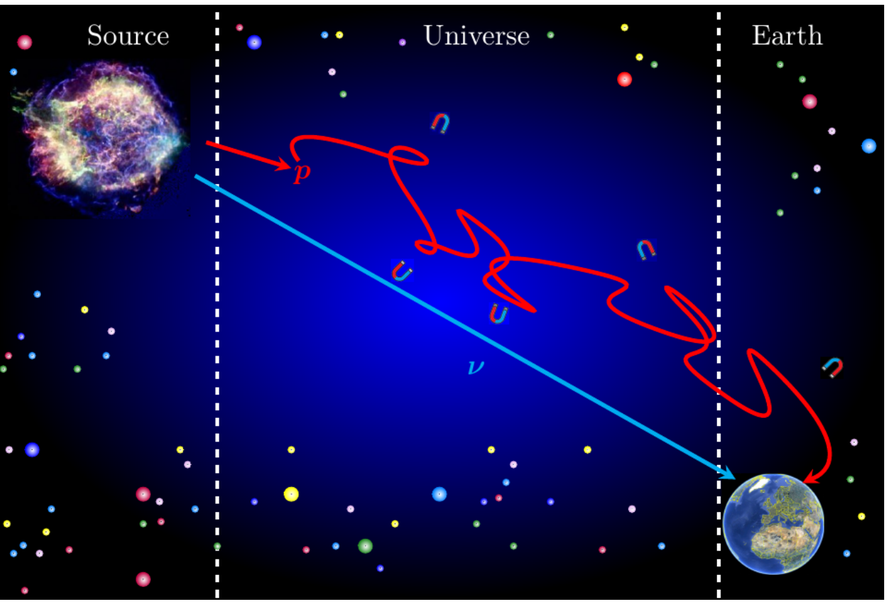

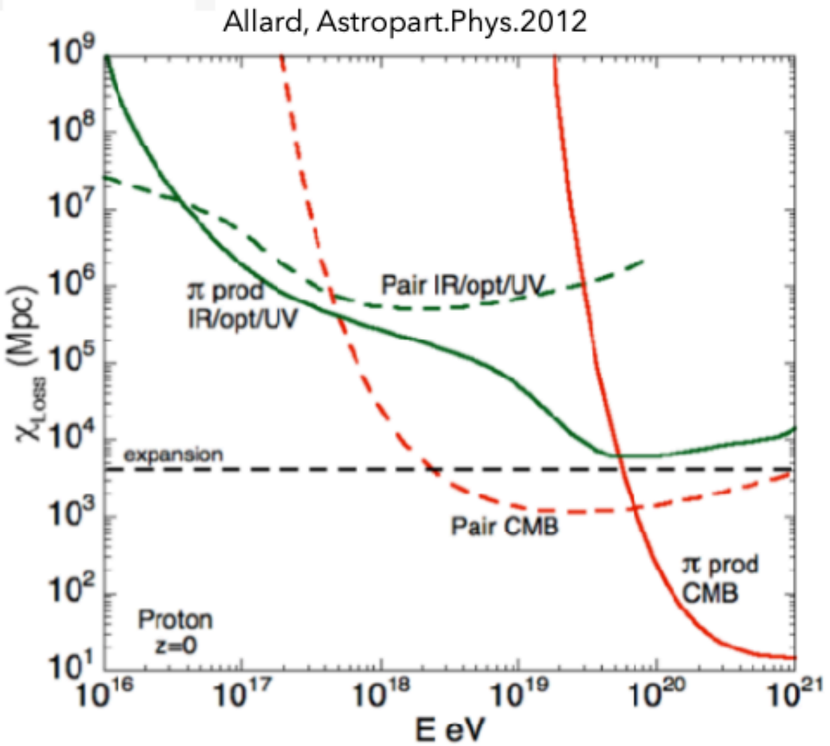

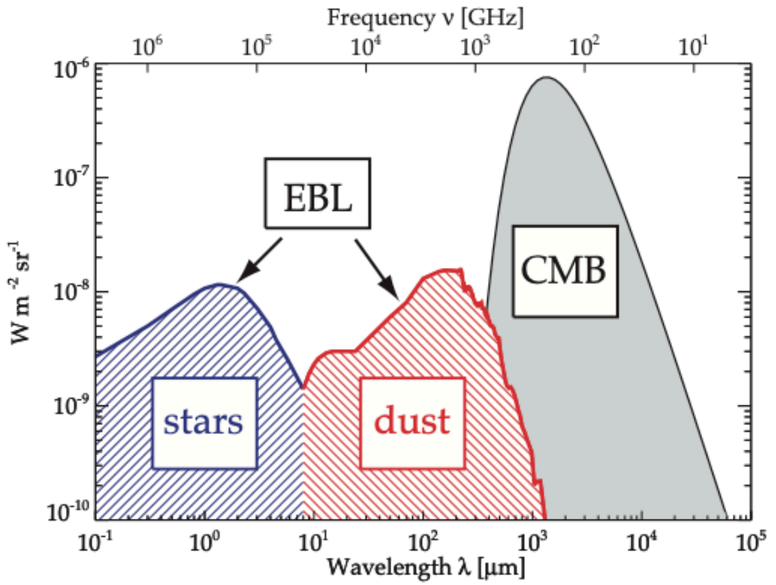

Energy losses in extragalactic space

- Adiabatic expansion of the Universe
- Electron-positron production, photopion production due to interactions with CMB and EBL.
- **Universe in UHECRs is not visible above a few hundreds of Mpc**

D. Mazin, AIP Conference Proceedings **1112**, 111 (2009)

Indirect detection: Extensive Air Shower (EAS)

The collision of cosmic rays with the atmospheric molecules produces a cascade of particles, called Extensive Air Shower (EAS).

The particles of an EAS initiated by a proton or a nucleus can be roughly divided into three components:

- Hadronic (mostly pions)
- Electromagnetic (e^+, e^-, γ)
- Penetrant (muons and neutrinos)

A key information to infer about properties of the primary particle is the depth of the shower maximum

$$X_{max} \propto lg(E/A)$$

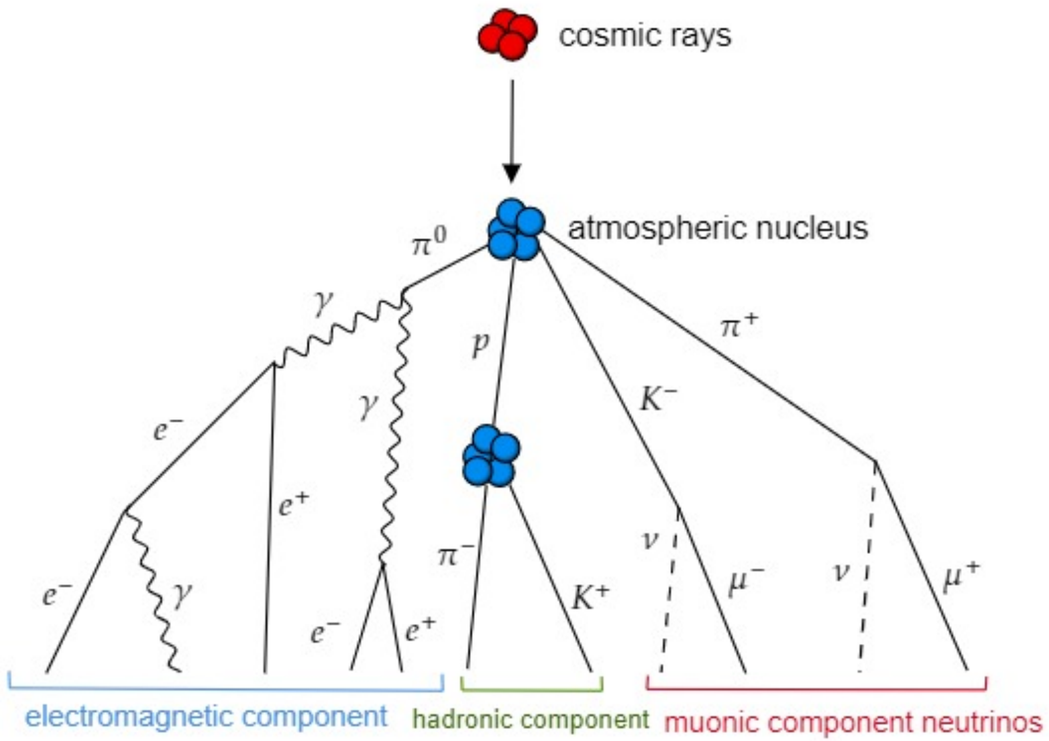

The Pierre Auger Observatory

Hybrid detector

Fluorescence detector (FD)

duty cycle 15%

24+3 fluorescence telescopes

Surface detector (SD)

duty cycle 100%

1660 water-Cherenkov detectors

Radio detector (RD)

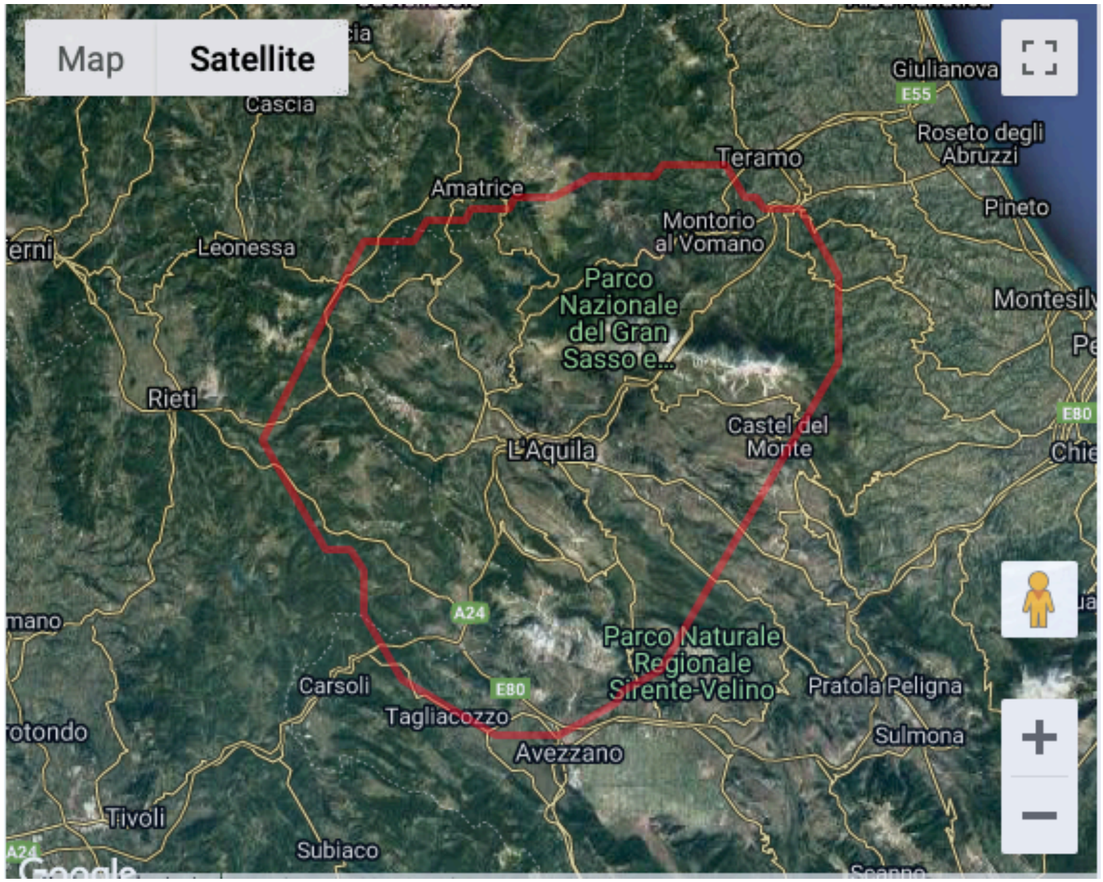

The Pierre Auger Observatory

Hybrid detector

Fluorescence detector (FD)

duty cycle 15%

24+3 fluorescence telescopes

Surface detector (SD)

duty cycle 100%

1660 water-Cherenkov detectors

Radio detector (RD)

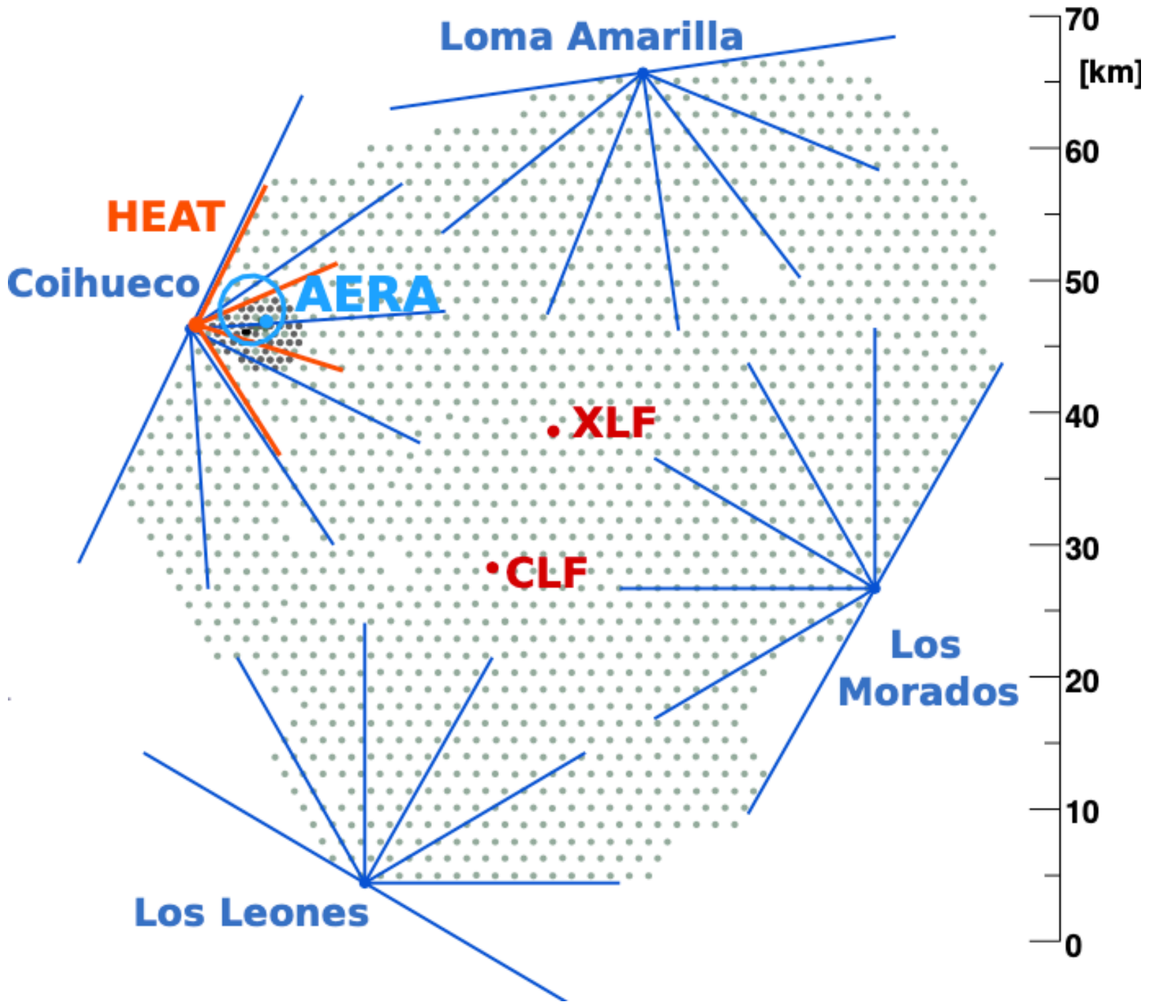

The hybrid detection

FD telescopes at Los Morados

elevation 1.5° – 30°

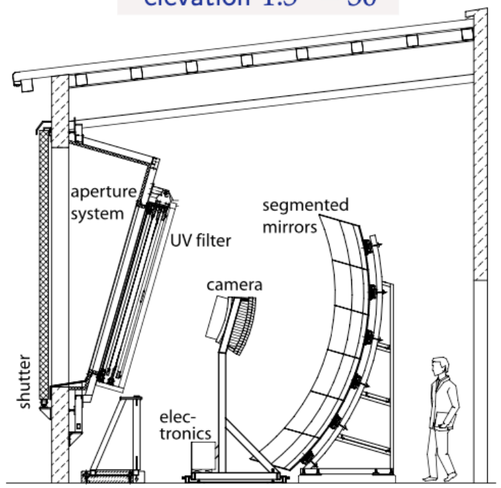

Water-Cherenkov station

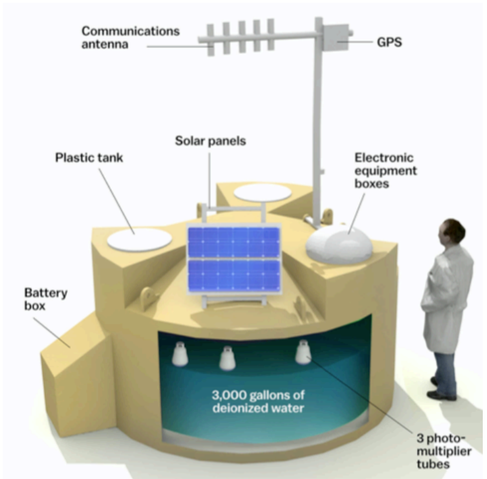

$$E_{\mathrm{cal}} = \int_0^{\infty} \left(\frac{\mathrm{d}E}{\mathrm{d}X}\right)_{\mathrm{obs}} \mathrm{d}X$$

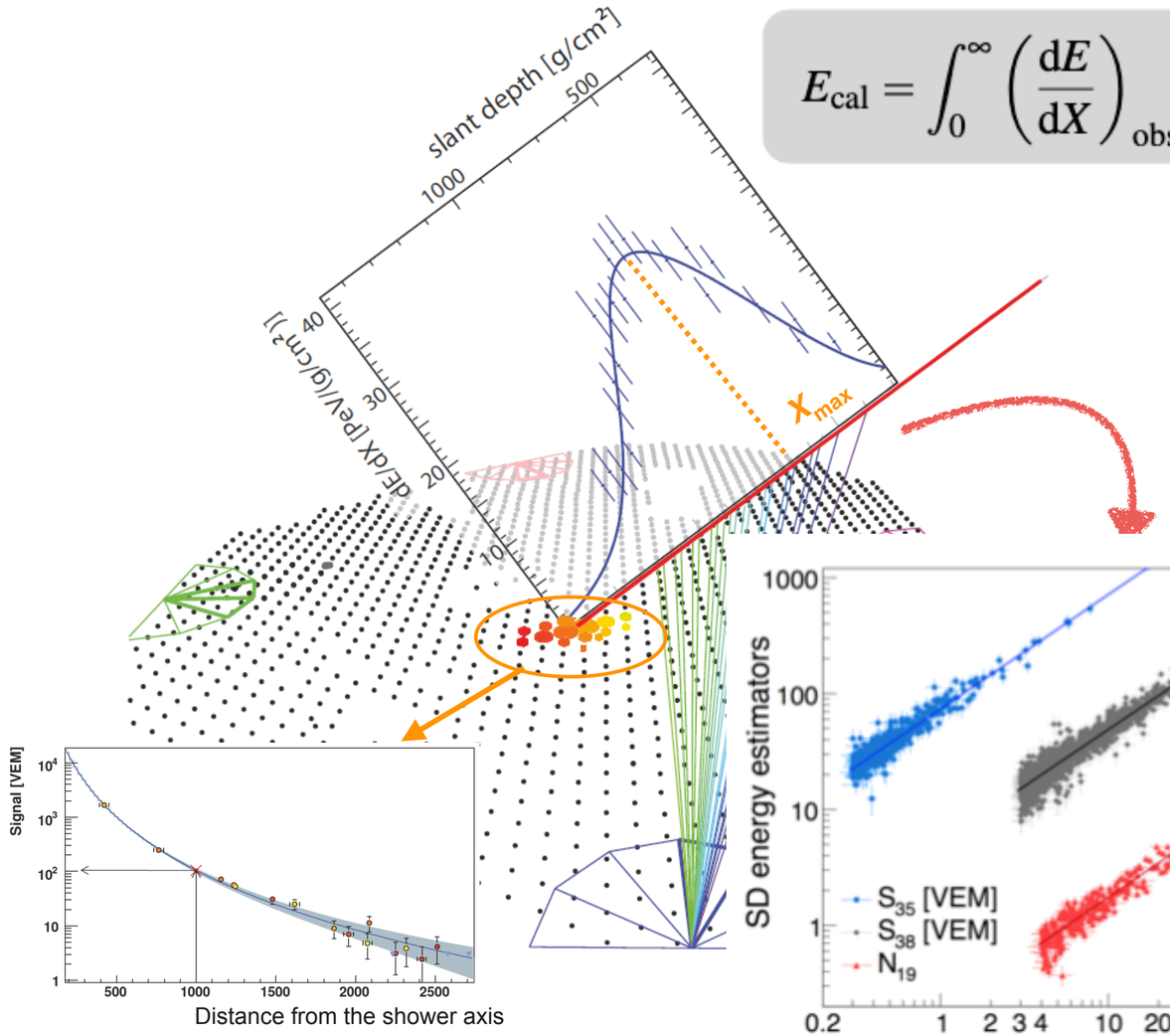

Highlight results: spectrum and composition

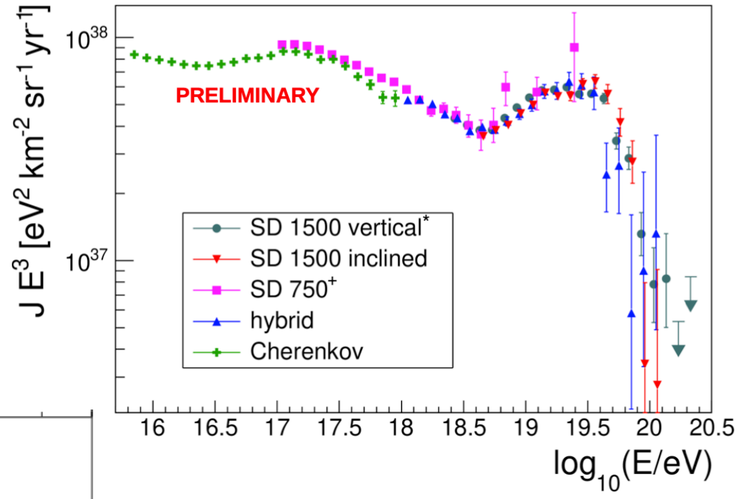

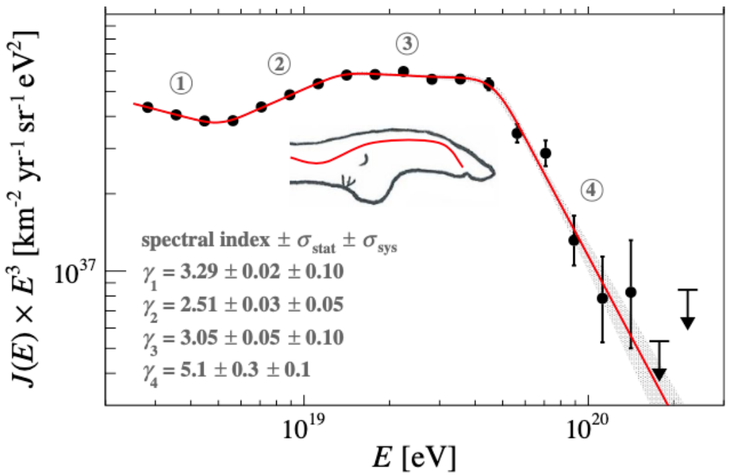

New features in the vertical spectrum.

It can be addressed to astrophysical processes!

The primary mass cannot be measured on an event-by-event basis.

It must be inferred statistically from the distribution of shower maxima of an ensemble of air showers.

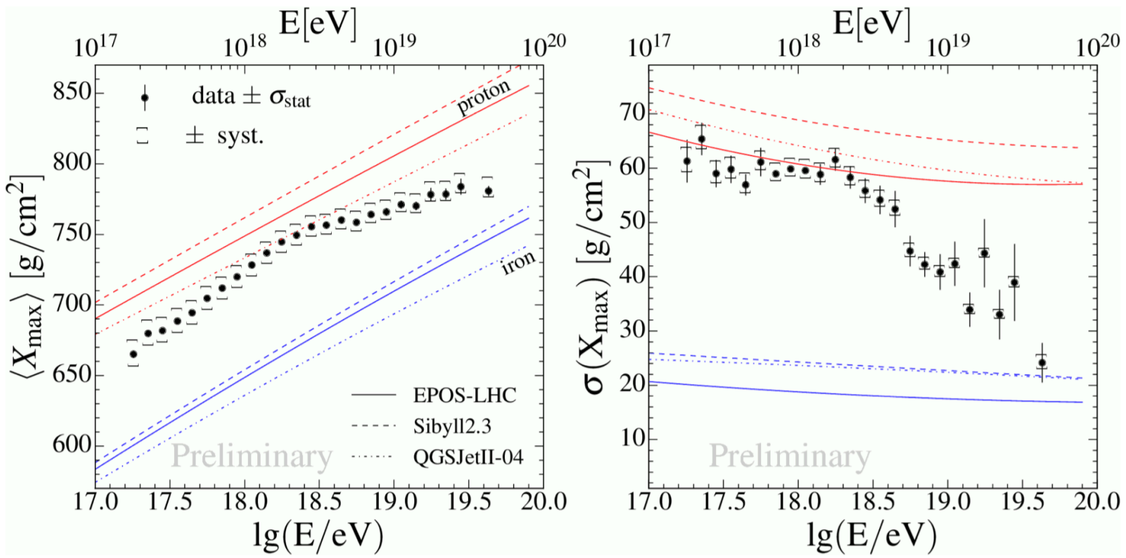

A. Aab *et al*. (The Pierre Auger Collaboration) Phys. Rev. Lett. **125**, 121106

V. Novothny for the Pierre Auger collaboration, ICRC2021

A. Yushkov for the Pierre Auger collaboration. DOI: 10.22323/1.358.0482

Large and intermediate scale anisotropy

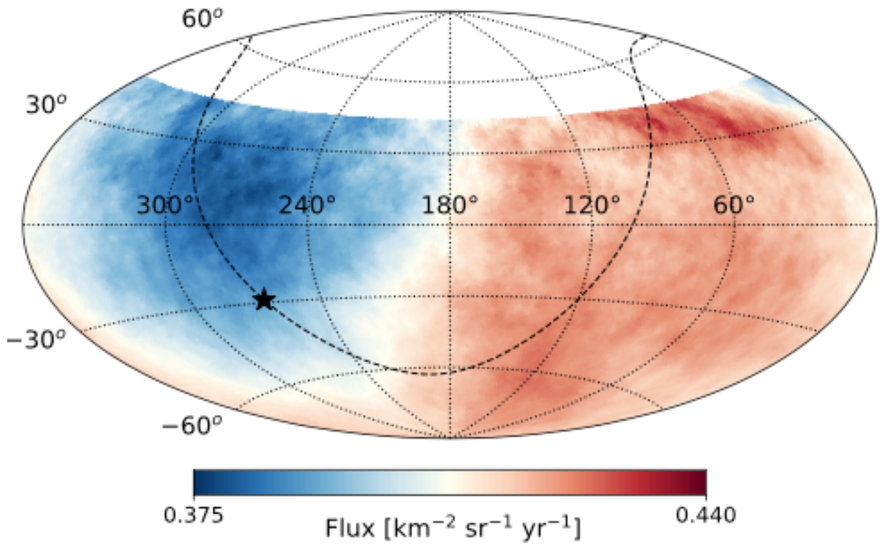

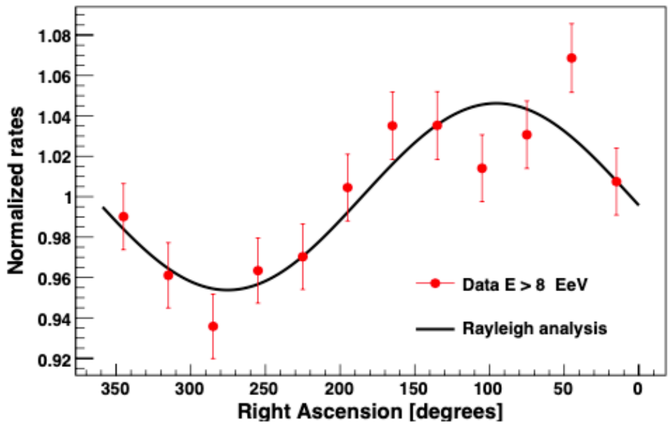

Catalog	E_{th} [EeV]	Ψ [deg]	α [%]	TS	Post-trial p-value
All galaxies (IR)	40	24^{+16}_{-8}	15^{+10}_{-6}	18.2	6.7×10^{-4}
Starbursts (radio)	38	25^{+11}_{-7}	9^{+6}_{-4}	24.8	3.1×10^{-5}
All AGNs (X-rays)	41	27^{+14}_{-9}	8^{+5}_{-4}	19.3	4.0×10^{-4}
Jetted AGNs (γ-rays)	40	23^{+9}_{-8}	6^{+4}_{-3}	17.3	1.0×10^{-3}

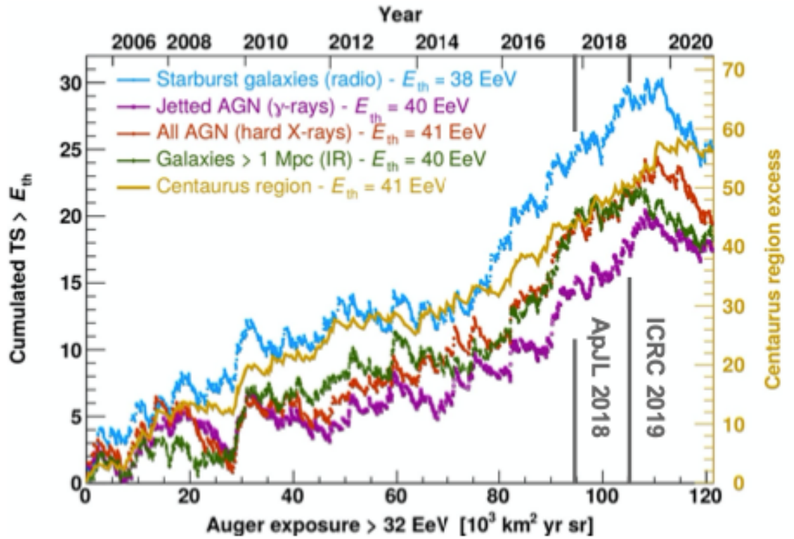

4.0σ

3.1σ

Combined fit above the ankle

Motivation: ankle interpretation

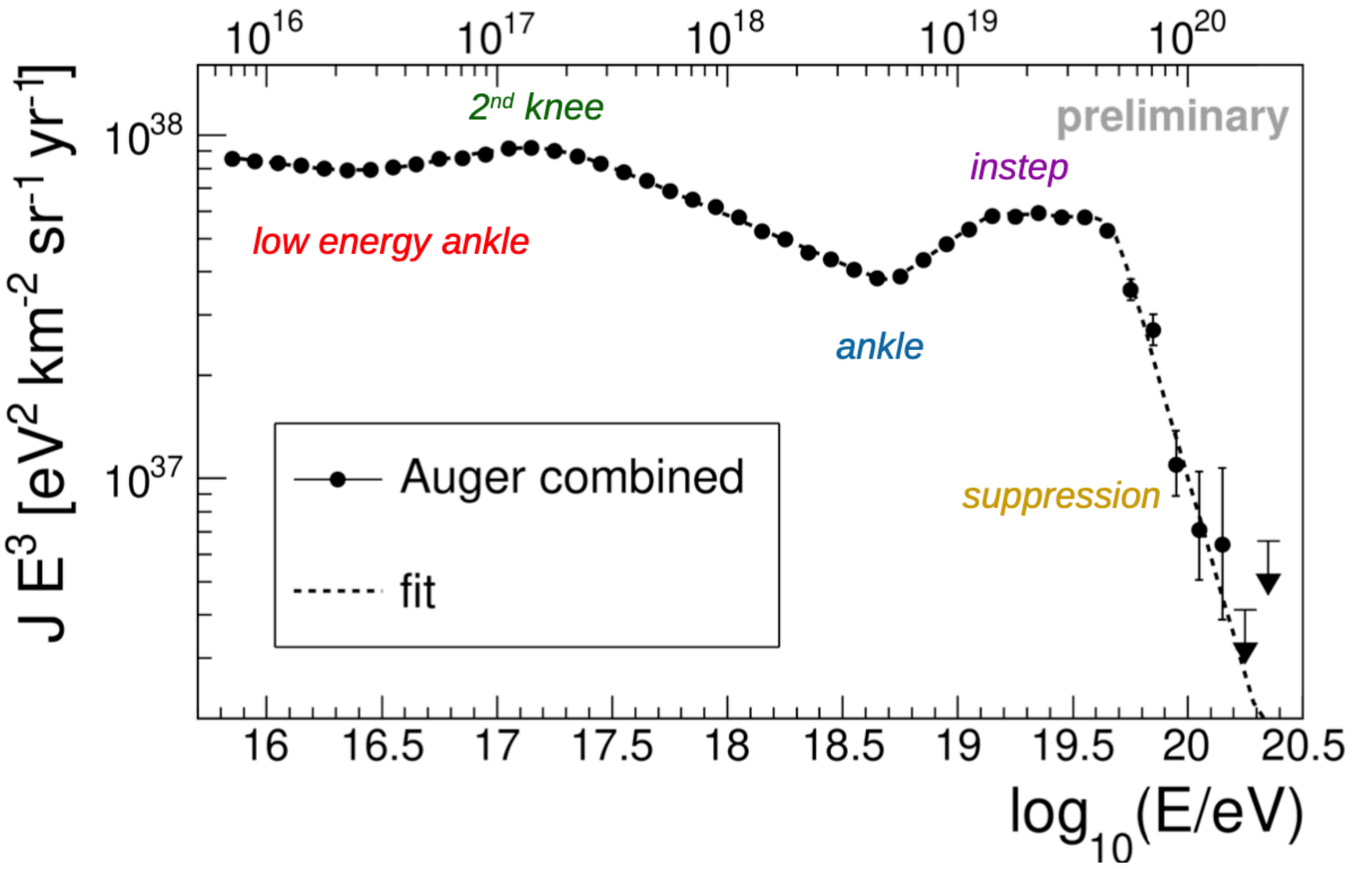

It is possible to link features in the UHECRs to astrophysical processes?

Several possible explanations:

- Transition model;
- Pure proton scenario;
- Mixed composition scenario;

How could the mass composition measurements help to understand these features?

Transition model

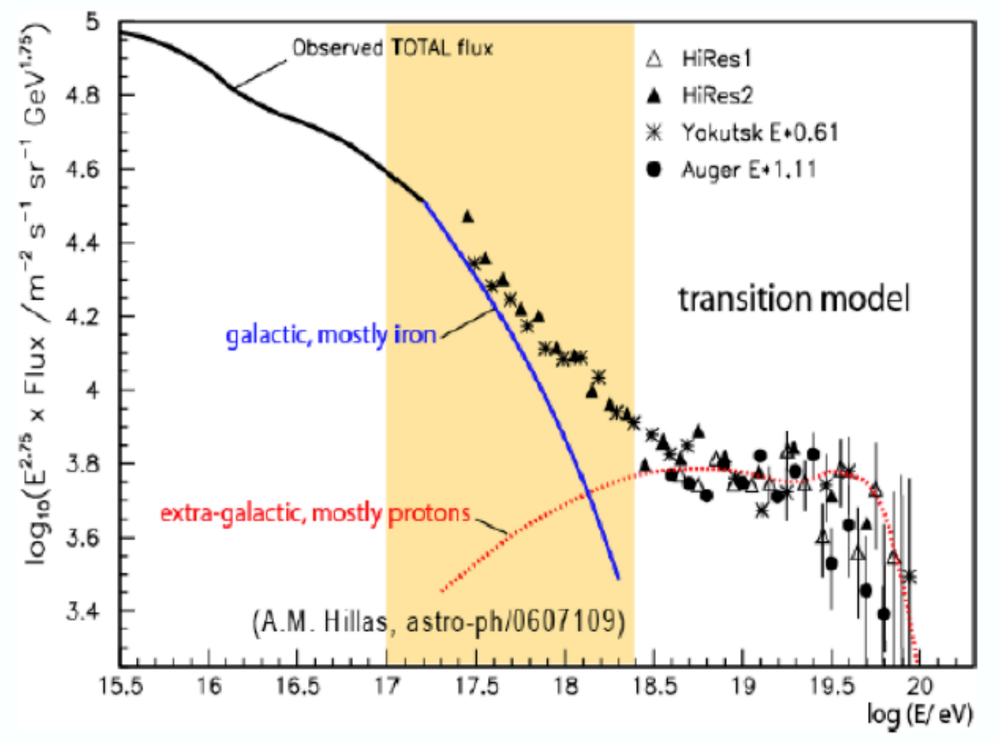

- The ankle could be the transition point between galactic and extragalactic cosmic rays.

Transition model

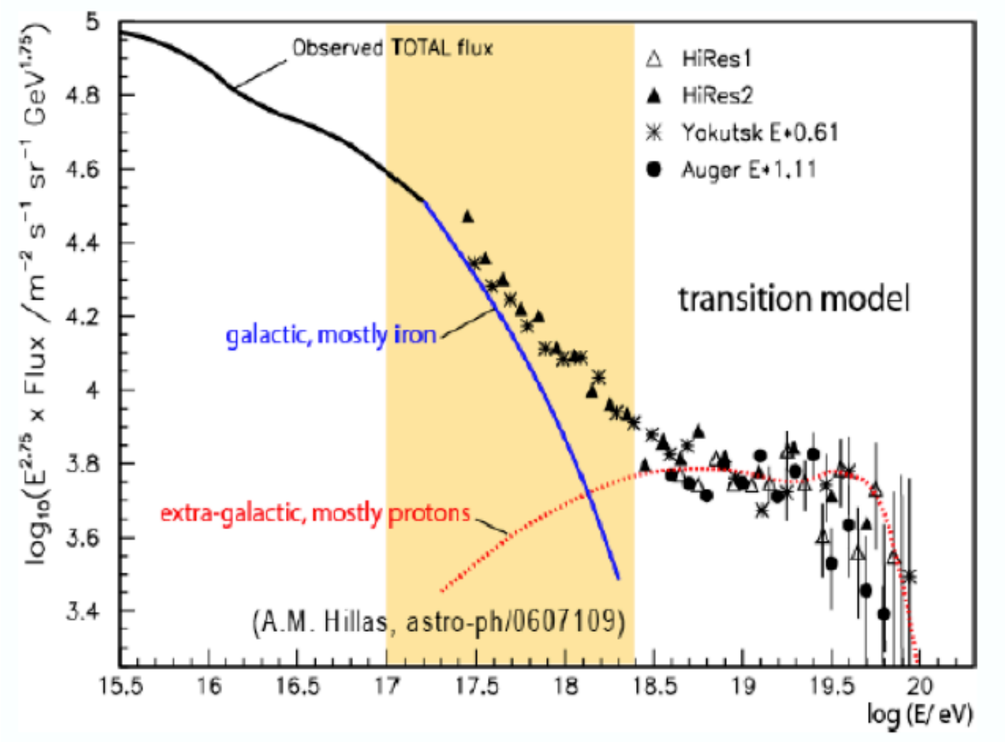

- The ankle could be the transition point between galactic and extragalactic cosmic rays.
- ✗ Hard to find Galactic sources capable to accelerate up to 10^{18} eV.
- ✗ Light composition at the ankle.

Pure proton scenario

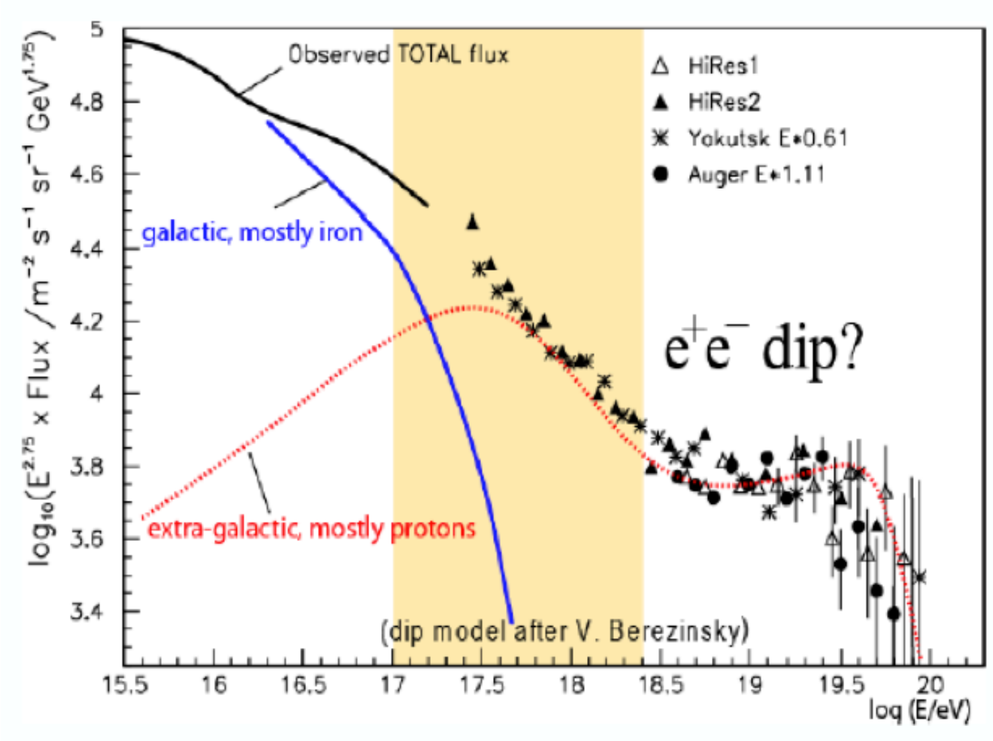

- Assuming only proton spectrum → feature of the propagation;

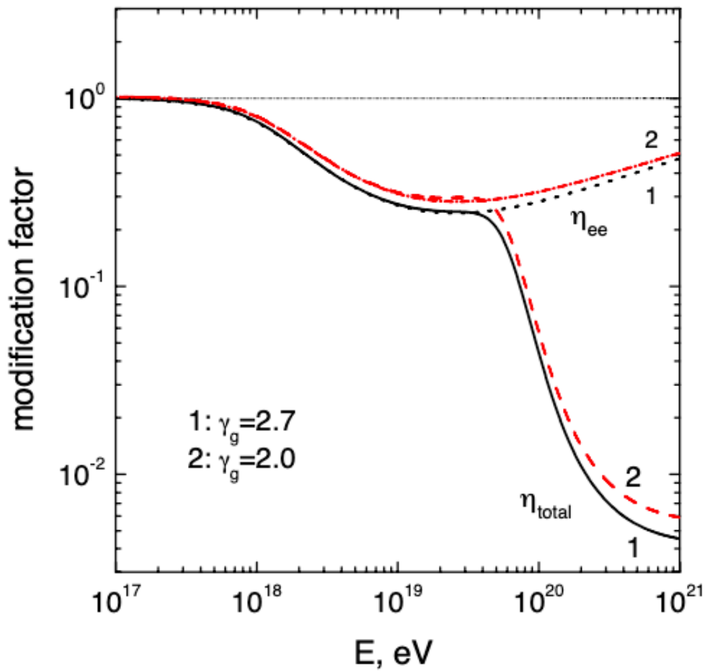

Pure proton scenario

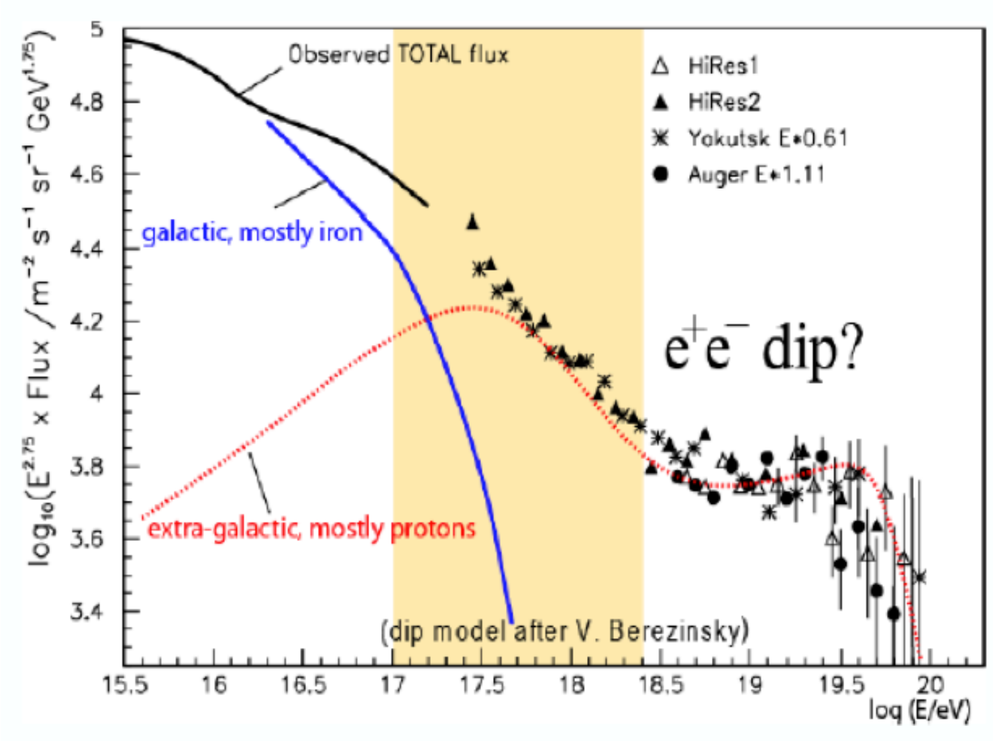

- Assuming only proton spectrum → feature of the propagation;

✘ The UHECRs are not only protons!

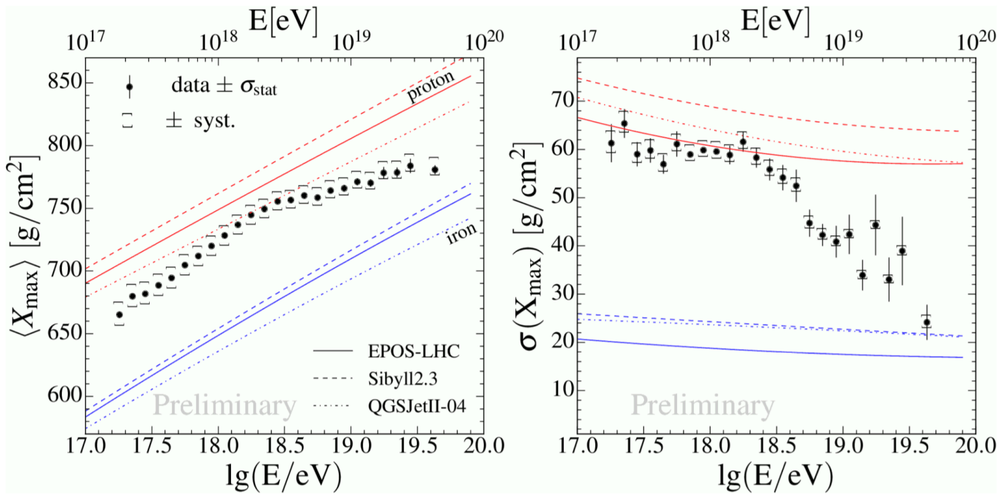

Mixed composition scenario

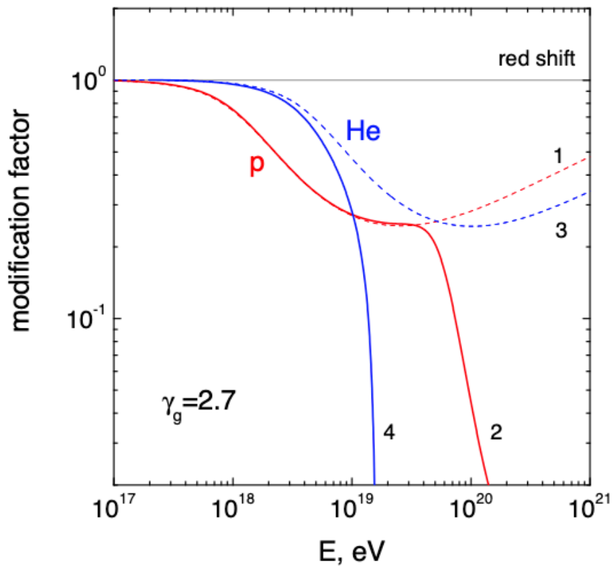

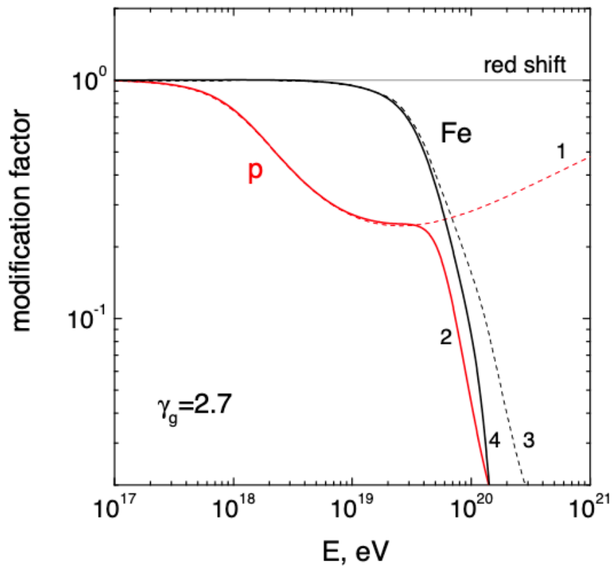

- Assuming nuclei-> the ankle feature is not reproduced.

R. Aloisio et al, Astropart.Phys. 27 (2007) 76-91
astro-ph/0608219

Mixed composition scenario

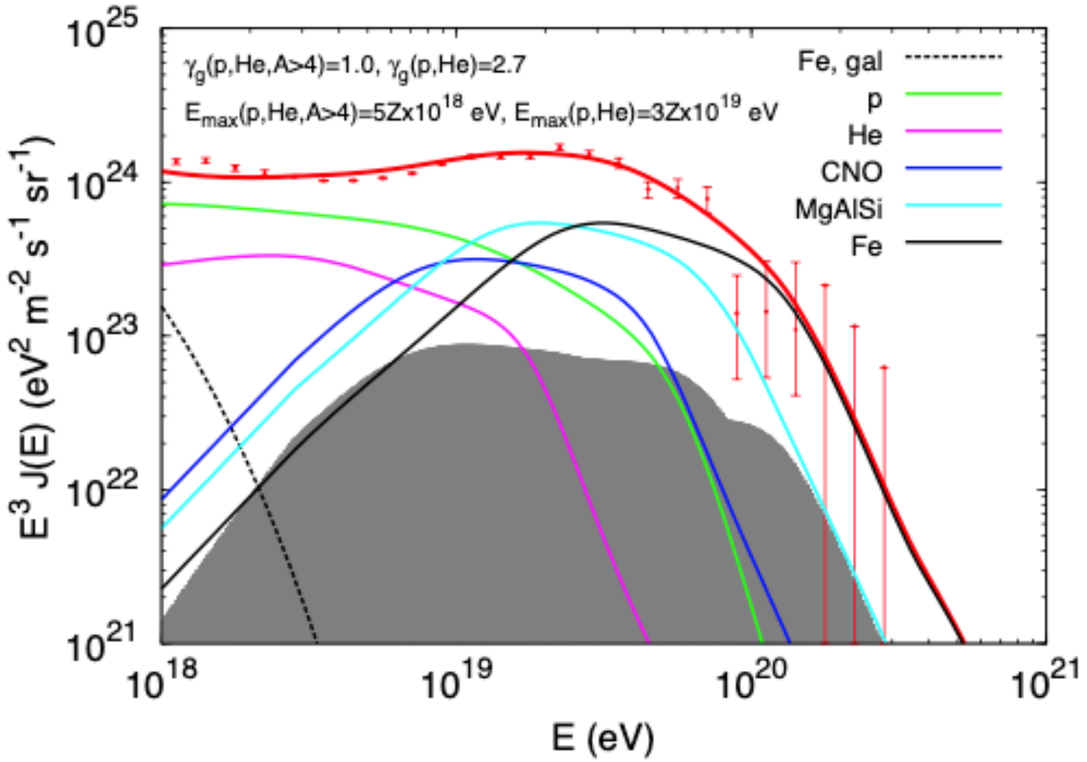

- Assuming nuclei-> the ankle feature is not reproduced.

- With a hard injection spectrum and maximum energy at the source it is possible to describe the spectrum above the ankle.

R. Aloisio et al. , JCAP 10 (2014) 020

Take-home message

- In the pure proton scenario, the features of the energy spectrum are due primarily to the interactions with the CMB.
- In the mixed composition scenario, the suppression of the flux at the highest energies would be due to the photo-disintegration of nuclei.
- The spectrum remains ambiguous concerning astrophysical interpretation;
- Fitting both the spectrum and composition, one can remove this degeneracy and infer information about the source scenarios which are compatible to data.

Combined fit above the ankle: ingredients

- Assuming point-like sources identical and uniformly distributed;
- Acceleration of five representative masses: Hydrogen, Helium, Nitrogen, Silicon and Iron.
- The injected flux for each mass is a power law with a broken-exponential cutoff.

$$J_k(E_i) = f_k J_0 \left(\frac{E_i}{E_0}\right)^{-\gamma} \cdot f_{\rm cut}(E_i, Z \cdot R_{\rm cut})$$

$$f_{\rm cut}(E_i, Z \cdot R_{\rm cut}) = \begin{cases} 1 & E_i < Z\ R_{\rm cut} \\ \exp\left(1 - \dfrac{E_i}{Z \cdot\ R_{\rm cut}}\right) & E_i > Z\ R_{\rm cut} \end{cases}$$

- The injected flux are propagated through the extra-galactic space and fitted to the Auger energy spectrum and composition.
- Free parameters of the fit are: $J_0, \gamma, R_{\rm cut}$ and $(N-1)\, f_k$.
- The total deviance is considered as the sum of the deviance of the spectrum and the deviance of the composition.

A.Aab et al. (The Pierre Auger Collaboration), JCAP04(2017)038

Simulation of extra-galactic propagation

To interpret the measured spectrum and mass composition data in terms of astrophysical scenarios, some tools are needed in order to take into account the role of the propagation.

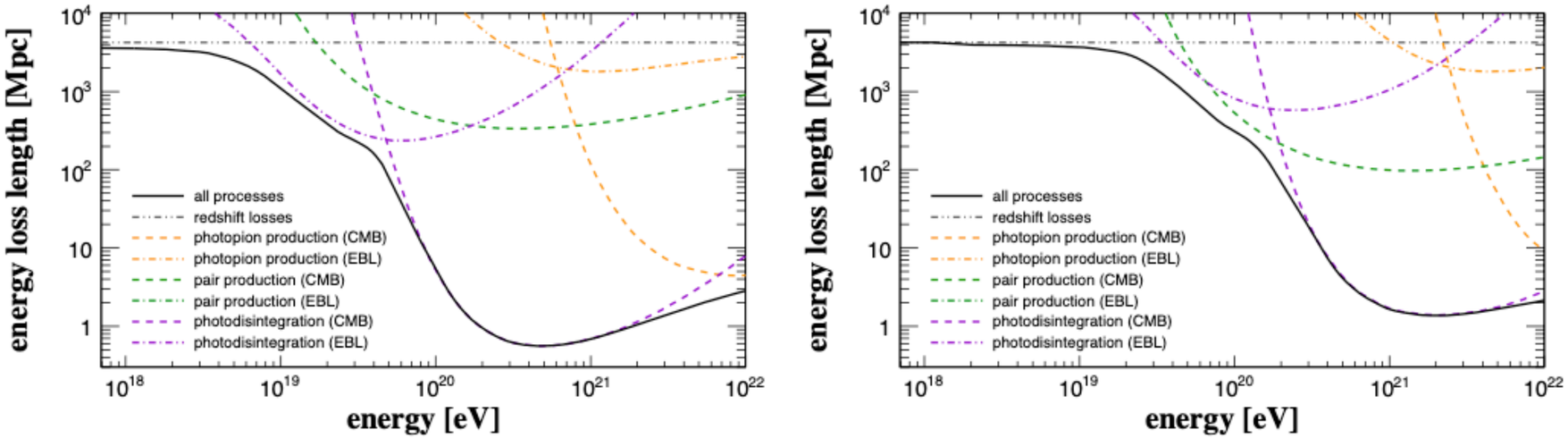

The SimProp software

- SimProp is a Monte Carlo simulation code for the propagation of UHECRs through the Universe.
- Particles injected with a flat distribution in energy and source redshift uniformly distributed.
- The propagation of particles is followed, along with that of the secondary particles produced during propagation.
- Different models for the Photo-disintegration cross section and EBL model.

R. Aloisio et al. JCAP11(2017)009

R. Alves Batista et al, JCAP10(2015)063

Combined fit above the ankle: results

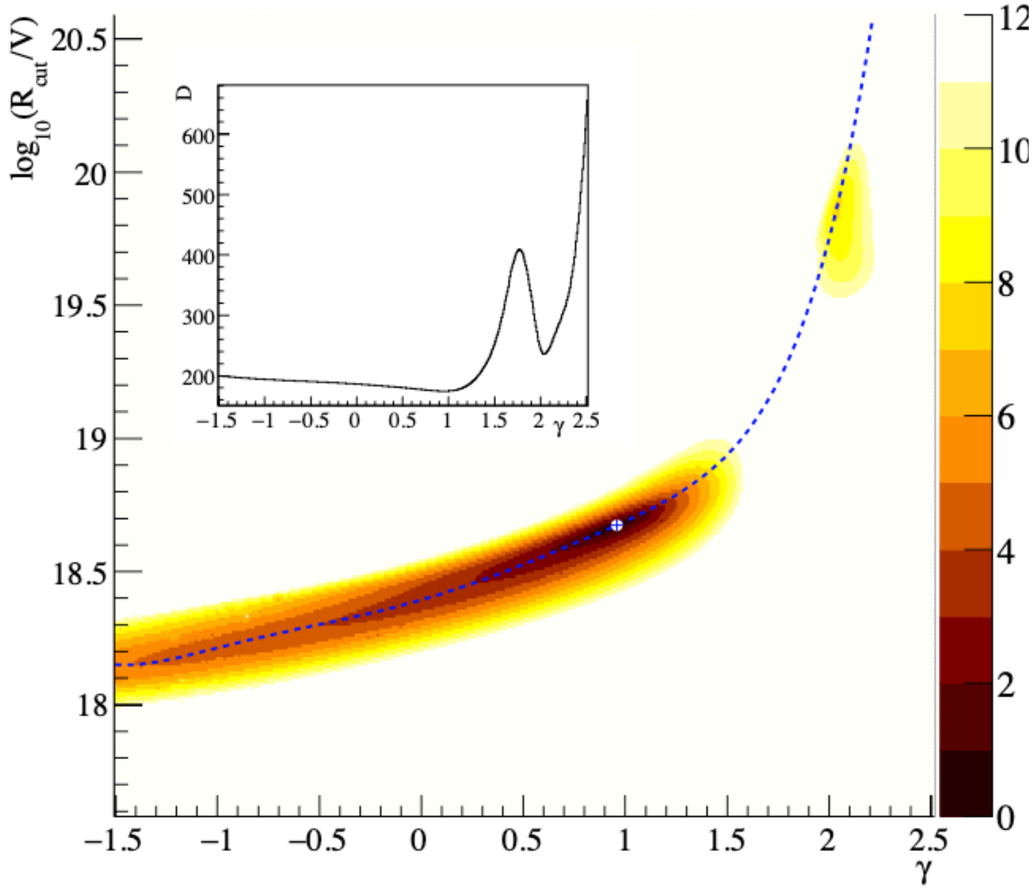

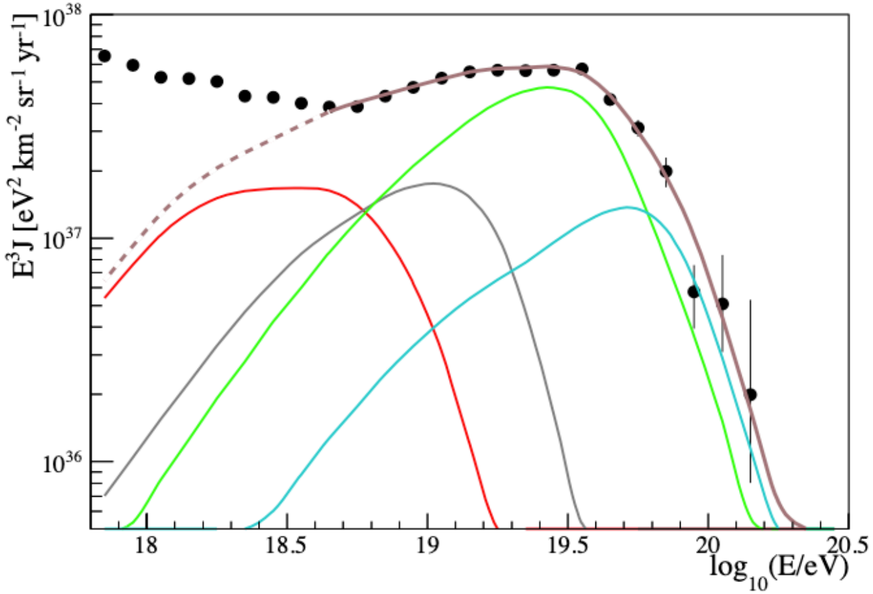

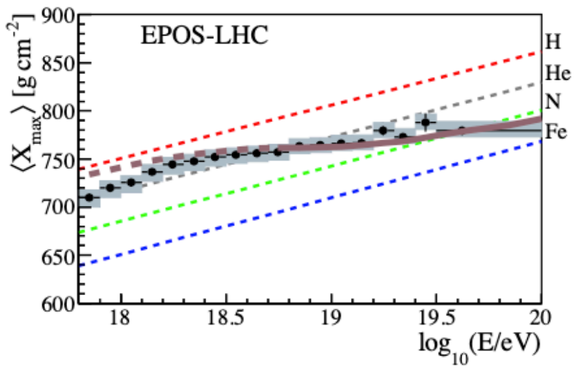

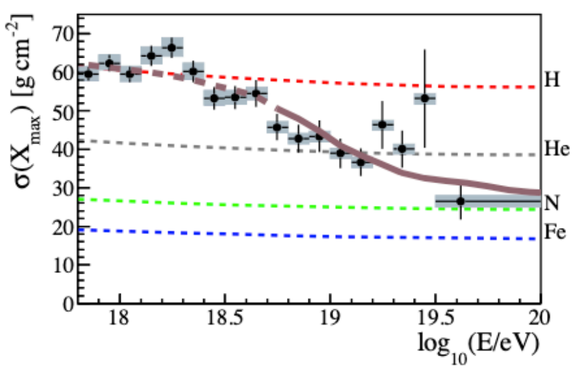

A new combined fit

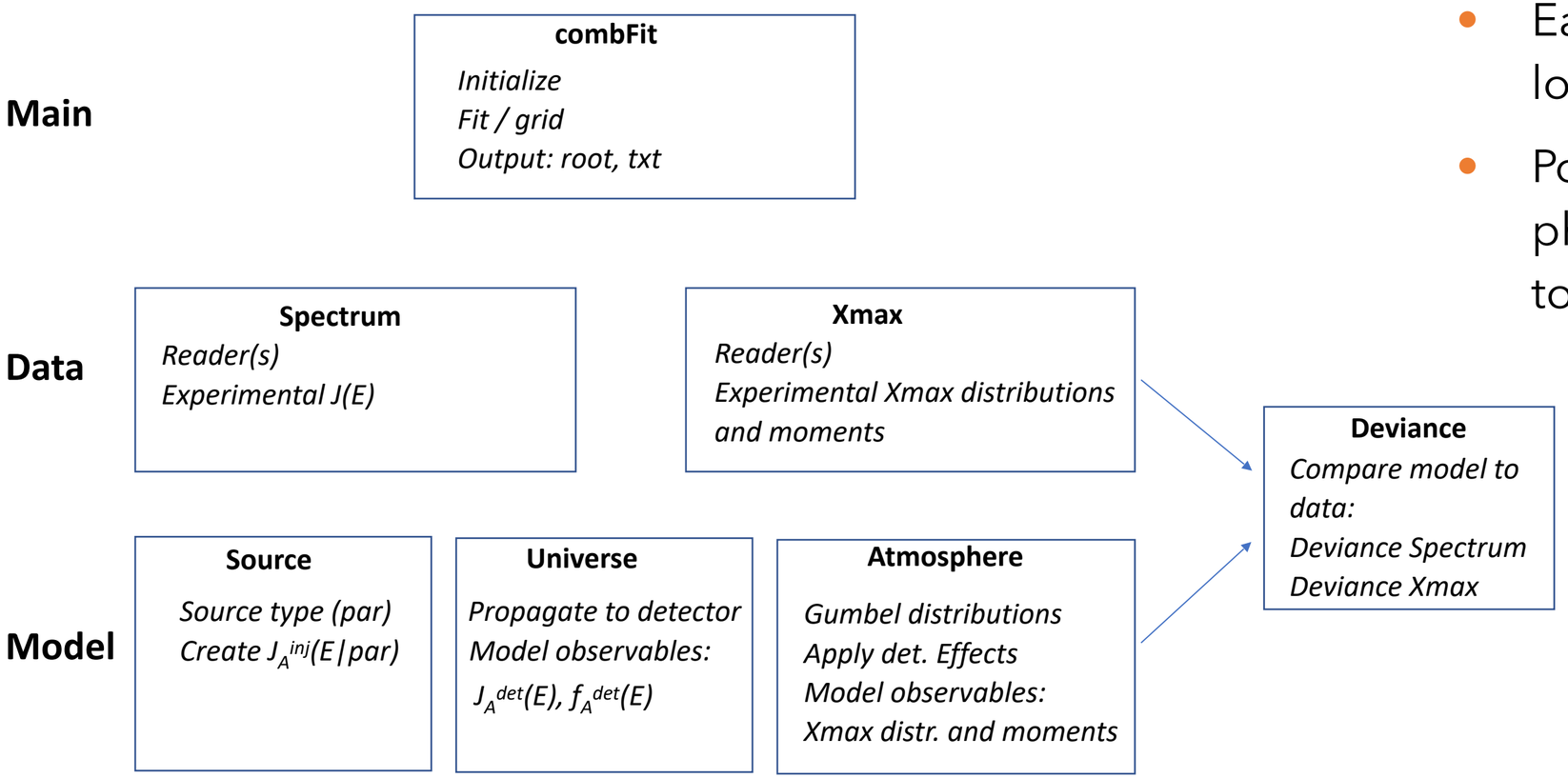

- Easy to extend to lower energies.
- Powerful phenomenological tool (es. FractionFit).

Updating dataset

ICRC2017

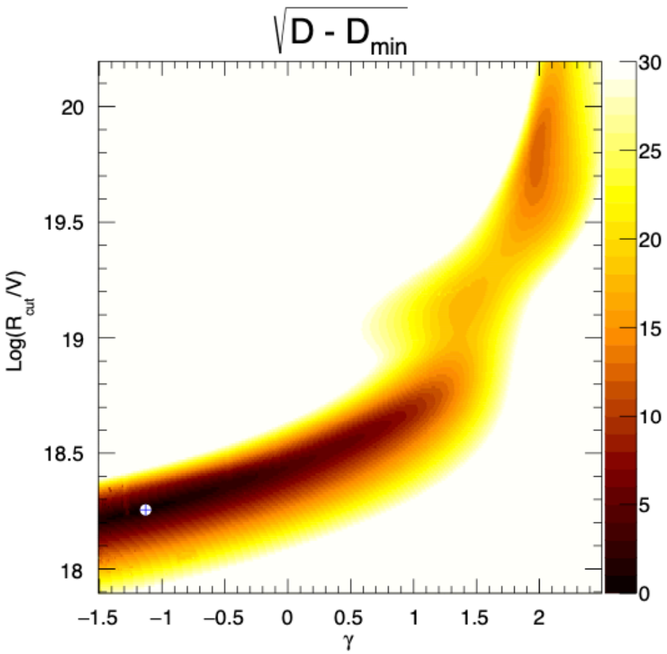

JCAP2017

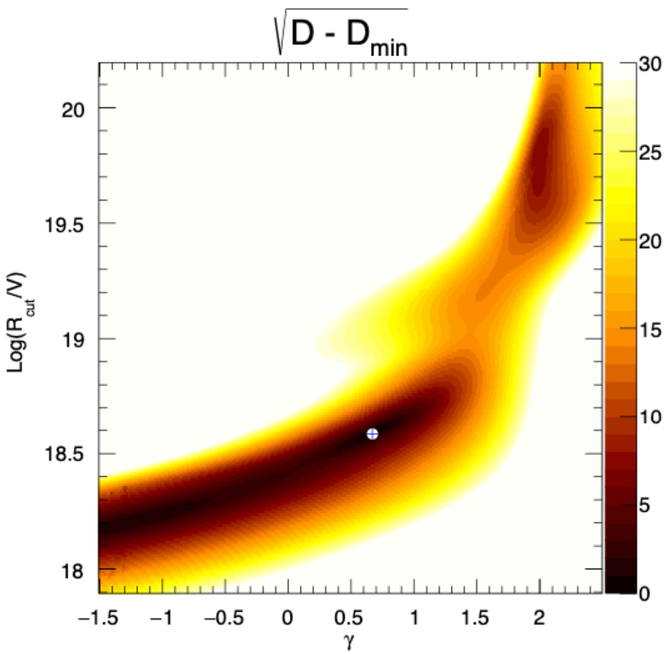

Parameter	JCAP2017	ICRC2017
$f_{\rm H}(\%)$	0.00	75.5 ± 8
$f_{\rm He}(\%)$	80.6 ± 3	24.2 ± 7
$f_{\rm N}(\%)$	16.8 ± 3	0.3 ± 0.1
$f_{\rm Si}(\%)$	2.4 ± 0.5	$O(10^{-4})$
$f_{\rm Fe}(\%)$	0.00	0.00
γ	$0.69^{+0.12}_{-0.12}$	-1.15 ± 0.27
$\log_{10}(R_{\rm cut}/{\rm V})$	$18.59^{+0.03}_{-0.03}$	18.27 ± 0.04
D_J	21.1(15)	14.9(15)
$D_{X_{\rm max}}$	174.6 (110)	237.9 (109)
D_{tot}	195.7(125)	252.8(124)

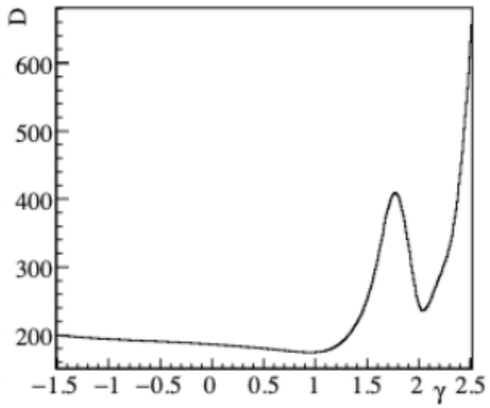

Including over-density correction

$$\frac{\rho_{\text{local}}}{\rho_{\text{Universe}}} = 1 + \left(\frac{r_0}{r}\right)^{-\gamma}$$

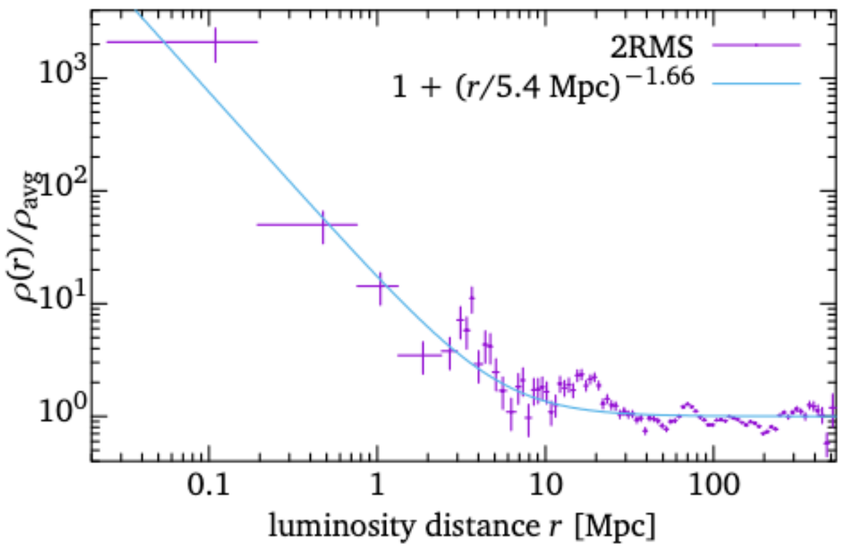

Parameter	JCAP2017	JCAP2017 OD	ICRC2017	ICRC2017 OD
$I_{\text{H}}(\%)$	0.00	0.00	13.4 ± 1	0.00
$I_{\text{He}}(\%)$	41.4 ± 1	39 ± 1	42.1 ± 12	45.5 ± 1
$I_{\text{N}}(\%)$	43.3 ± 9	61 ± 1	32.6 ± 16	48.4 ± 7
$I_{\text{Si}}(\%)$	15.2 ± 4	$O(10^{-4})$	9.9 ± 16	5.9 ± 2
$I_{\text{Fe}}(\%)$	0.00	0.00	2 ± 2	0.00
γ	$0.69^{+0.12}_{-0.12}$	0.74 ± 0.08	-1.12 ± 0.28	0.45 ± 0.09
$\log_{10}(R_{\text{cut}}/\text{V})$	$18.59^{+0.03}_{-0.03}$	18.59 ± 0.01	18.23 ± 0.04	18.53 ± 0.02
D_{J}	21.1(15)	28.6(15)	14.9(15)	32.5(15)
$D_{X_{\text{max}}}$	174.6(110)	153.9(110)	237.9(109)	202.6(109)
D_{tot}	195.7(125)	182.5(125)	252.8(124)	235.1(124)

Short summary: Combined fit above the ankle

Parameter	ICRC2019	ICRC2019 OD
$I_{\mathrm{H}}(\%)$	11.2 ± 9	0.00
$I_{\mathrm{He}}(\%)$	44.7 ± 12	46.5 ± 1
$I_{\mathrm{N}}(\%)$	28.7 ± 15	46.8 ± 6
$I_{\mathrm{Si}}(\%)$	15.4 ± 12	6.7 ± 0.1
$I_{\mathrm{Fe}}(\%)$	0.00	0.00
γ	-1.1 ± 0.25	0.36 ± 0.09
$\log_{10}(\mathrm{R_{cut}/V})$	18.5 ± 0.01	18.5 ± 0.01
D_{J}	23(15)	49.5(15)
$D_{X_{\mathrm{max}}}$	293.7 (121)	259.7 (121)
D_{tot}	316.7(136)	309.2(136)

- The best fit solution estimates a very hard injection spectrum, providing a reasonable description of the features in the observed energy spectrum, which are more and more pronounced because of the increased number of events.
- The mass composition at the sources is largely dominated by light masses, with a relatively small amount of nitrogen.
- With this methods it is possible to describe energy spectrum and composition at Earth, despite the fact that the fit is worse if compared to the previous dataset.

Extended combined fit

Additional component

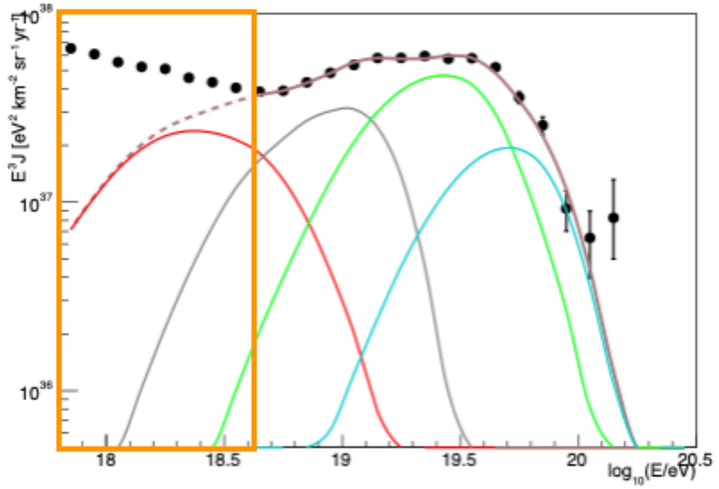

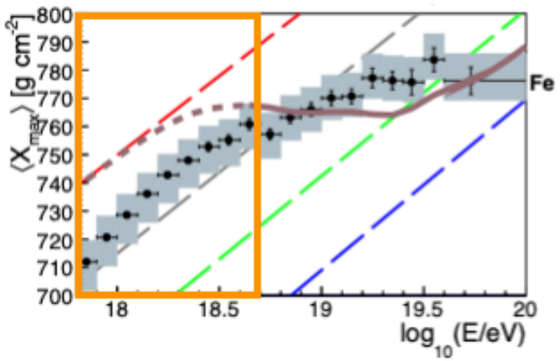

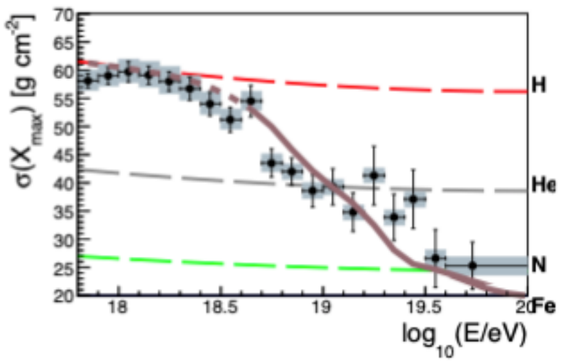

- Taking into account only propagation effects, it is impossible to generate the ankle feature using nuclei rather than proton.
- A second extra-galactic component, independent of the one used to fit the data above the ankle, is required.

Implementation of the extended combined fit

$$J_k^{\mathrm{LE}}(E) = J_0^{\mathrm{LE}}\ f_k^{\mathrm{LE}} \left(\frac{E}{E_0}\right)^{-\gamma^{\mathrm{LE}}} \cdot f_{\mathrm{cut}}(E, Z \cdot R_{\mathrm{cut}}^{\mathrm{LE}})$$

$$J_k^{\mathrm{HE}}(E) = J_0^{\mathrm{HE}}\ f_k^{\mathrm{HE}} \left(\frac{E}{E_0}\right)^{-\gamma^{\mathrm{HE}}} \cdot f_{\mathrm{cut}}(E, Z \cdot R_{\mathrm{cut}}^{\mathrm{HE}})$$

- Duplicating the combined fit structure using two extra-galactic components;
- The free parameters are duplicated with respect to the previous case.

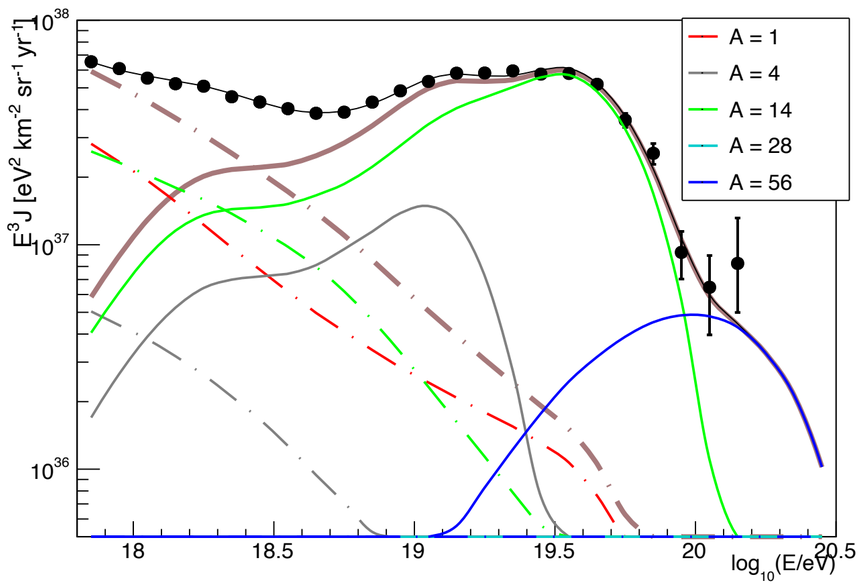

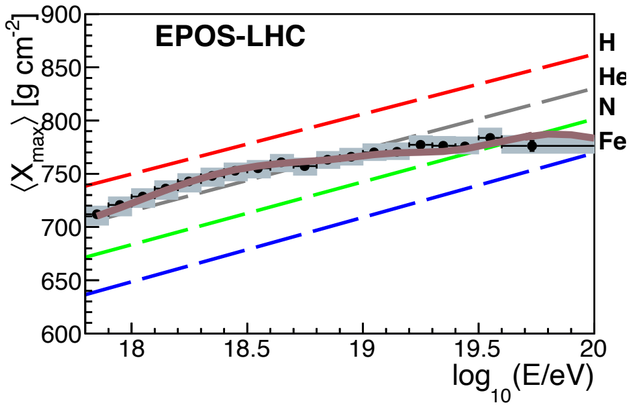

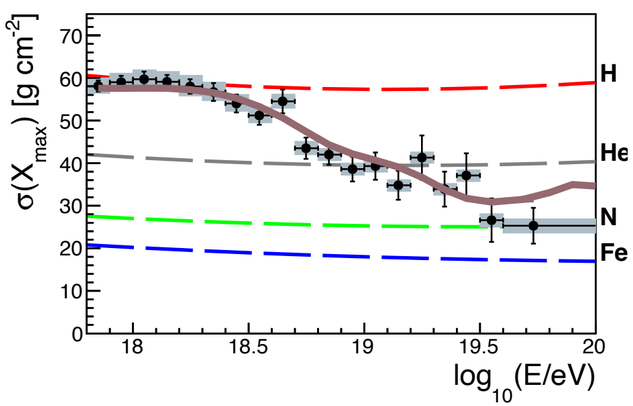

Implementation of the extended combined fit

	OD		NO OD	
Parameter	**LE**	**HE**	**LE**	**HE**
$I_{\rm H}(\%)$	49 ± 0.1	$O(10^{-9})$	49.5 ± 0.3	$O(10^{-6})$
$I_{\rm He}(\%)$	8 ± 0.1	27.8 ± 0.1	5.8 ± 0.1	25 ± 0.3
$I_{\rm N}(\%)$	43 ± 0.3	70.4 ± 10	44.7 ± 0.1	60.8 ± 0.3
$I_{\rm Si}(\%)$	$O(10^{-10})$	$O(10^{-6})$	$O(10^{-10})$	13 ± 0.1
$I_{\rm Fe}(\%)$	$O(10^{-10})$	$1.8 + 0.6$	$O(10^{-10})$	$1.2 + 0.01$
γ	3.46 ± 0.1	-1.96 ± 0.1	3.5 ± 0.1	-2.21 ± 0.1
$\log_{10}(R_{\rm cut}/{\rm V})$	19.6 ± 1.5	18.15 ± 0.01	21 ± 4	18.12 ± 0.01
$D_{\rm J}$	$39(24)$		$37.2(24)$	
$D_{X_{\rm max}}$	$514.2\ (329)$		$522.4\ (329)$	
$D_{\rm tot}$	$553.3(353)$		$559.6(353)$	

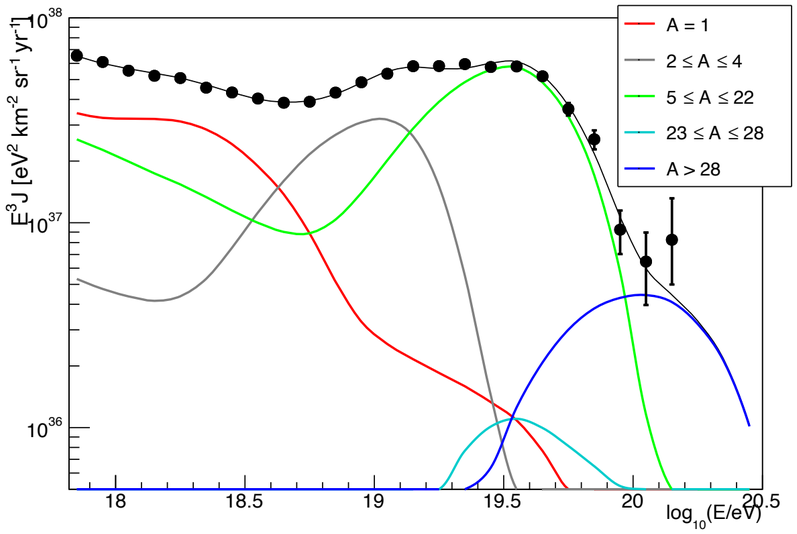

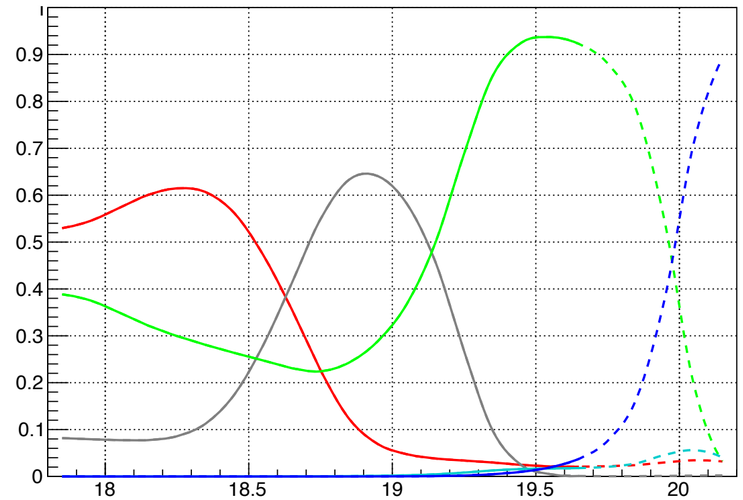

- The high-energy component consists of a hard injection spectrum ($\gamma \simeq -2$) and a low energy cutoff at the sources.
- The low-energy component presents an extremely soft injected energy spectrum, with a spectral index larger than 3.

Taking into account the end of the Galactic spectrum

$$J(E) = J_0^{\mathrm{G}} \cdot \begin{cases} E^{-\gamma_1} & E \leq E_b \\ E^{-\gamma_2} & E > E_b \end{cases} \qquad f_{\mathrm{cut}}(E, E_{\mathrm{cut}}^G) = \exp\left(- \frac{E}{E_{\mathrm{cut}}^G} \right)$$

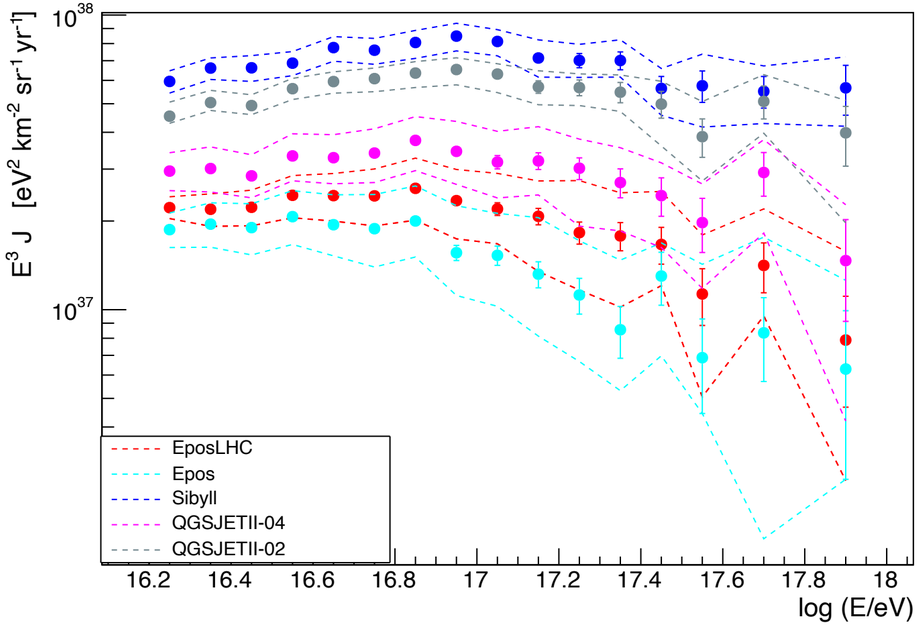

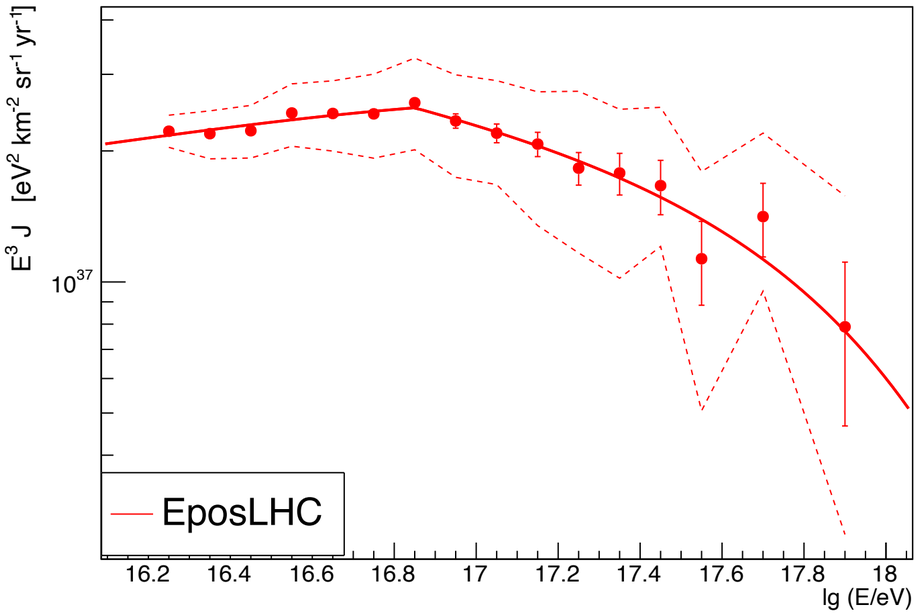

Param.	value
J_0^{G} $(\mathrm{eV}^{-1}\mathrm{km}^{-2}\mathrm{s}^{-1}\mathrm{sr}^{-1})$	$(7.61 \pm 0.04) \cdot 10^{-14}$
γ_1	2.86 ± 0.01
γ_2	3.19 ± 0.04
$\log_{10}(E_{\mathrm{b}}/\mathrm{eV})$	16.85 ± 0.001

M. Bertaina [Kascade-Grande coll.], *PoS* ICRC2015 (2016) 359
W.-D. Apel et al. - [KASCADE-Grande Coll.], *Phys. Rev. D* **87** (2013) 081101

Taking into account the end of the Galactic spectrum

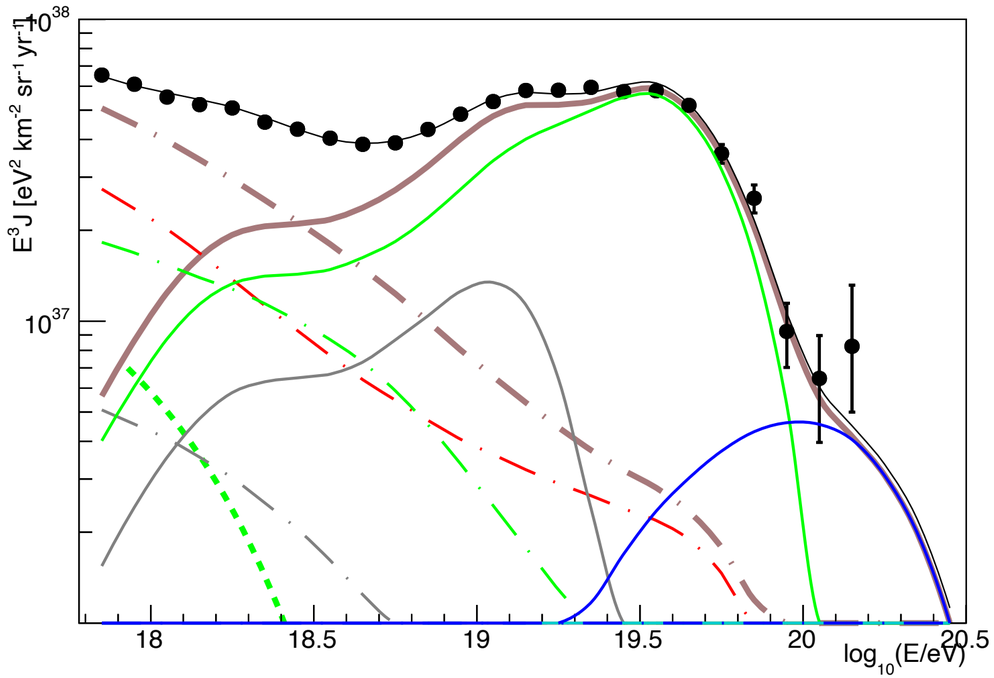

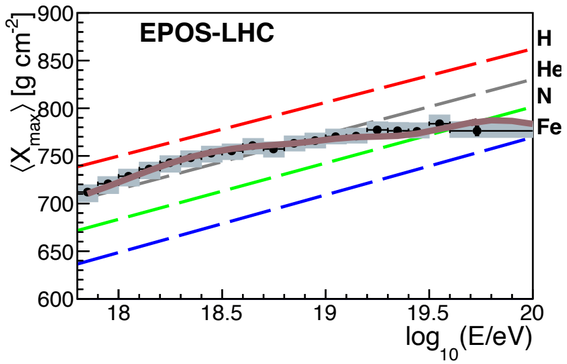

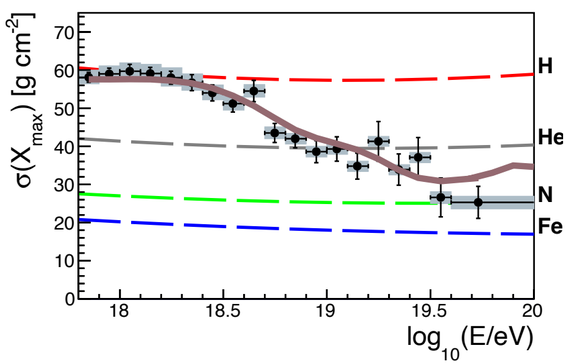

- The presence of an iron component at low energies is strongly disfavored.
- The fit is not able to distinguish between a galactic and an extra-galactic contribution at low energies. The Galactic intermediate composition is favored.

Low energy component made of protons

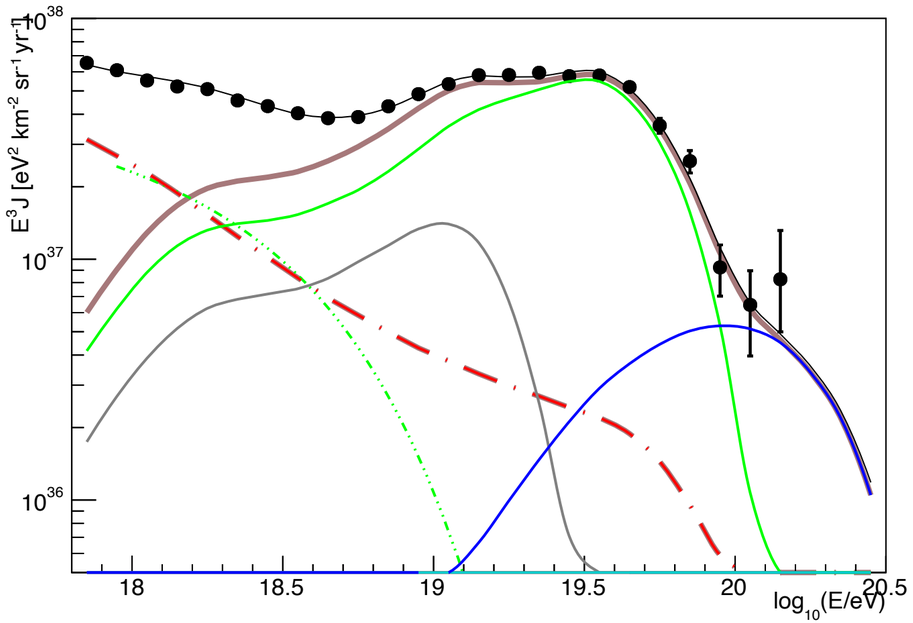

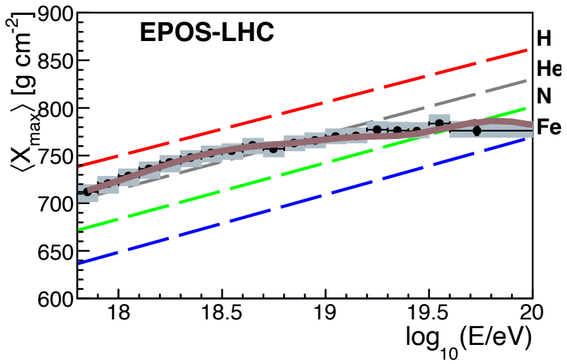

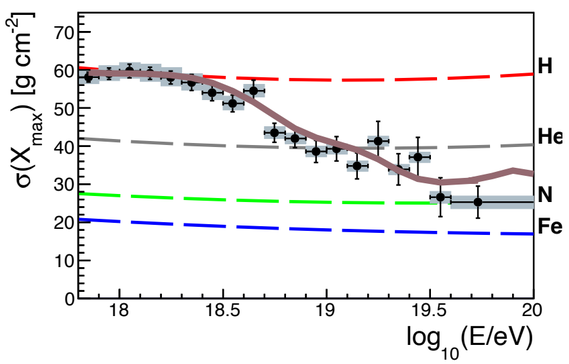

- Test a different scenarios inspired by source-propagation model.
- Low energy component made only by protons;
- Fitting the normalization and the cutoff of the Galactic component.

- It requires a Galactic flux two times higher than KG electron-poor component.
- The fit is slightly worse with respect to the previous case.

Associated cosmogenic neutrino fluxes

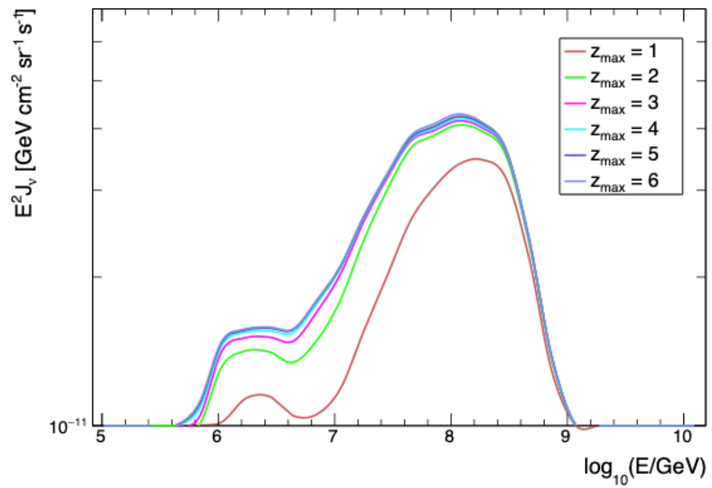

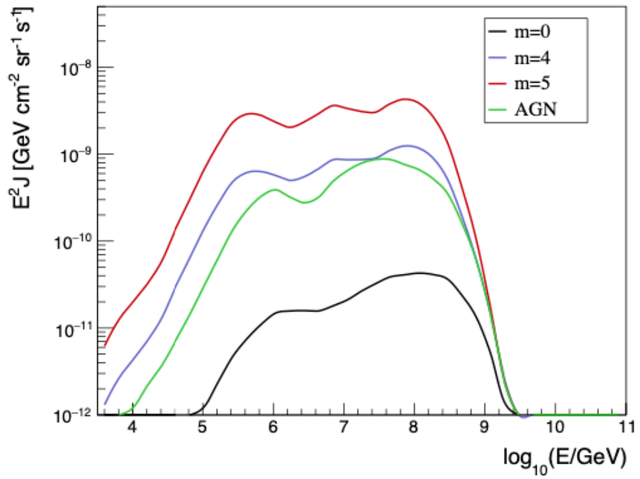

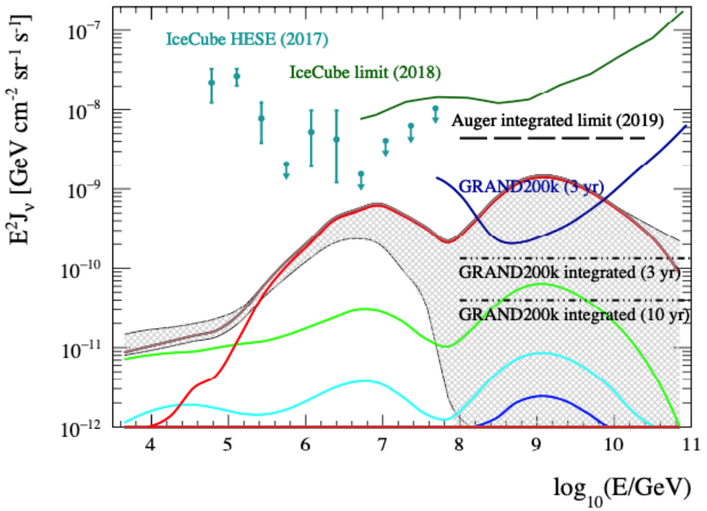

$$S(z) \propto (1+z)^m$$

Neutrinos (1 component): assuming m = 0, several order of magnitude below the experimental data and limits.

Neutrinos (2 components): affected by big uncertainties in the maximum energy –> future neutrino detectors could constrain maximum energy for this model.

Short summary: Extended combined fit

- The HE component requires an hard injection spectrum: the additional component below the ankle does not spoil the main features of the fit shown in the combined fit above the ankle;
- The LE component requires a soft injection spectrum.
- The fit is not able to distinguish between a galactic + extra-galactic contribution and a pure extra-galactic contribution at low energies.
- An intermediate composition is favored at low energies, while the presence of an Iron galactic component is strongly disfavored.

Source-propagation model

Ankle interpretation

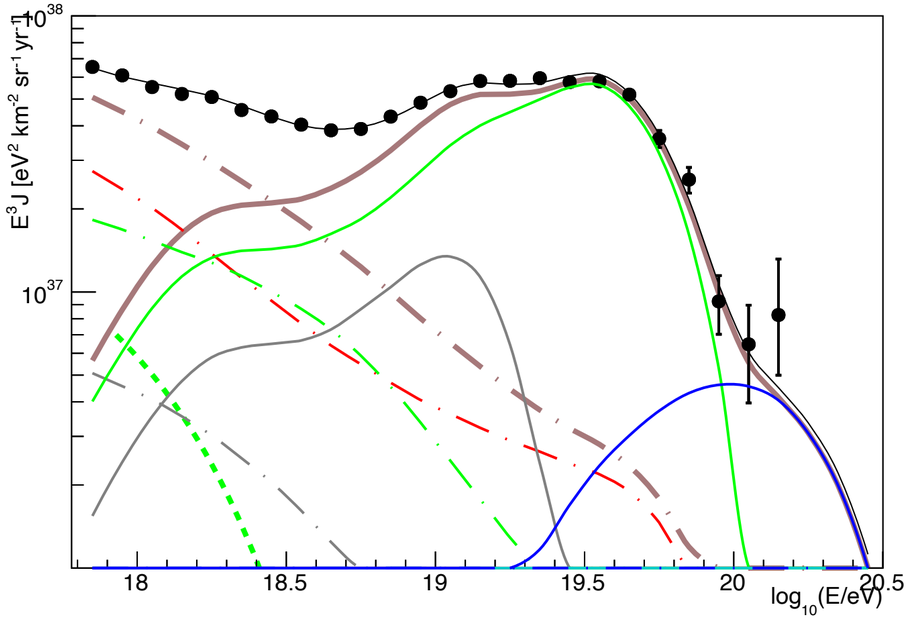

Description of the Auger data over a large energy range using two populations: one with a hard injection spectrum at high energies and a second one with a soft injection spectrum at low energies.

Different classes of sources

Mechanism at the source

Source-propagation model

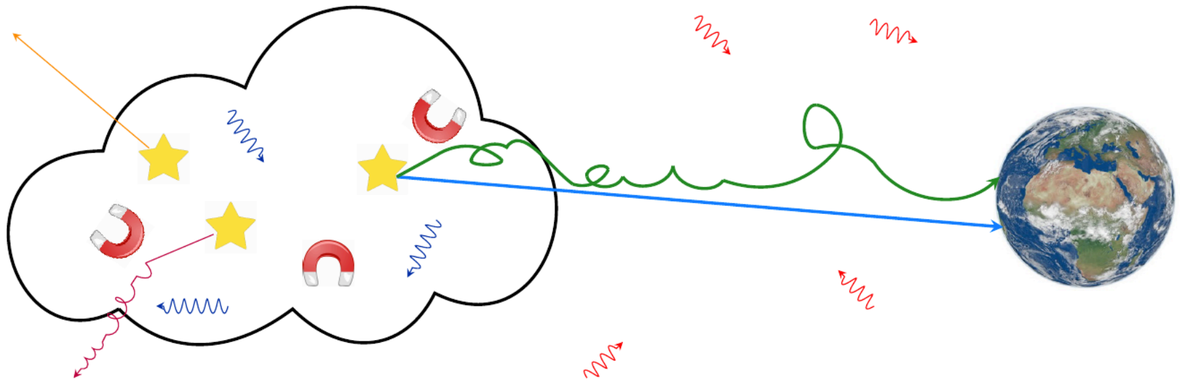

In a system in which the accelerator is embedded in an environment in which the cosmic rays are confined in presence of a photon field:

- High energy particles are able to escape with no interactions;
- Low energy particles loses energy and mass, creating a pile-up of nucleons at low energies.
- The interplay of the two components can describe both UHECRs spectrum and composition at Earth.

M. Unger, G.R. Farrar and L.A. Anchordoqui, Phys. Rev. D 92, 123001 (2015)

UFA model

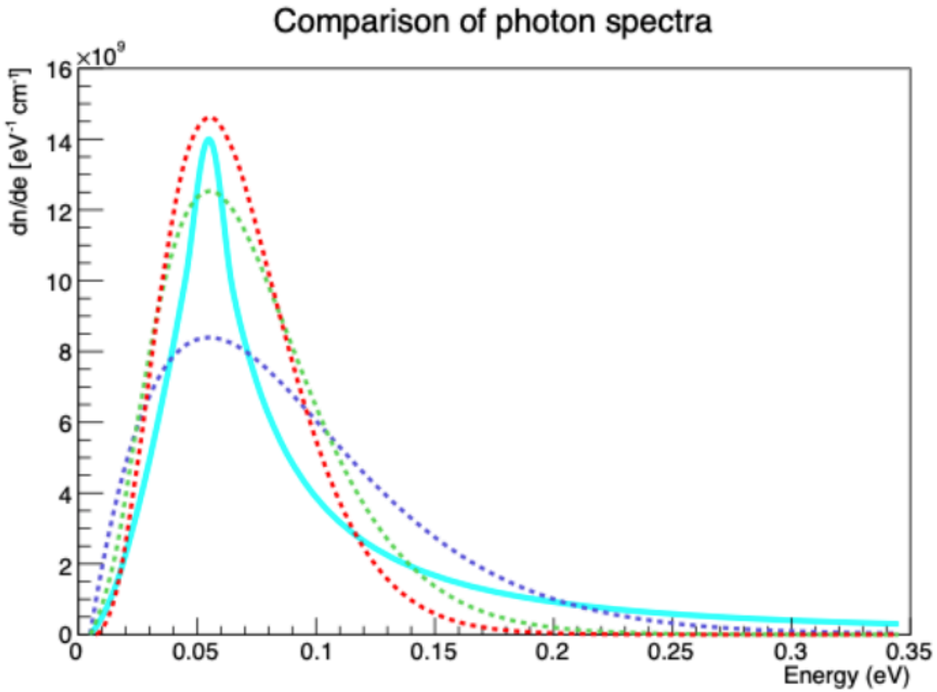

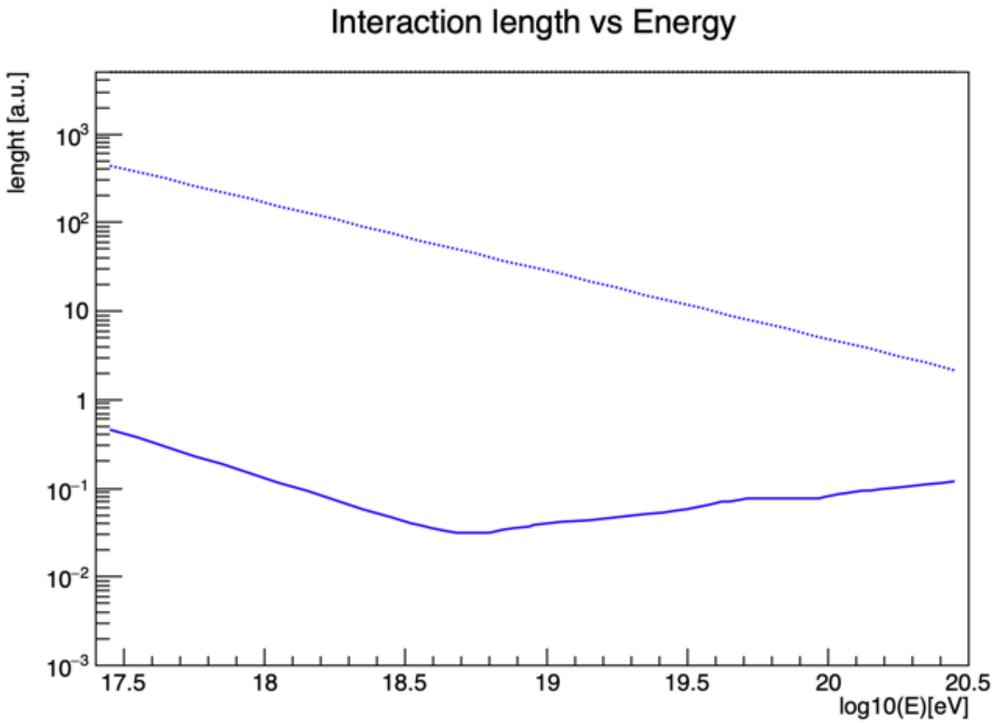

$$\frac{1}{\tau} = \frac{1}{2\Gamma^2} \int_{\epsilon'_{\min}}^{2\Gamma\epsilon} \int_{\epsilon=0}^{+\infty} \frac{n_\gamma(\epsilon)}{\epsilon^2} \, \mathrm{d}\epsilon \, \sigma(\epsilon') \epsilon' \, \mathrm{d}\epsilon'$$

M. Unger, G.R. Farrar and L.A. Anchordoqui, Phys. Rev. D 92, 123001 (2015)

R. Aloisio et al. JCAP11(2017)009

UFA model

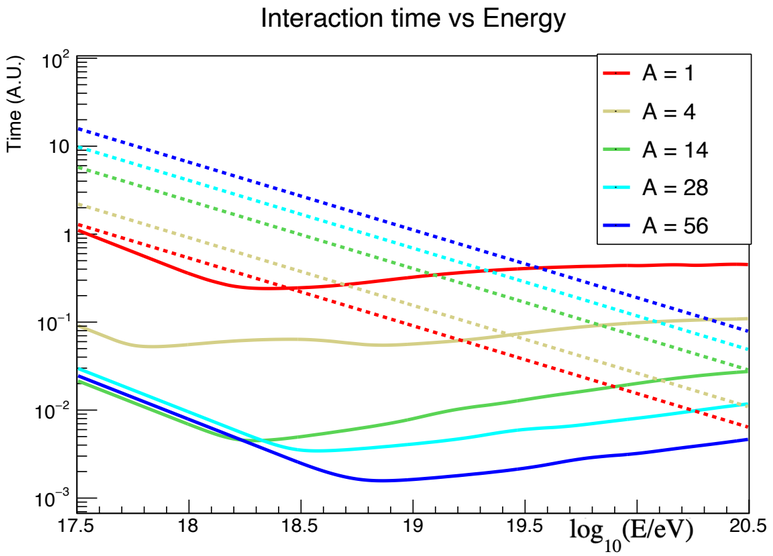

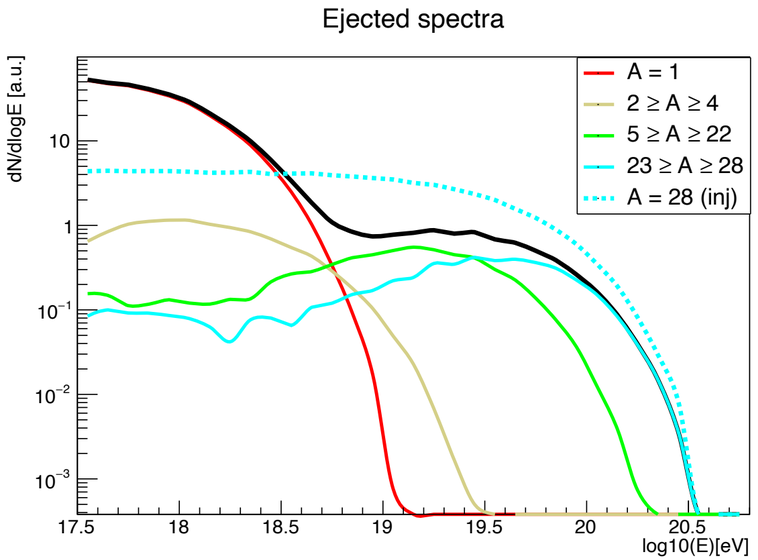

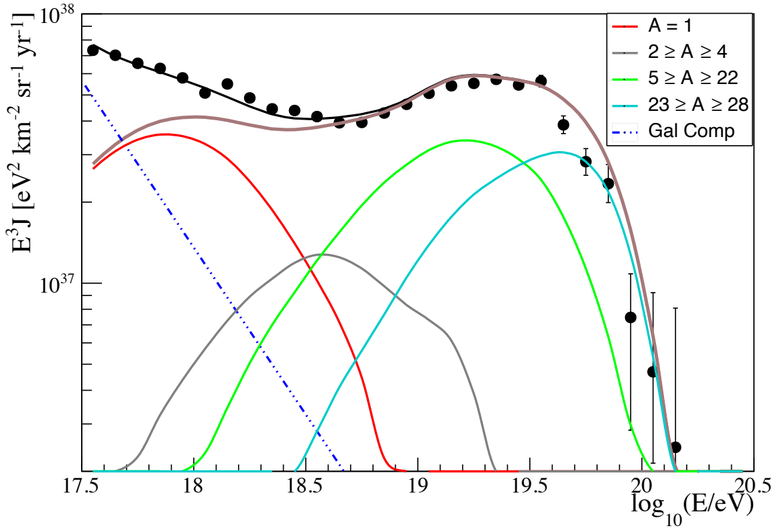

M. Unger, G.R. Farrar and L.A. Anchordoqui, Phys. Rev. D 92, 123001 (2015)

Methodology of source-propagation model

- A single nuclear specie is injected in the environment surrounding the source;
- Interaction and escaping times are computed: if a particle escapes is not propagated anymore, otherwise the computation of energy and mass losses is performed;
- We are assuming that all the sources are identical and distributed up to a maximum redshift.
- The fluxes escaping from the sources are propagated thought the extra-galactic space and compared to the data at Earth.

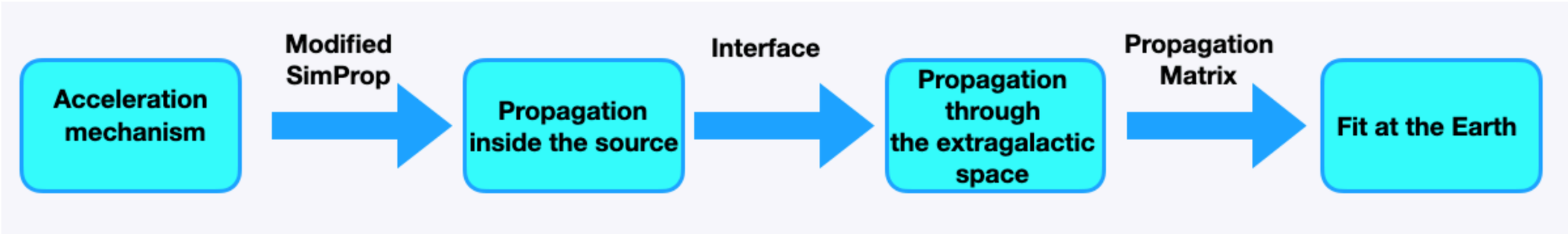

Application to Starburst Galaxies

- Motivation: Acceleration & Correlation.
- Benchmark model: M82.
- Leaky box model: computation of interaction and escape times.

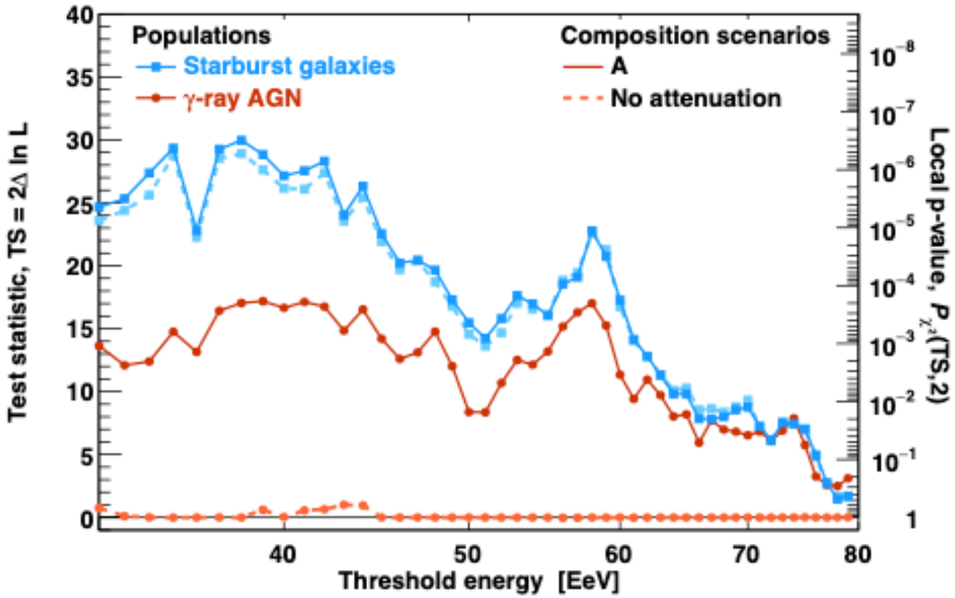

G. E. Romero, A. L. Müller and M. Roth, Astron. Astrophys. 616 (2018), A57
L. A. Anchordoqui, Phys. Rev. D **97** (2018) no.6, 063010

A Aab et al. [Pierre Auger], Astrophys. J. Lett. 853 (2018) no.2, L29

Photo-interaction time

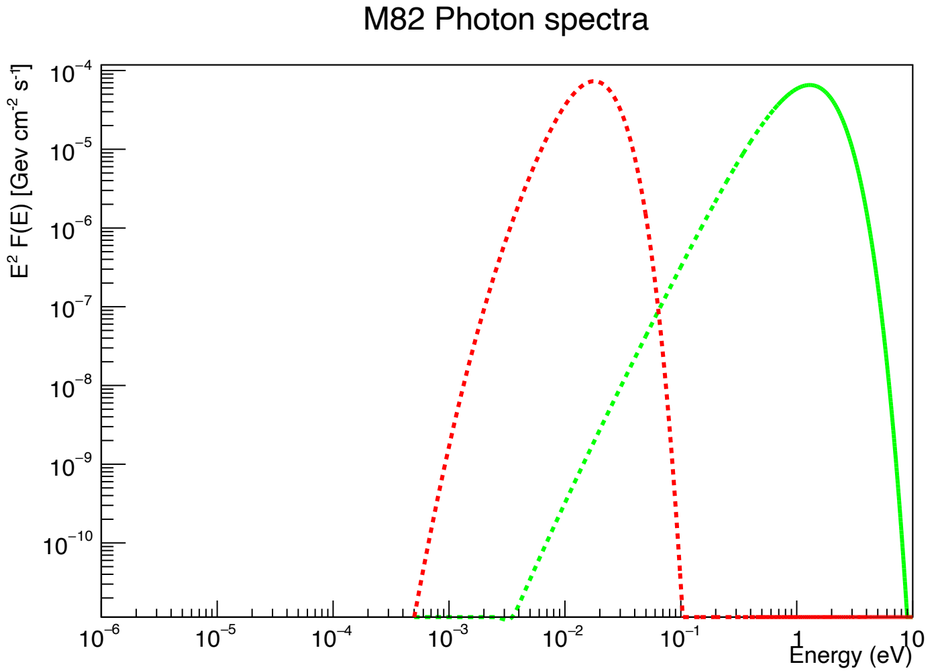

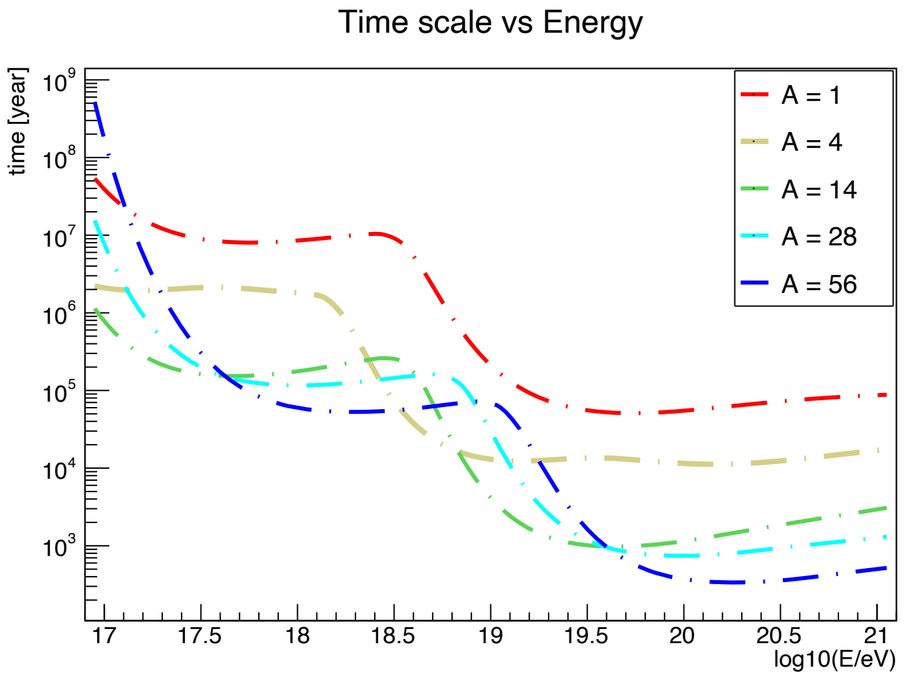

$$\frac{1}{\tau} = \frac{1}{2\Gamma^2} \int_{\epsilon'_{\min}}^{2\Gamma\epsilon} \int_{\epsilon=0}^{+\infty} \frac{n_\gamma(\epsilon)}{\epsilon^2} \, \mathrm{d}\epsilon \, \sigma(\epsilon') \epsilon' \, \mathrm{d}\epsilon'$$

E. Peretti et al. Mon. Not. Roy. Astron. Soc. 487 (2019) no.1, 168-180

Escape time

Diffusion

$$\tau_D = \frac{R^2}{D}$$

Depends on the magnetic field B , on the coherence lenght l_c and on the strength of the turbulence $\frac{\delta B}{B}$

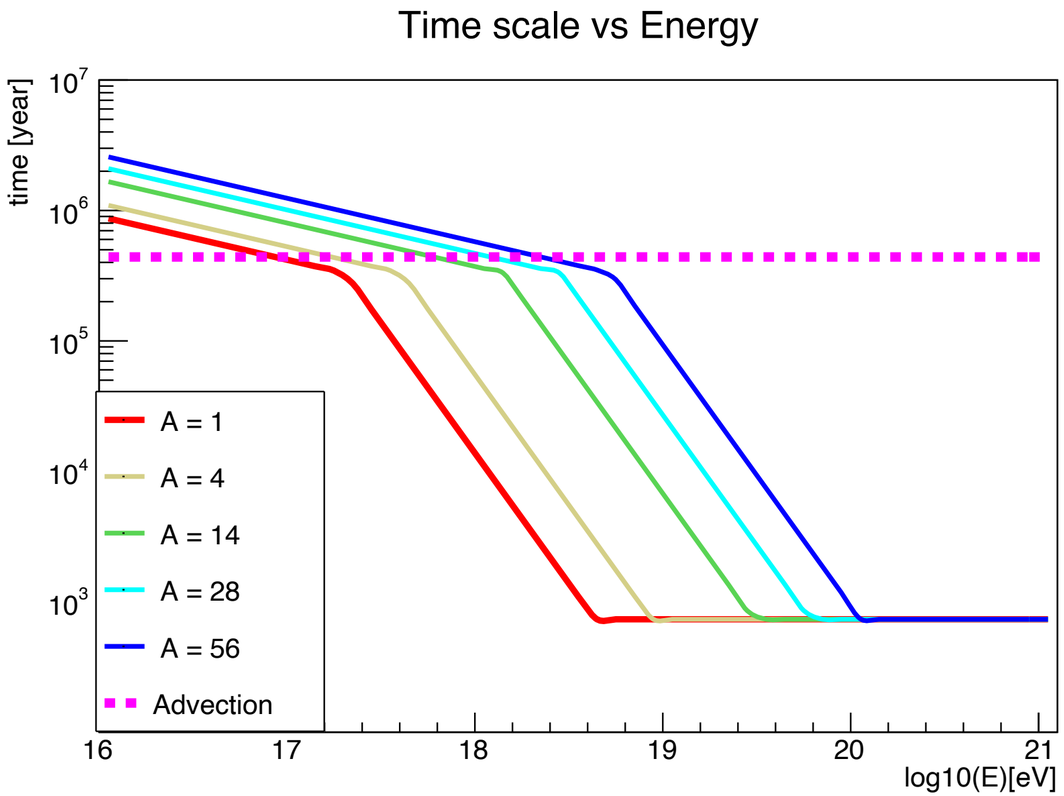

Advection

$$\tau_{\mathrm{adv}} = \frac{R}{v_w}$$

P. Subedi et al, 2017 ApJ 837 140

M82 test

Using the starting prototype a good agreement with respect to data was not found:
M82 configuration does not disintegrate enough injected particles!

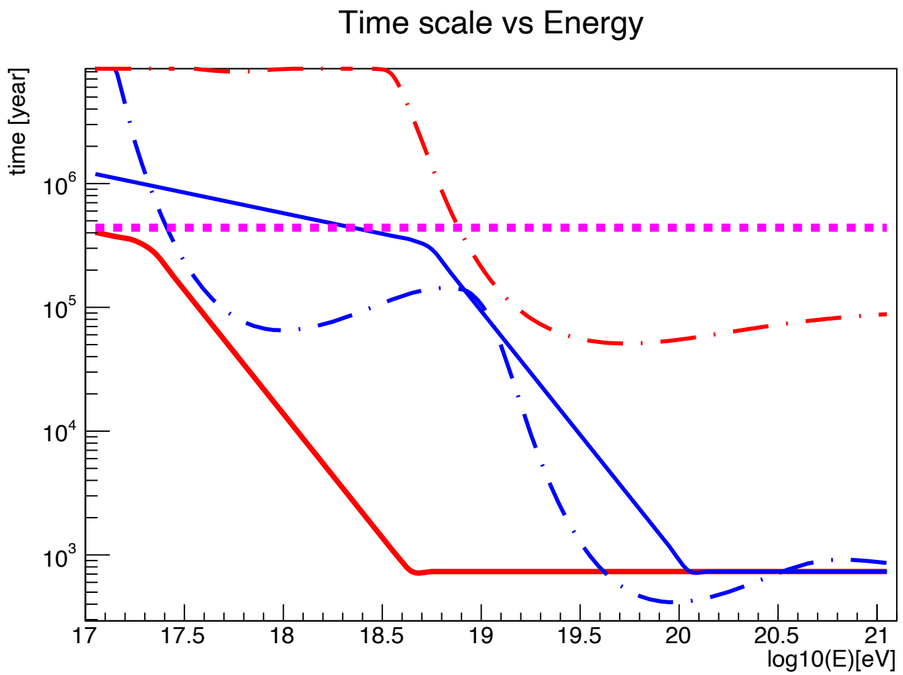

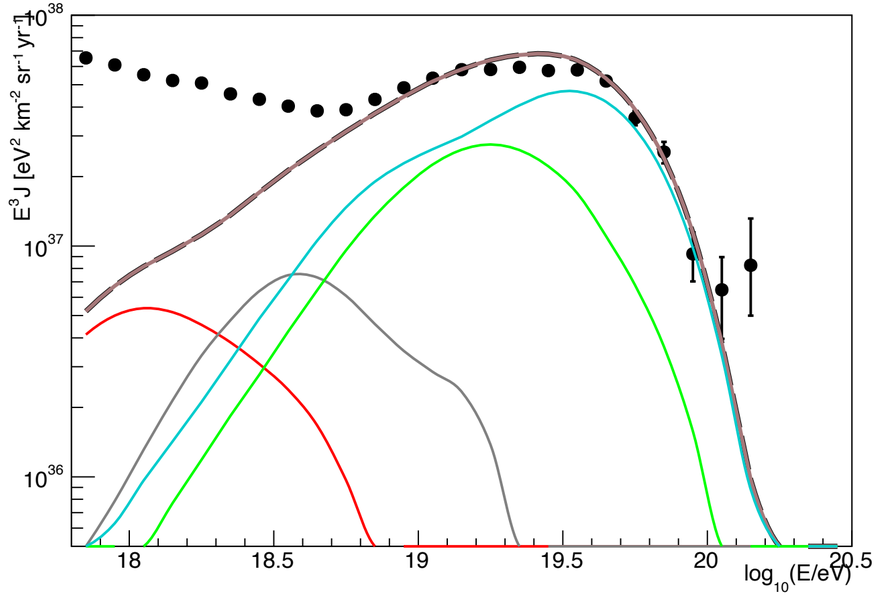

Including hadronic interactions

- The p-p and p-A cross section σ are used to calculate the interaction time
- If a hadronic interaction happens, then the interacting nucleus A is disintegrated in a nucleus $A_{\mathrm{frag}} < A$, producing $A - A_{\mathrm{frag}}$ nucleons.
- For each interaction a certain number of charged pions $N_{\pi^{\pm}}$ are produced according to a flat distribution in rapidity.

σ, A_{frag} and $N_{\pi^{\pm}}$ are obtained using Sibyll 2.3d.

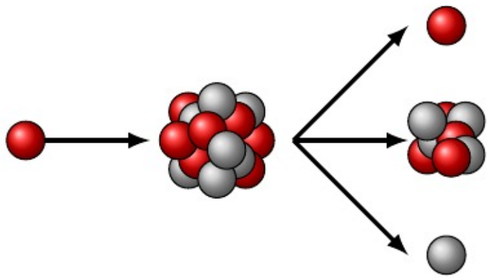

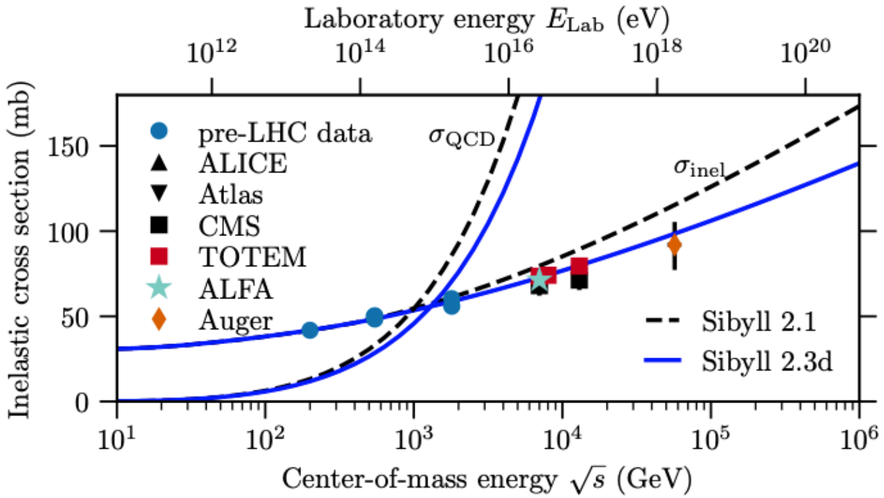

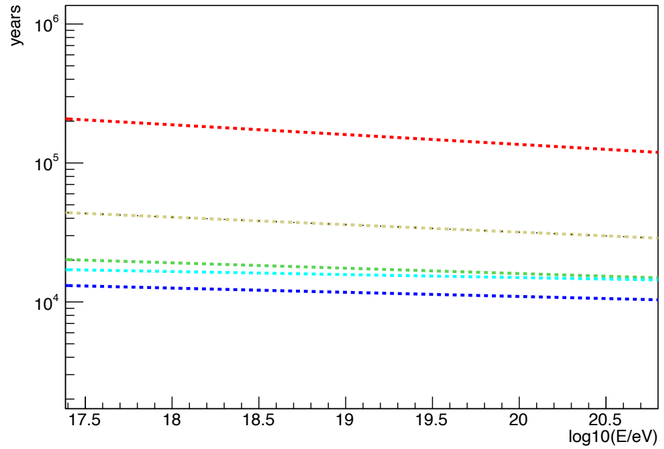

Varying the parameter space

Parameter	Space Parameter	
Radius of SBN	$\in [150,300]$ pc	Internal parameter of the SBGs
Density of ISM	$\in [125,12500]$ p/cm^3	
Luminosity of IR photon field	$\in [44,46]$ $\log(L/(erg/s))$	
Mass at the injection	$\in [1,56]$	Accelerator features
Spectral index	$\in [1,2]$	
Rigidity cutoff	$\in [18,19]$	
Evolution of the sources	Flat, SFR	Distribution of sources and Extra-galactic propagation
Photodisintegration cross section	Talys, PSB	
EBL model	Gilmore, Dominguez	

The Kennicutt-Schmid Law in Star Forming Galaxies

$$\Sigma_{SFR} = A\,\Sigma_{gas}^{N}$$

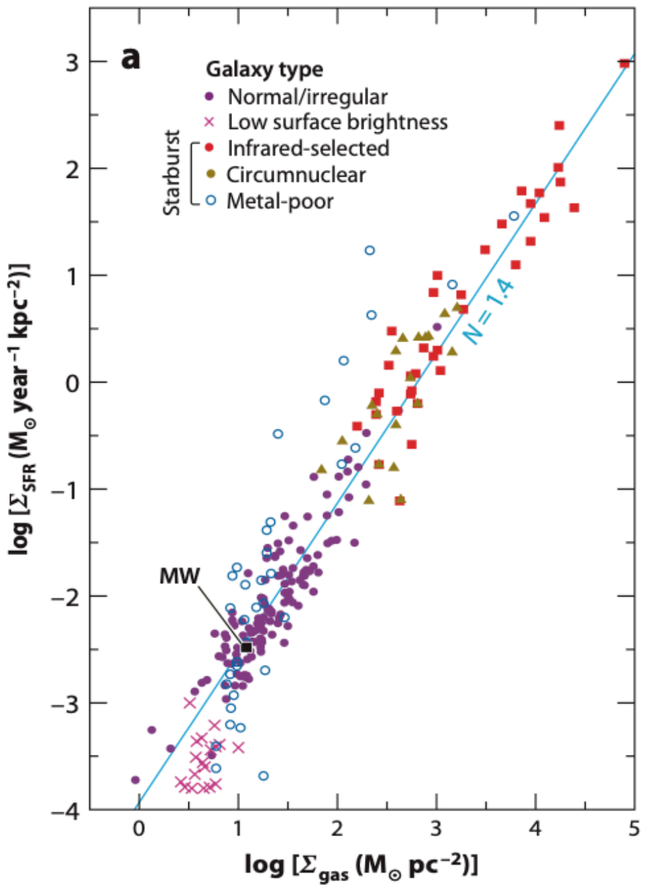

$$\dot{M}_*[\mathrm{M}_\odot\,\mathrm{yr}^{-1}] = 1.7\times10^{-10}\epsilon\,L_{\mathrm{IR}}[\mathrm{L}_\odot],$$

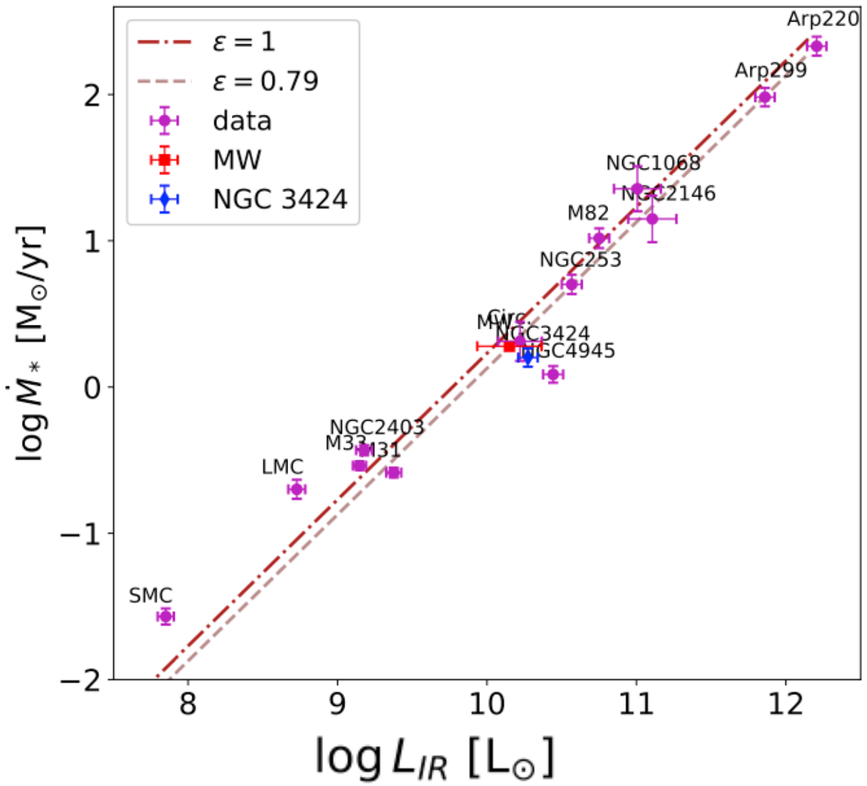

R. C. Kennicutt, Jr., Astrophys. J. 498 (1998), 541

P. Kornecki et al, A. & A., 641 (Sept. 2020), A14

Comparison to the experimental data

- A single nuclear specie (A = 28) is propagated inside the source. Sources are considered identical and distributed up to a maximum redshift.

- The escaping fluxes from sources are propagated through the Universe and compared to the experimental data.

- The chosen prototype is not able to describe the data at Earth;

- Within the parameter space, a set of parameters at the source that can describe energy spectrum and composition at Earth was found.

Comparison to the experimental data

- A single nuclear specie (A = 28) is propagated inside the source. Sources are considered identical and distributed up to a maximum redshift.
- The escaping fluxes from sources are propagated through the Universe and compared to the experimental data.
- The chosen prototype is not able to describe the data at Earth;
- Within the parameter space, a set of parameters at the source that can describe energy spectrum and composition at Earth was found.

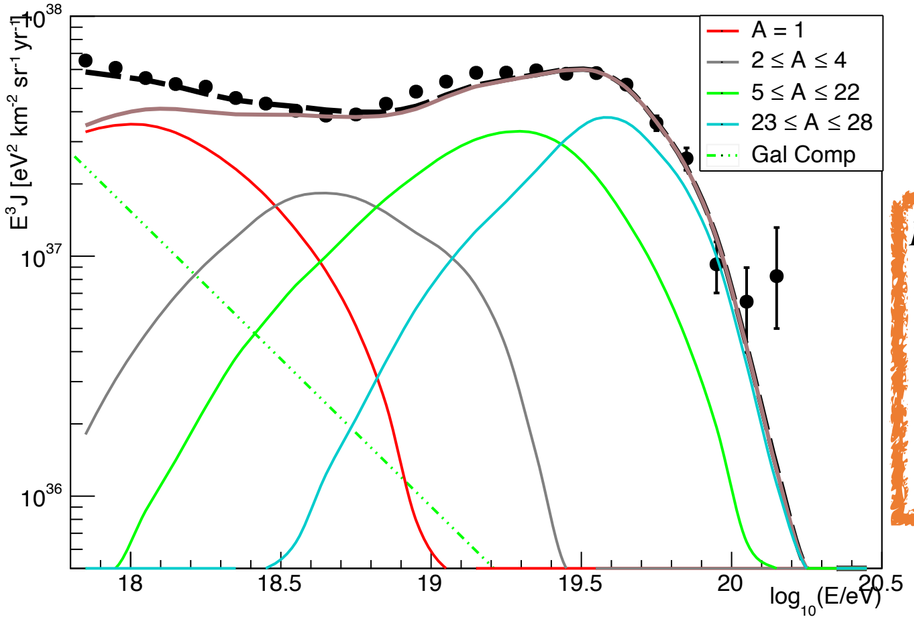

$L_{IR} = 3.46 \cdot 10^{45} \mathrm{erg/s}$

$R = 225\ \mathrm{pc}$

$n_{\mathrm{ISM}} = 1875\ \mathrm{cm}^{-3}$

$\gamma^* = 1$

$\log_{10}(R^*_{\mathrm{cut}}/V) = 18.5$

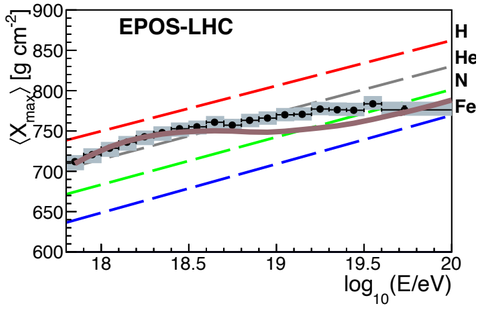

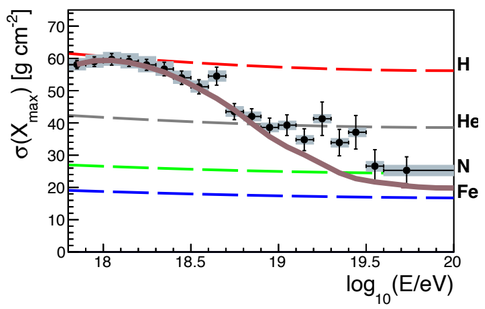

* assuming an injection shape $\frac{dN}{dE} \propto E^{-\gamma} \cdot f(E, Z \cdot R_{\mathrm{cut}})$

Associated neutrino fluxes

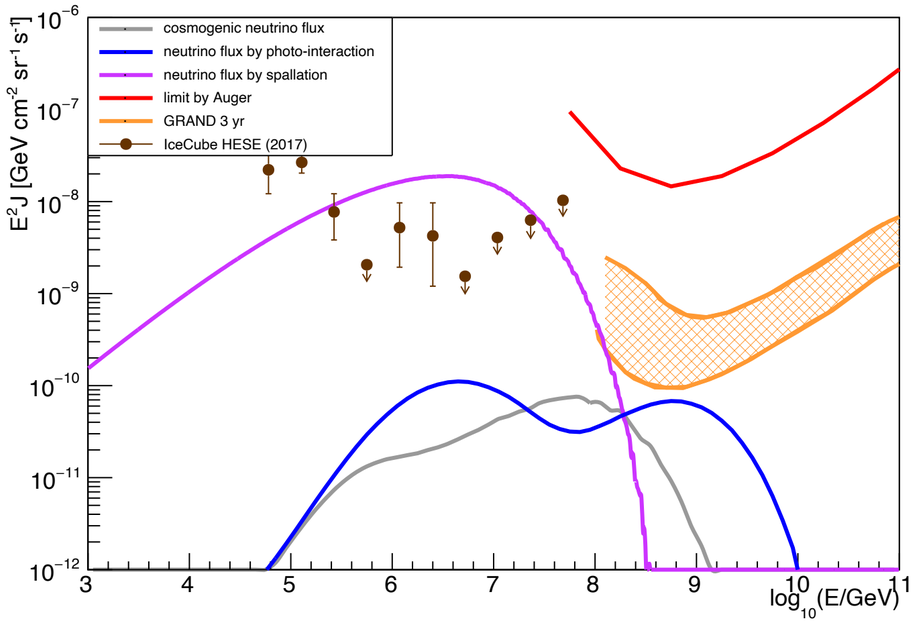

- In this configuration cosmogenic neutrinos are comparable to photo-interaction neutrinos produced in the source.

- Once taken into account also the hadronic interactions, the expected neutrino flux is larger and can be used to constrain plausible scenarios that describe the UHECR data.

Associated neutrino fluxes

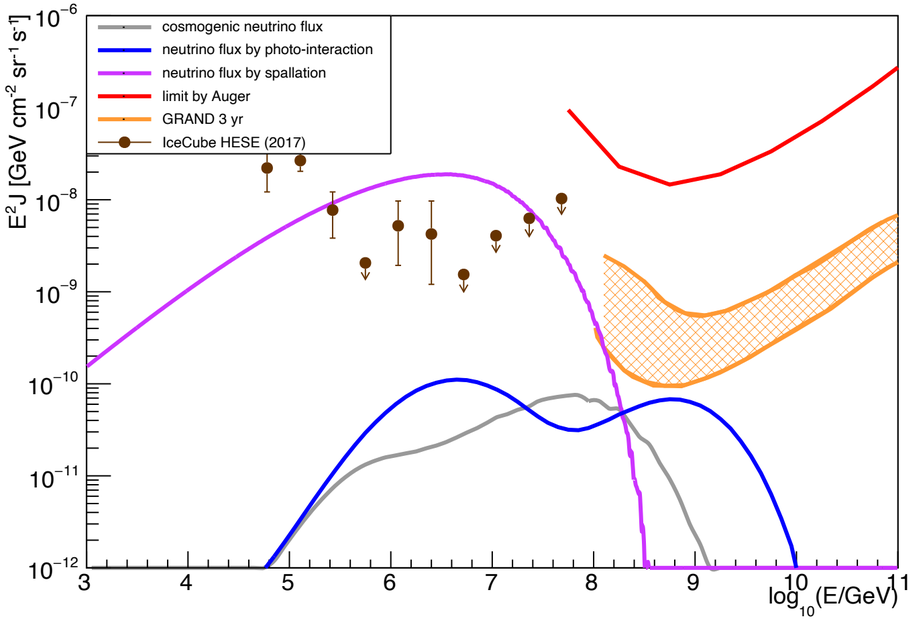

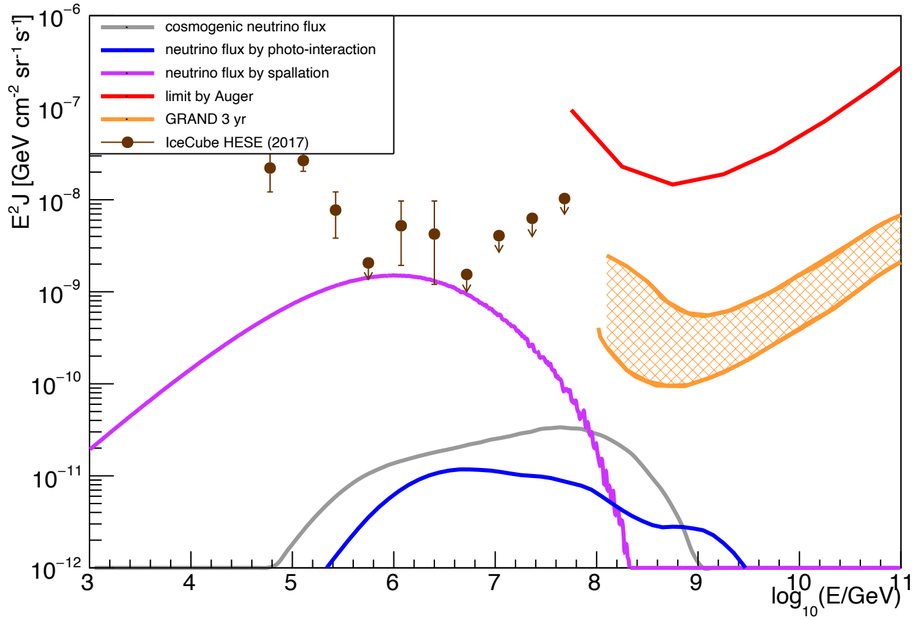

- Decreasing the luminosity, the neutrino fluxes from source decrease ;
- A detailed study of the parameter space is foreseen.

Cross-check on the number of sources

$$n_{\mathrm{SBG}} = \frac{\varepsilon_{\mathrm{CR}}}{\alpha \cdot L_{\mathrm{IR}}} = 1.8 \cdot 10^{-6} \left[\frac{\alpha}{0.1}\right]^{-1} \mathrm{Mpc}^{-3}$$

From the comparison to the data

Cross-check on the number of sources

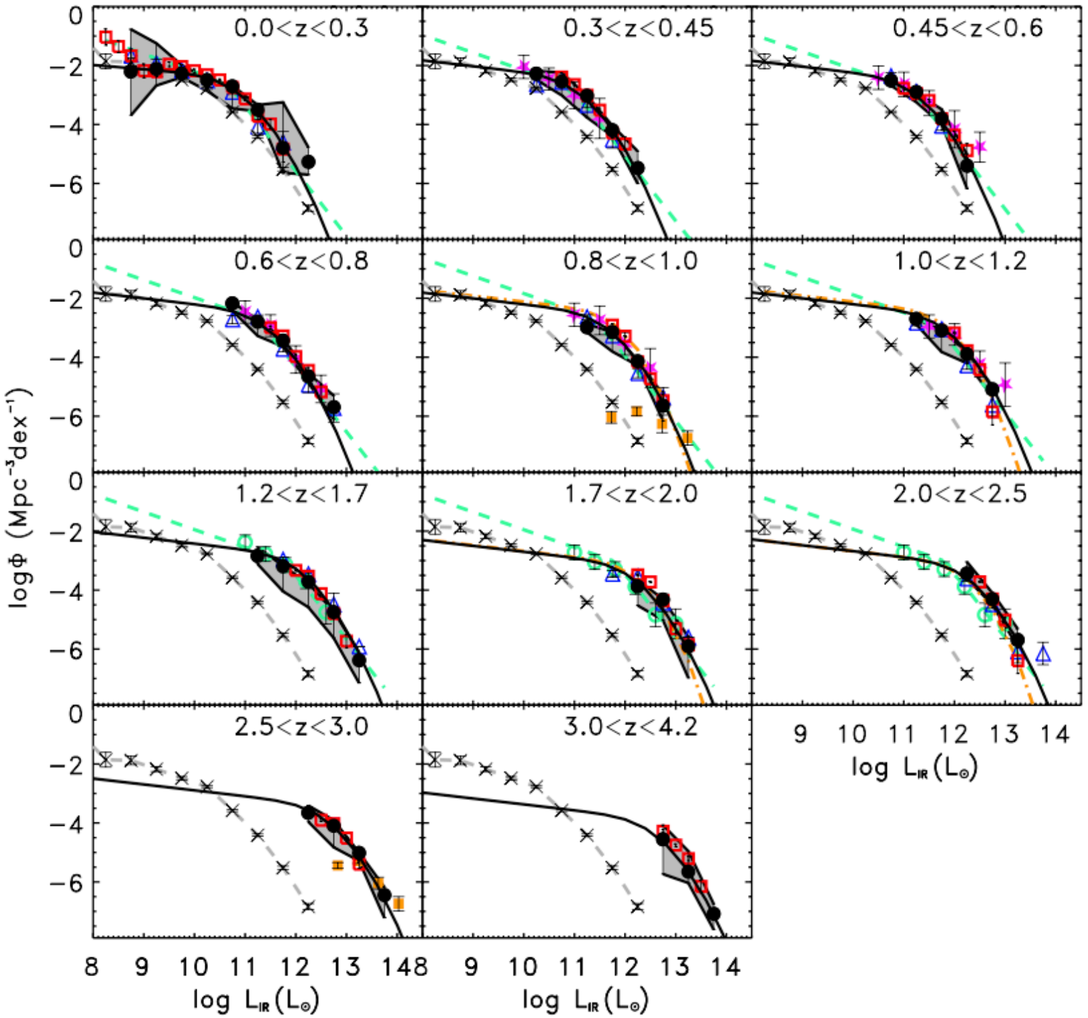

$$n_{\rm SBG} = \frac{\varepsilon_{\rm CR}}{\alpha \cdot L_{\rm IR}} = 1.8 \cdot 10^{-6} \left[\frac{\alpha}{0.1}\right]^{-1} \ {\rm Mpc}^{-3}$$

From the comparison to the data

Using the luminosity functions

$$n_{\rm SBG} \simeq 3 \cdot 10^{-5} \ {\rm Mpc}^{-3}$$

G. Gruppioni et al,
DOI: https://doi.org/10.1093/mnras/stt308

Summary and future perspectives

Combined fit above the ankle

- ☑ Re-organization the combined fit code;
- ☑ Updating to new datasets;
- ☑ Including over-density correction;
- ☑ A hard injection spectrum and low rigidity cutoff is required.
- ☑ The composition at sources is dominated by light and intermediate-mass elements.

Extended combined fit

- ☑ Extension of the combined fit below the ankle using two components;
- ☑ Take into account the end of the Galactic spectrum.
- ☑ Hard injection spectrum at high energies vs soft injection at low energies.
- ☑ Intermediate nuclei required at low energies.
- ☑ Iron Galactic flux strongly disfavored.

Summary and future perspectives

Source-propagation model

- ☑ Source-propagation model in a generic source: UFA model (introducing a generic photon field in SimProp);
- ☑ Source-propagation model in a Starburst Galaxy : M82;
- ☑ Introducing hadronic interaction in SimProp;
- ☑ Exploring the parameter space in order to describe both the energy spectrum and composition;
- ☑ Cosmogenic and source neutrino fluxes for each configuration;
- ☑ Cross-check using luminosity functions.

Future perspectives

- ☐ Using arrival direction information;
- ☐ Including photons propagation in SimProp;
- ☐ Application to other candidates.

GRAN SASSO
SCIENCE INSTITUTE

THANKS FOR YOU ATTENTION!

Antonio Condorelli

antonio.condorelli@gssi.it
https://www.gssi.it/people/students/students-physics/item/2054-condorelli-antonio

www.gssi.it

Cap 1 & 2

Cap 1: Distance of UHECRs

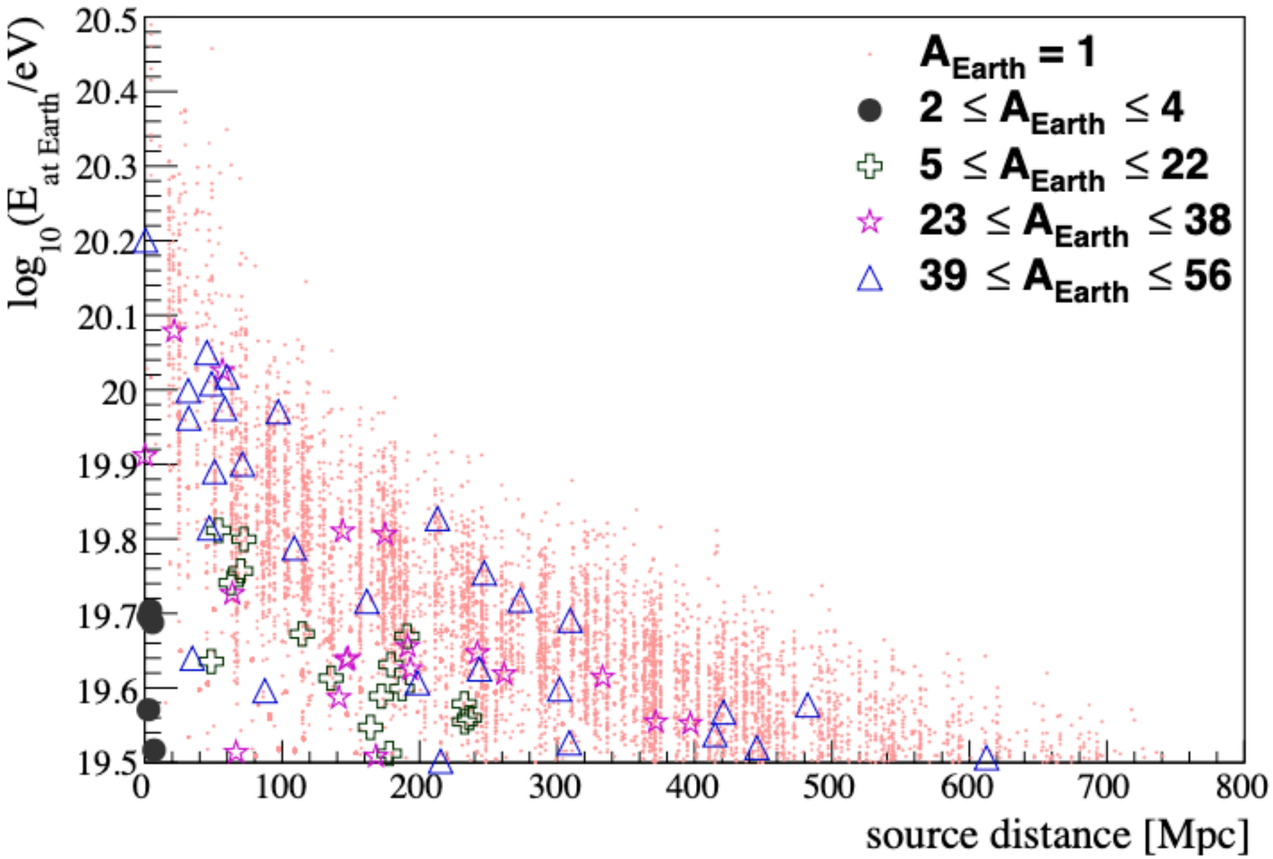

Interactions

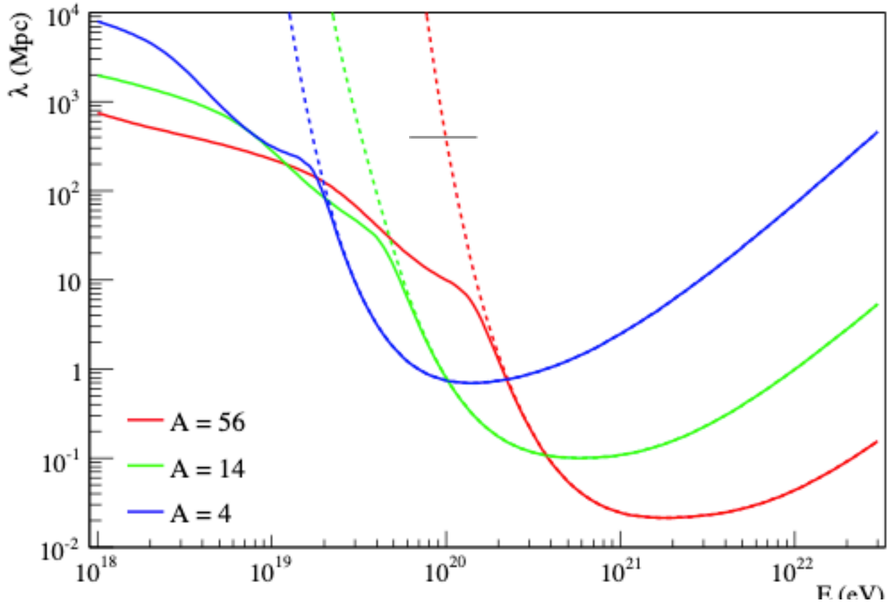

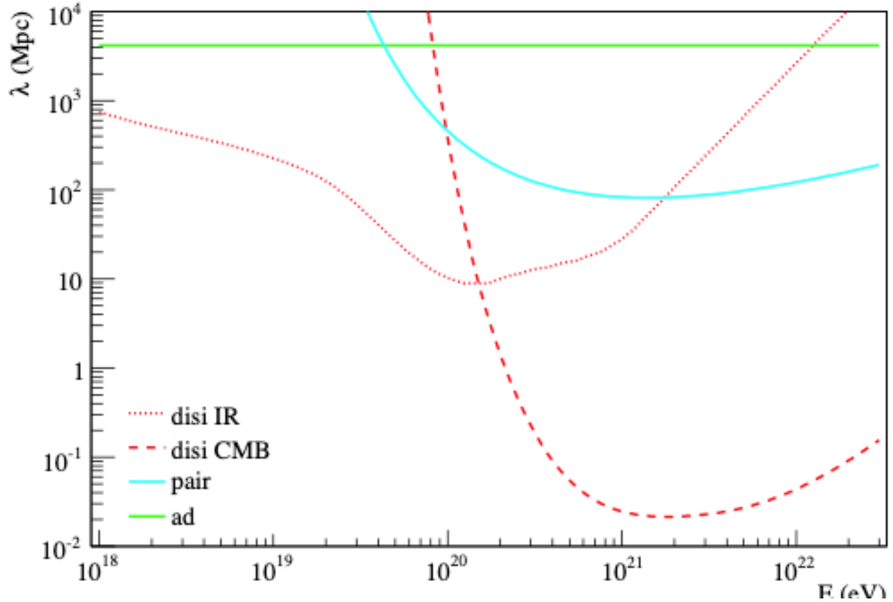

pair production energy threshold: 1 MeV and monotonically decrease (scale as Z^2/A)

Photodisintegration 8 MeV

Photopion 145 MeV —-> E/A matters

$$\beta_{ad}(A,Z) = -\frac{1}{E}\frac{dE}{dz}\left(\frac{dt}{dz}\right)^{-1} = H_0\sqrt{(1+z)^3\Omega_m + \Omega_\Lambda} = H(z)$$

As a consequence of the expansion of the Universe, relativistic particles are observed today with an energy E(z = 0) redshifted with respect to the initial one E(z) according to E(0) = E(z)(1+z) ^{-1}
Dominant at low energy (10^{18})

Detail of the detectors

ICRC 2013

Systematic uncertainty in the energy scale	
Fluorescence yield	3.6%
Atmosphere	3.4% – 6.2%
FD calibration	9.9%
FD profile recon.	6.5% – 5.6%
Invisible energy	3% – 1.5%
Stability of energy scale	5%
TOTAL	14%

SD events

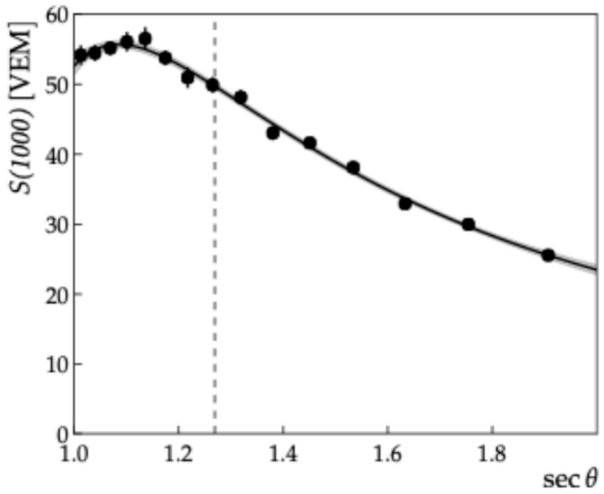

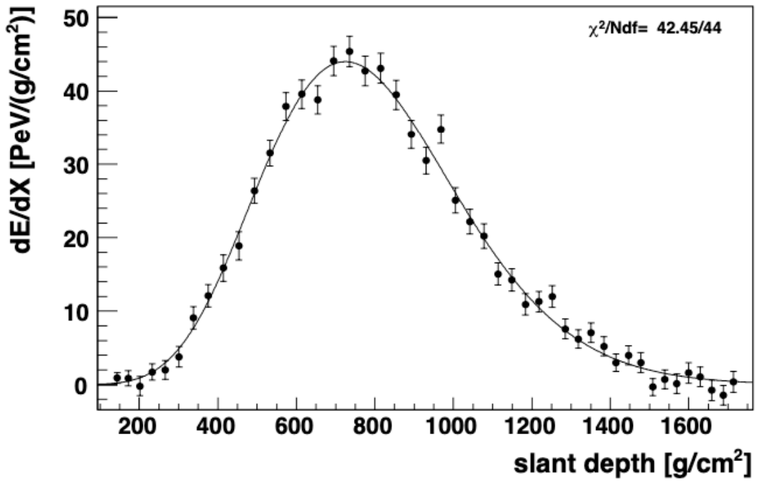

Evolution of the shower front

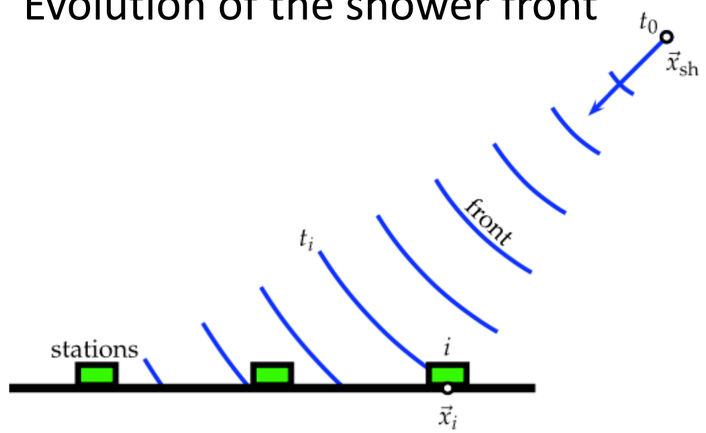

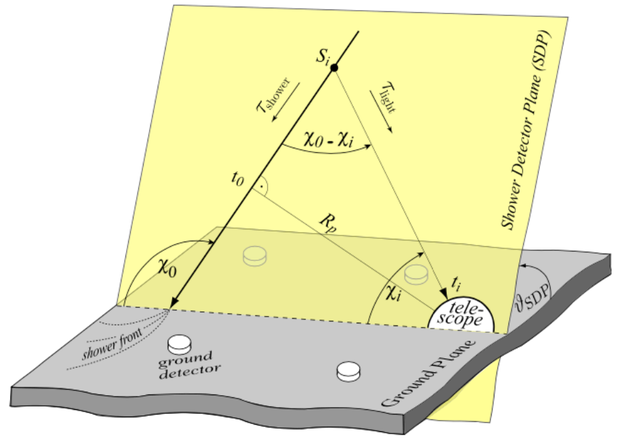

What is the instep?

$$J(E;\mathbf{s}) = J_0 \left(\frac{E}{E_0}\right)^{-\gamma_1} \left[1 + \left(\frac{E}{E_{12}}\right)^{\frac{1}{\omega_{12}}}\right]^{(\gamma_1-\gamma_2)\omega_{12}} \times \frac{1}{1+(E/E_s)^{\Delta\gamma}}.$$

Old—> 6 fitted parameters!

$$J(E;\mathbf{s}) = J_0 \left(\frac{E}{E_0}\right)^{-\gamma_1} \prod_{i=1}^{3} \left[1 + \left(\frac{E}{E_{ij}}\right)^{\frac{1}{\omega_{ij}}}\right]^{(\gamma_i-\gamma_j)\omega_{ij}}$$

New-> 8 fitted parameters! (4 spectral indexes, 3 transition energies and a normalization)

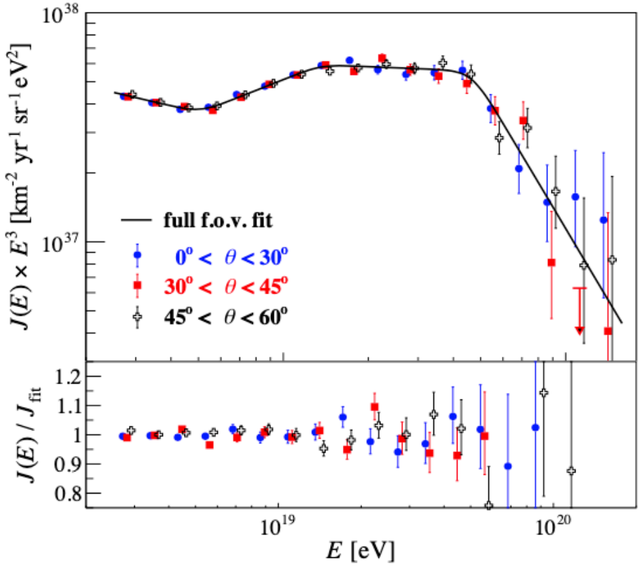

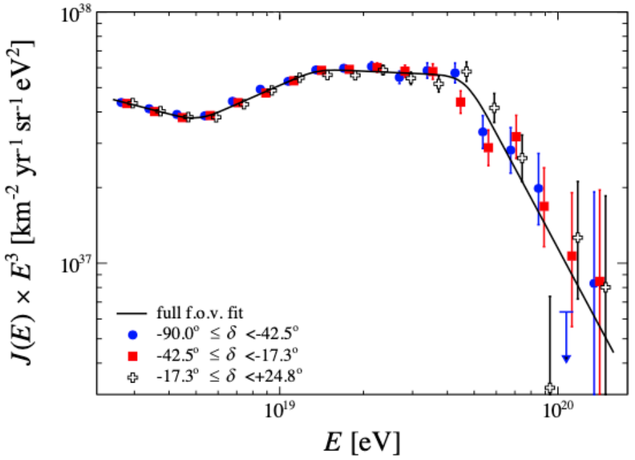

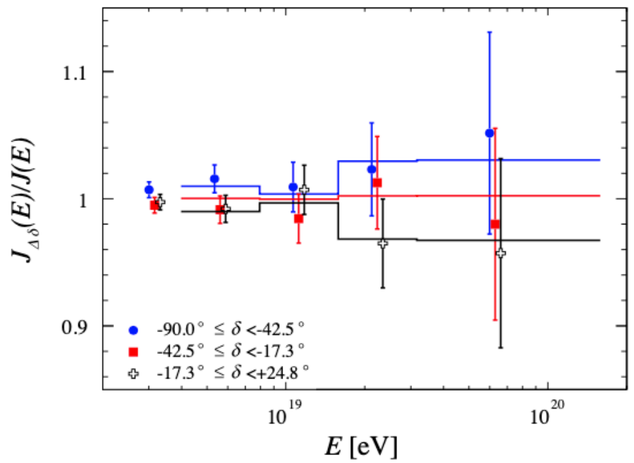

64

What is the instep?

Cosmic ray flux (isotropic, spectral flux)

$$\phi(E) = \frac{\mathrm{d}N}{\mathrm{d}E\,\mathrm{d}A\,\mathrm{d}t\,\mathrm{d}\Omega}$$

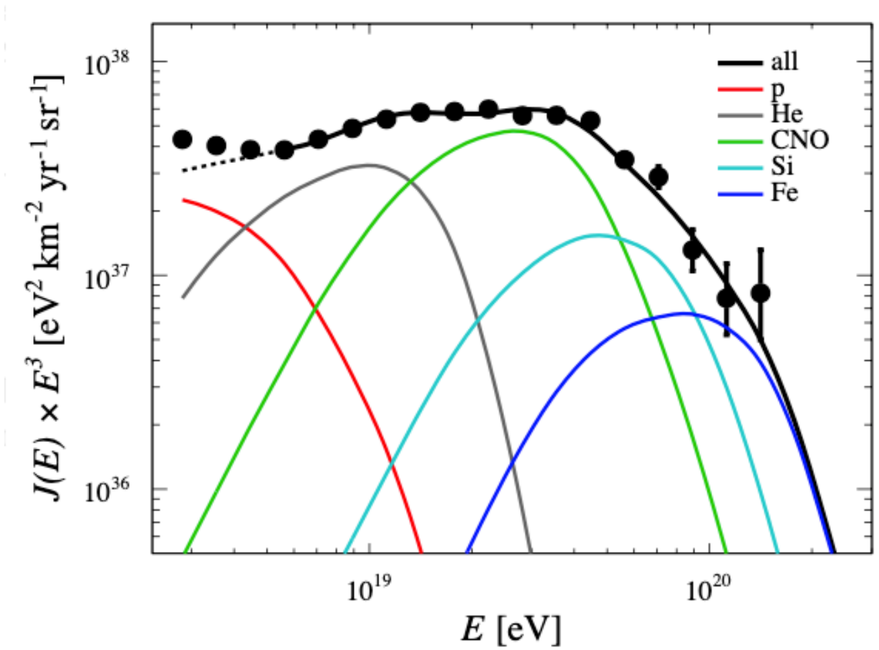

Spectral particle number density (differential in energy)

$$n(E, \vec{x}) = \frac{\mathrm{d}N}{\mathrm{d}E\,\mathrm{d}^3x} = \frac{4\pi}{\beta c}\,\phi(E)$$

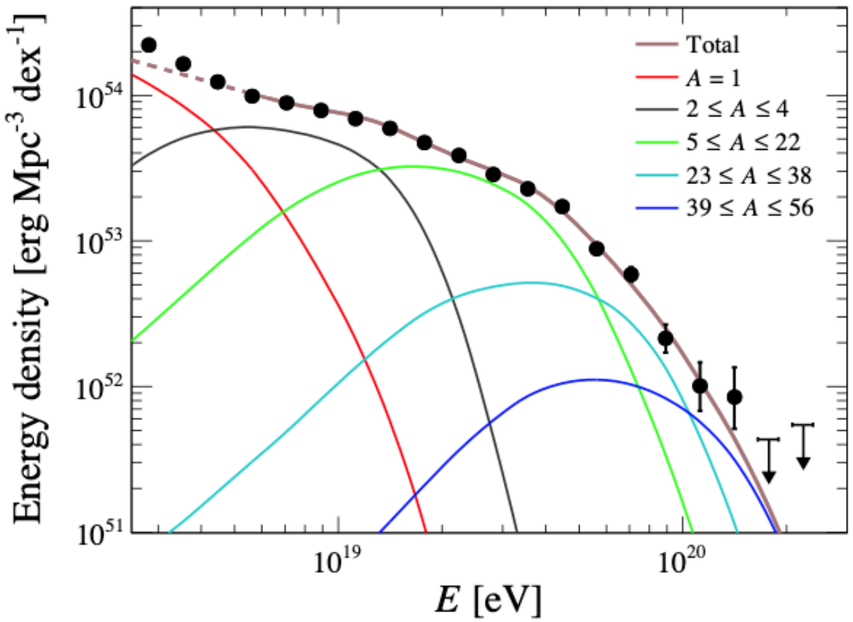

Large scale anisotropies

Rayleigh analysis in right ascension

$$a_\alpha = \frac{2}{\mathcal{N}} \sum_{i=1}^{N} w_i \cos \alpha_i, \qquad b_\alpha = \frac{2}{\mathcal{N}} \sum_{i=1}^{N} w_i \sin \alpha_i.$$

Fourier transform: classical approach to study the large-scale anisotropies in the arrival directions of cosmic rays

The amplitude r_α and phase φ_α of the first harmonic of the modulation are obtained from

$$r_\alpha = \sqrt{a_\alpha^2 + b_\alpha^2}, \qquad \tan \varphi_\alpha = \frac{b_\alpha}{a_\alpha}.$$

Energy [EeV]	**Number of events**	**Fourier coefficient a_α**	**Fourier coefficient b_α**	**Amplitude r_α**	**Phase φ_α [°]**	**Probability $P(\geq r_\alpha)$**
4 to 8	81,701	0.001 ± 0.005	0.005 ± 0.005	$0.005^{+0.006}_{-0.002}$	80 ± 60	0.60
≥ 8	32,187	-0.008 ± 0.008	0.046 ± 0.008	$0.047^{+0.008}_{-0.007}$	100 ± 10	2.6×10^{-8}

Intermediate scale anisotropies

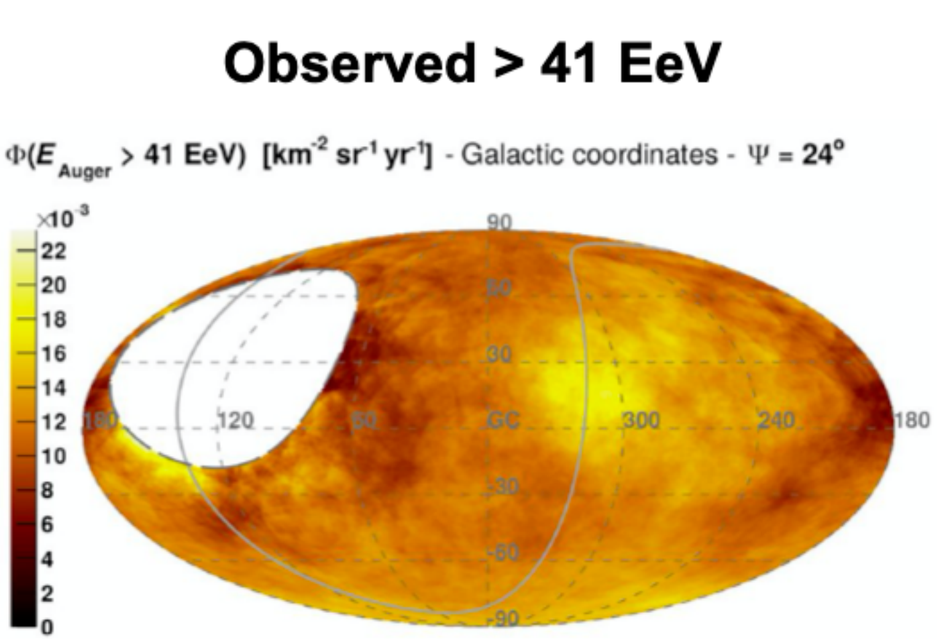

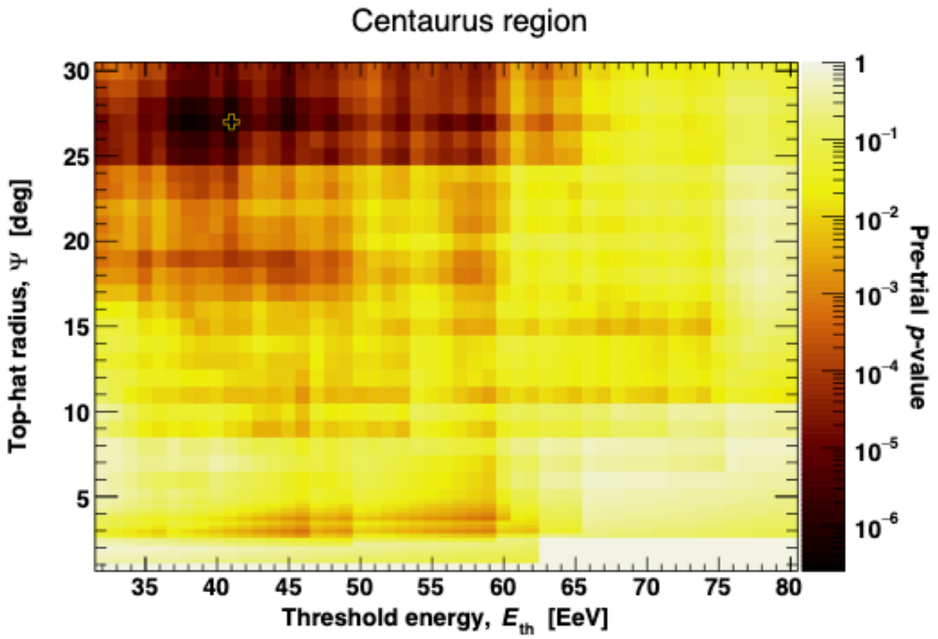

The number of events, N_{observed}, above an energy threshold E_{th} within a disc of radius Ψ centered on equatorial coordinates

(R.A.,Dec.) is compared with that expected, N_{expected}, from an isotropic distribution of arrival directions accounting for the geometric exposure of the Observatory.

The search is performed over a grid, by threshold steps of 1 EeV between 32 and 80 EeV, by radial steps of 1° between 1° and 30°, and on a directional grid of 1° spacing, a value which corresponds to the angular resolution of the Observatory at the energies of interest

A Aab et al. [Pierre Auger], Astrophys. J. Lett. 853 (2018) no.2, L29

Intermediate scale anisotropies

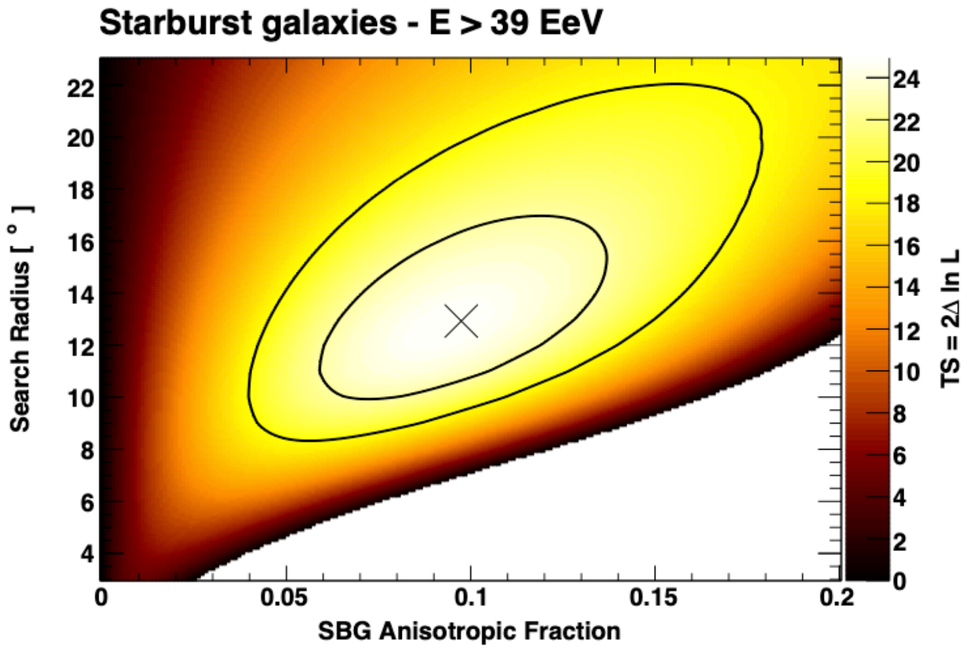

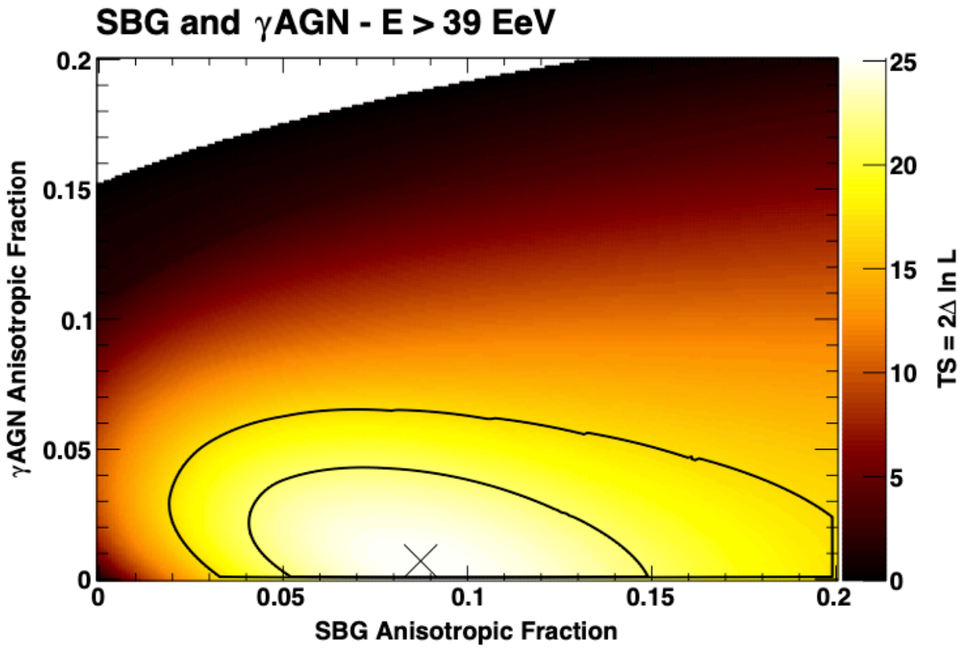

Test hypothesis	Null hypothesis	Threshold energy[a]	TS	Local p-value $\mathcal{P}_{\chi^2}(\mathrm{TS},2)$	Post-trial p-value	1-sided significance	AGN/other fraction	SBG fraction	Search radius
SBG + ISO	ISO	39 EeV	24.9	3.8×10^{-6}	3.6×10^{-5}	$4.0\,\sigma$	N/A	9.7 %	12.9°
γAGN + SBG + ISO	γAGN + ISO	39 EeV	14.7	N/A	1.3×10^{-4}	$3.7\,\sigma$	0.7 %	8.7 %	12.5°
γAGN + ISO	ISO	60 EeV	15.2	5.1×10^{-4}	3.1×10^{-3}	$2.7\,\sigma$	6.7 %	N/A	6.9°
γAGN + SBG + ISO	SBG + ISO	60 EeV	3.0	N/A	0.08	$1.4\,\sigma$	6.8 %	0.0 %[b]	7.0°
Swift-BAT + ISO	ISO	39 EeV	18.2	1.1×10^{-4}	8.0×10^{-4}	$3.2\,\sigma$	6.9 %	N/A	12.3°
Swift-BAT + SBG + ISO	*Swift*-BAT + ISO	39 EeV	7.8	N/A	5.1×10^{-3}	$2.6\,\sigma$	2.8 %	7.1 %	12.6°
2MRS + ISO	ISO	38 EeV	15.1	5.2×10^{-4}	3.3×10^{-3}	$2.7\,\sigma$	15.8 %	N/A	13.2°
2MRS + SBG + ISO	2MRS + ISO	39 EeV	10.4	N/A	1.3×10^{-3}	$3.0\,\sigma$	1.1 %	8.9 %	12.6°

SBG excess

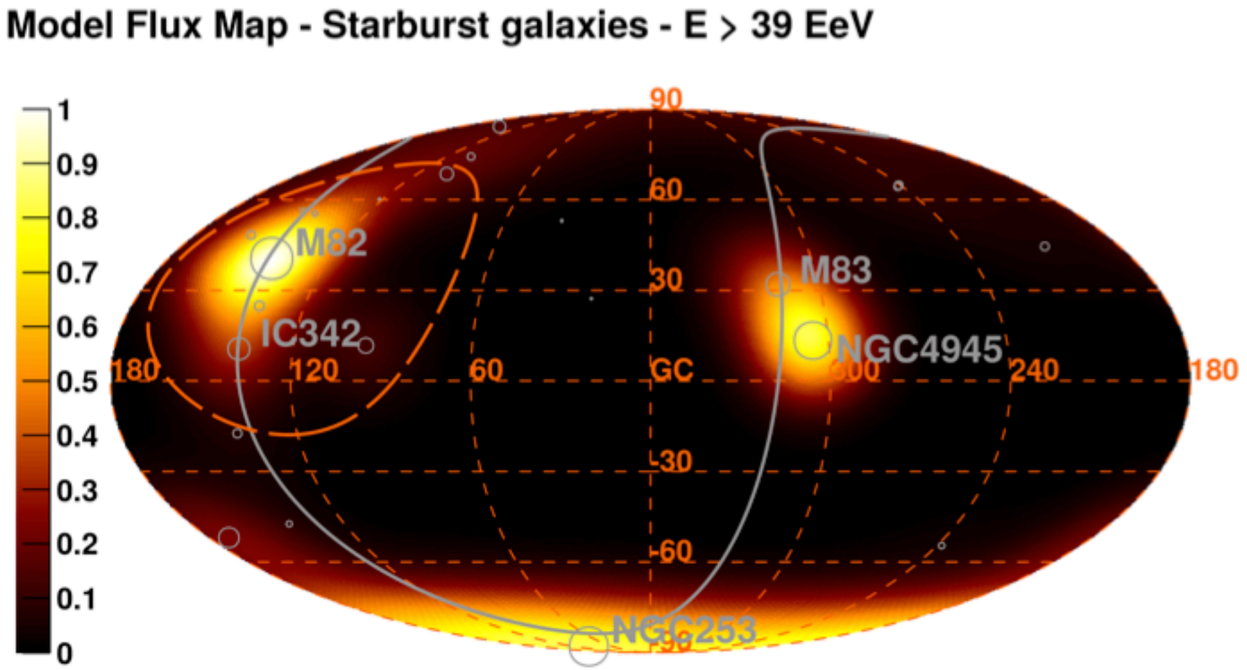

A Aab et al. [Pierre Auger], Astrophys. J. Lett. 853 (2018) no.2, L29

SBG list

SBGs	l [°]	b [°]	Distance[a] [Mpc]	Flux weight [%]	Attenuated weight: A / B / C [%]	% contribution[b]: A / B / C [%]
NGC 253	97.4	-88	2.7	13.6	20.7 / 18.0 / 16.6	35.9 / 32.2 / 30.2
M82	141.4	40.6	3.6	18.6	24.0 / 22.3 / 21.4	0.2 / 0.1 / 0.1
NGC 4945	305.3	13.3	4	16	19.2 / 18.3 / 17.9	39.0 / 38.4 / 38.3
M83	314.6	32	4	6.3	7.6 / 7.2 / 7.1	13.1 / 12.9 / 12.9
IC 342	138.2	10.6	4	5.5	6.6 / 6.3 / 6.1	0.1 / 0.0 / 0.0
NGC 6946	95.7	11.7	5.9	3.4	3.2 / 3.3 / 3.5	0.1 / 0.1 / 0.1
NGC 2903	208.7	44.5	6.6	1.1	0.9 / 1.0 / 1.1	0.6 / 0.7 / 0.7
NGC 5055	106	74.3	7.8	0.9	0.7 / 0.8 / 0.9	0.2 / 0.2 / 0.2
NGC 3628	240.9	64.8	8.1	1.3	1.0 / 1.1 / 1.2	0.8 / 0.9 / 1.1
NGC 3627	242	64.4	8.1	1.1	0.8 / 0.9 / 1.1	0.7 / 0.8 / 0.9
NGC 4631	142.8	84.2	8.7	2.9	2.1 / 2.4 / 2.7	0.8 / 0.9 / 1.1
M51	104.9	68.6	10.3	3.6	2.3 / 2.8 / 3.3	0.3 / 0.4 / 0.5
NGC 891	140.4	-17.4	11	1.7	1.1 / 1.3 / 1.5	0.2 / 0.3 / 0.3
NGC 3556	148.3	56.3	11.4	0.7	0.4 / 0.6 / 0.6	0.0 / 0.0 / 0.0
NGC 660	141.6	-47.4	15	0.9	0.5 / 0.6 / 0.8	0.4 / 0.5 / 0.6
NGC 2146	135.7	24.9	16.3	2.6	1.3 / 1.7 / 2.0	0.0 / 0.0 / 0.0
NGC 3079	157.8	48.4	17.4	2.1	1.0 / 1.4 / 1.5	0.1 / 0.1 / 0.1
NGC 1068	172.1	-51.9	17.9	12.1	5.6 / 7.9 / 9.0	6.4 / 9.4 / 10.9
NGC 1365	238	-54.6	22.3	1.3	0.5 / 0.8 / 0.8	0.9 / 1.5 / 1.6
Arp 299	141.9	55.4	46	1.6	0.4 / 0.7 / 0.6	0.0 / 0.0 / 0.0
Arp 220	36.6	53	80	0.8	0.1 / 0.3 / 0.2	0.0 / 0.2 / 0.1
NGC 6240	20.7	27.3	105	1	0.1 / 0.3 / 0.1	0.1 / 0.3 / 0.1

Could we have information about Galactic component at low energies

COSMIC-RAY ANISOTROPIES IN RIGHT ASCENSION MEASURED BY THE PIERRE AUGER OBSERVATORY

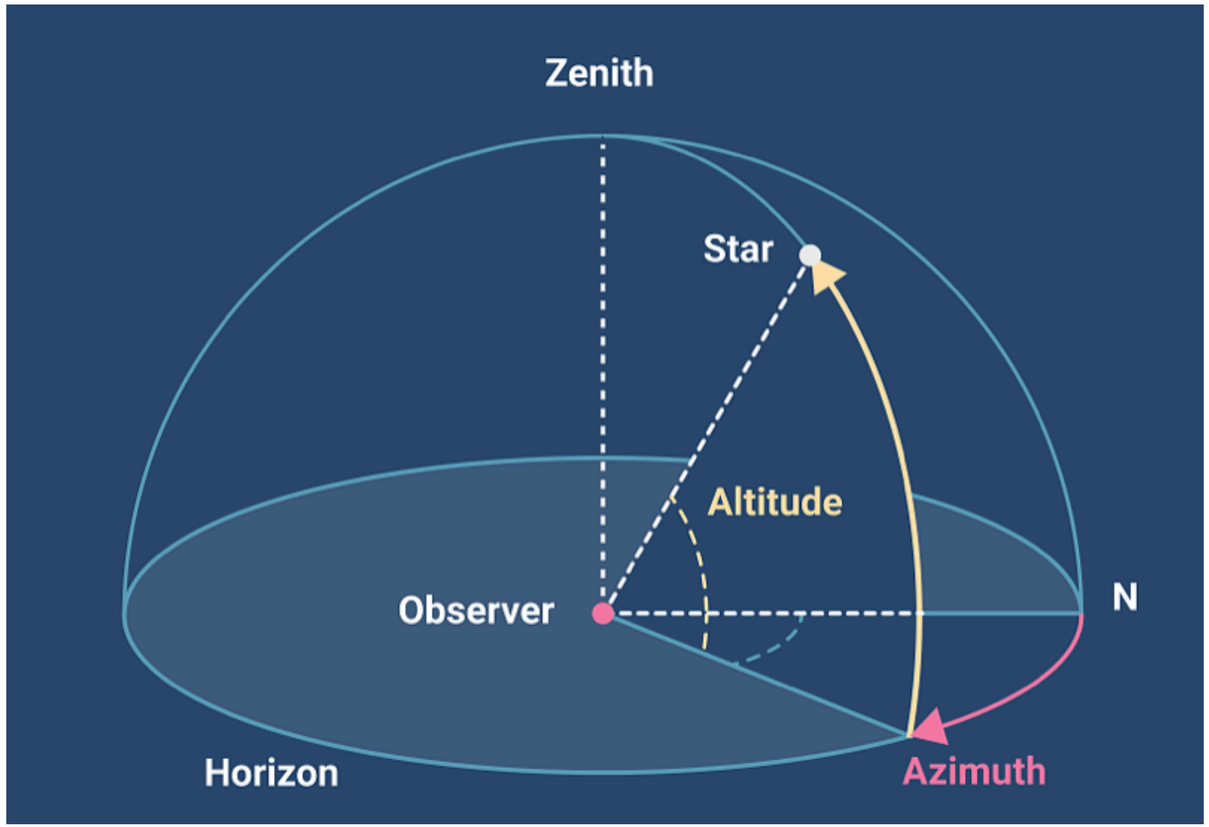

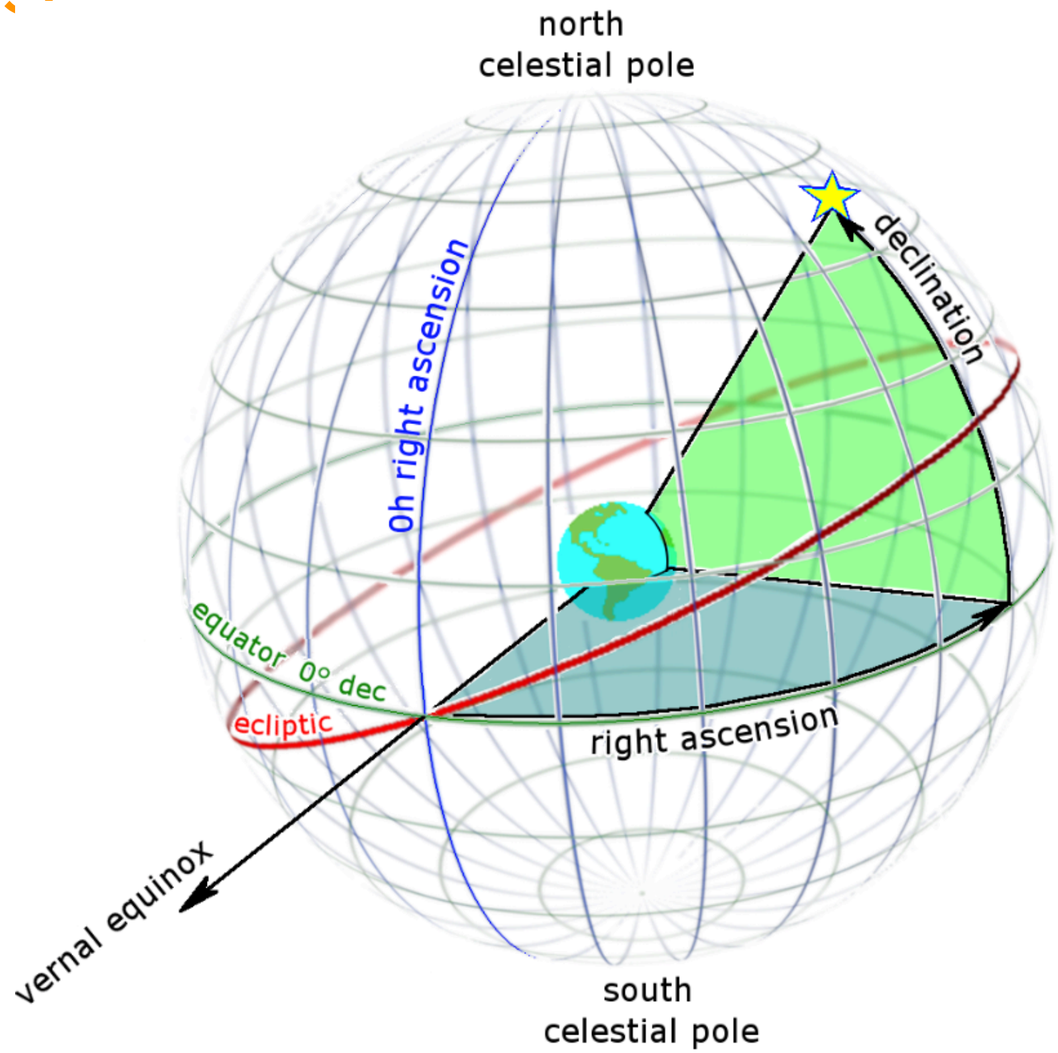

Cap 3

Modification factor

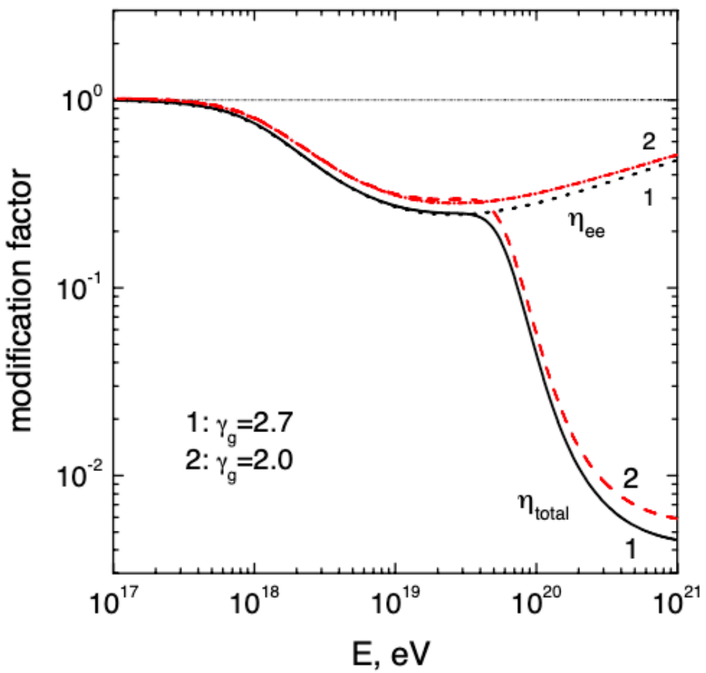

Only adiabatic energy loss

Then adiabatic + ee (η_{ee})

then also photopion production (η_{total})

$$\eta_{\rm p}(E) = \frac{J_{\rm p}(E)}{J_{\rm p}^{\rm unm}(E)}.$$

The formalism of the *modification factor* η_p in is commonly used to put in evidence the signatures of the energy losses suffered.by protons. It is defined as the ratio of the spectrum $J_p(E)$, where all the energy losses are included, to the so-called unmodified spectrum J_{unm}, where only adiabatic p energy losses are taken into account:

Modification factor

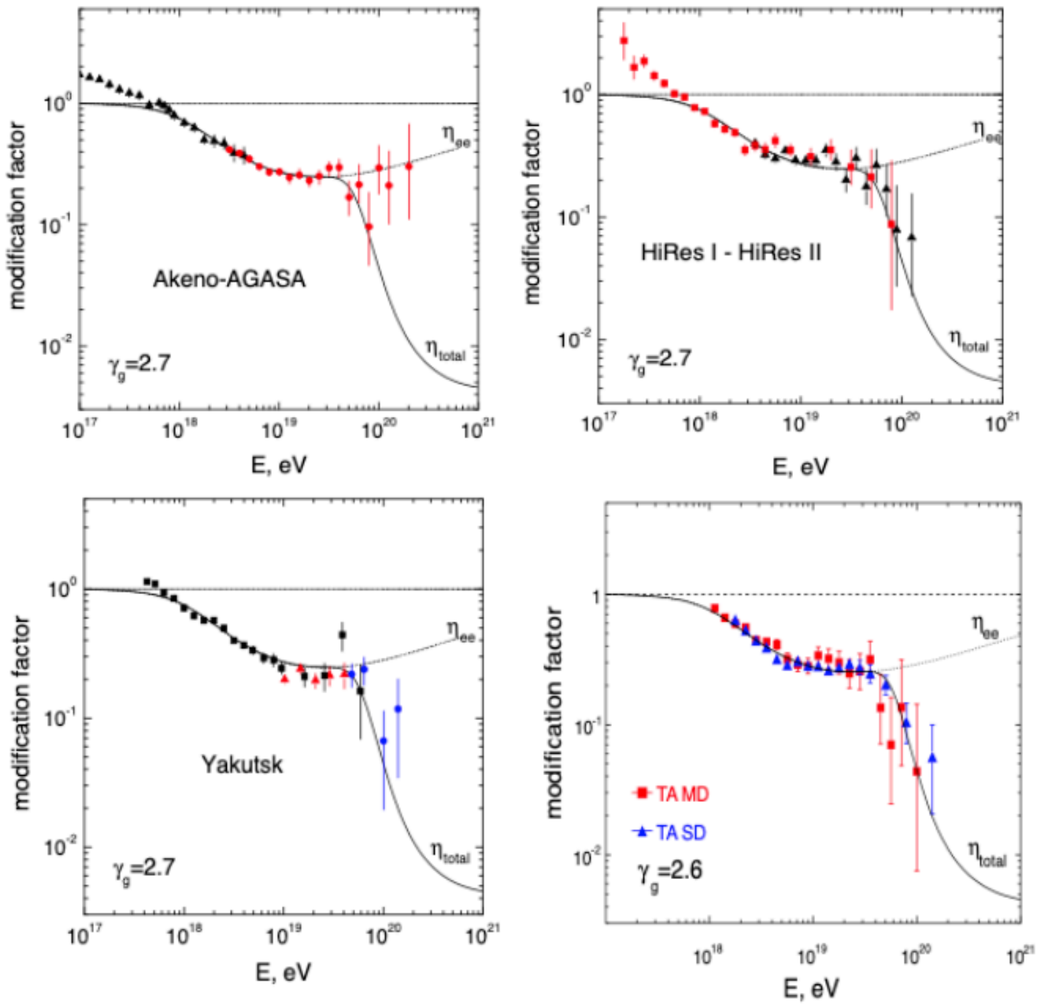

Negative spectral index

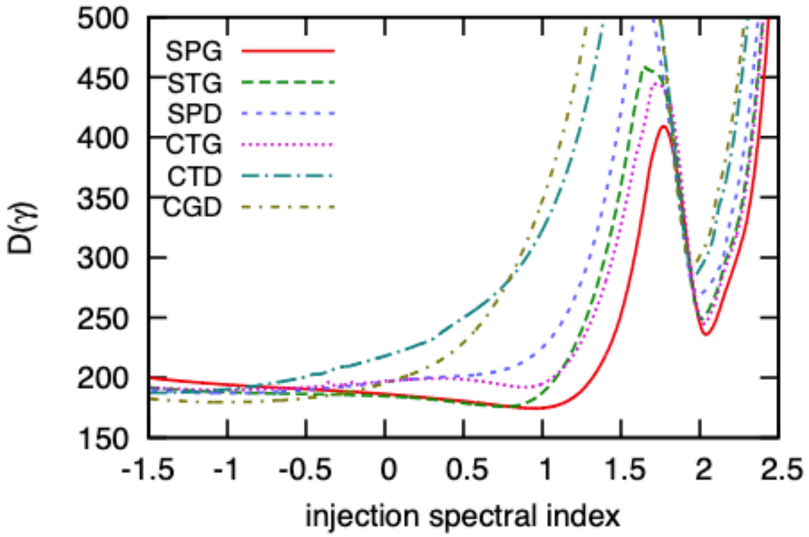

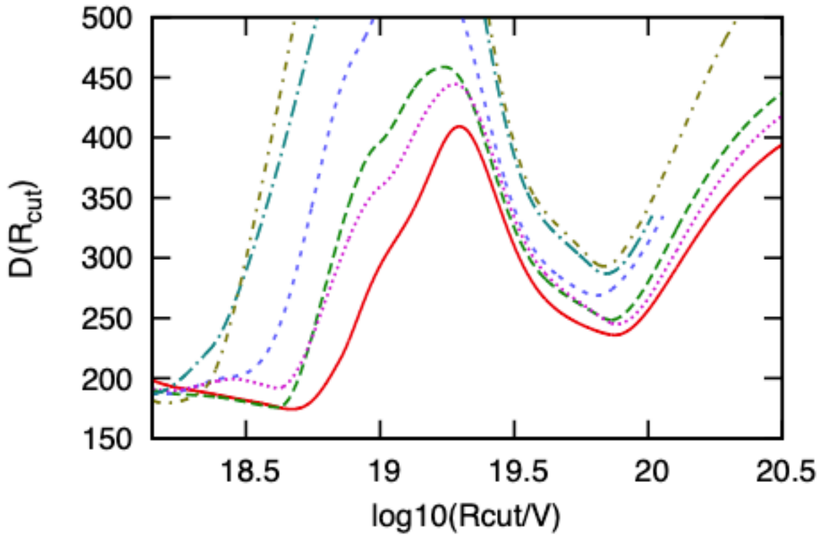

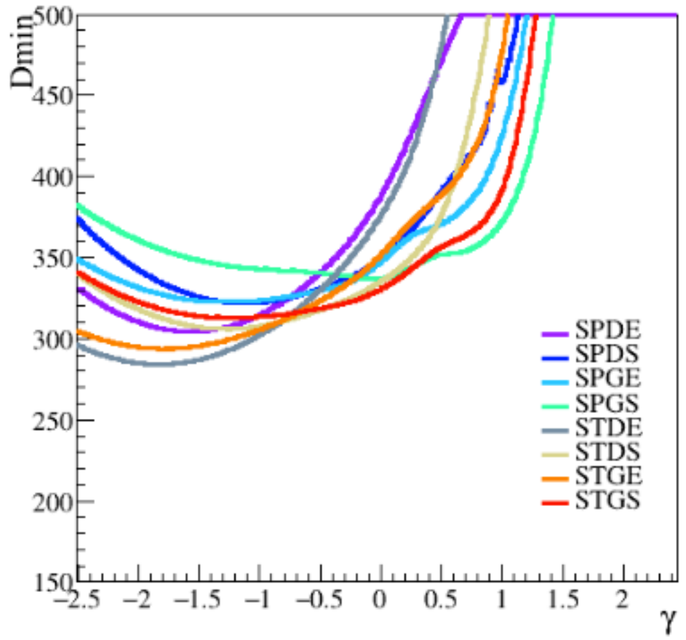

Figure: from Sergio Petrera

Fraction parameters

Decreasing R_{cut}, the propagated fluxes start to show the effect of the cutoff at the sources with the consequence that the maximum energy of secondary protons is pushed to low values, which in turn produces a less mixed composition in better agreement with data. In this region the observed spectrum starts to be reproduced by the envelope of hard elemental fluxes ($\gamma \approx 1$), cut by a decrease that is caused by both the source cutoff (for the secondary nucleons) and the photo-disintegration. In this region the spectral parameters appear to be degenerate

$$
\begin{aligned}
f_{\mathrm{H}} &= c_1^2 \\
f_{\mathrm{He}} &= (1 - c_1^2) \cdot c_2^2 \\
f_{\mathrm{N}} &= (1 - c_1^2) \cdot (1 - c_2^2) \cdot c_3^2 \\
f_{\mathrm{Si}} &= (1 - c_1^2) \cdot (1 - c_2^2) \cdot (1 - c_3^2) \cdot c_4^2 \\
f_{\mathrm{Fe}} &= (1 - c_1^2) \cdot (1 - c_2^2) \cdot (1 - c_3^2) \cdot (1 - c_4^2)
\end{aligned}
$$

Fraction parameters

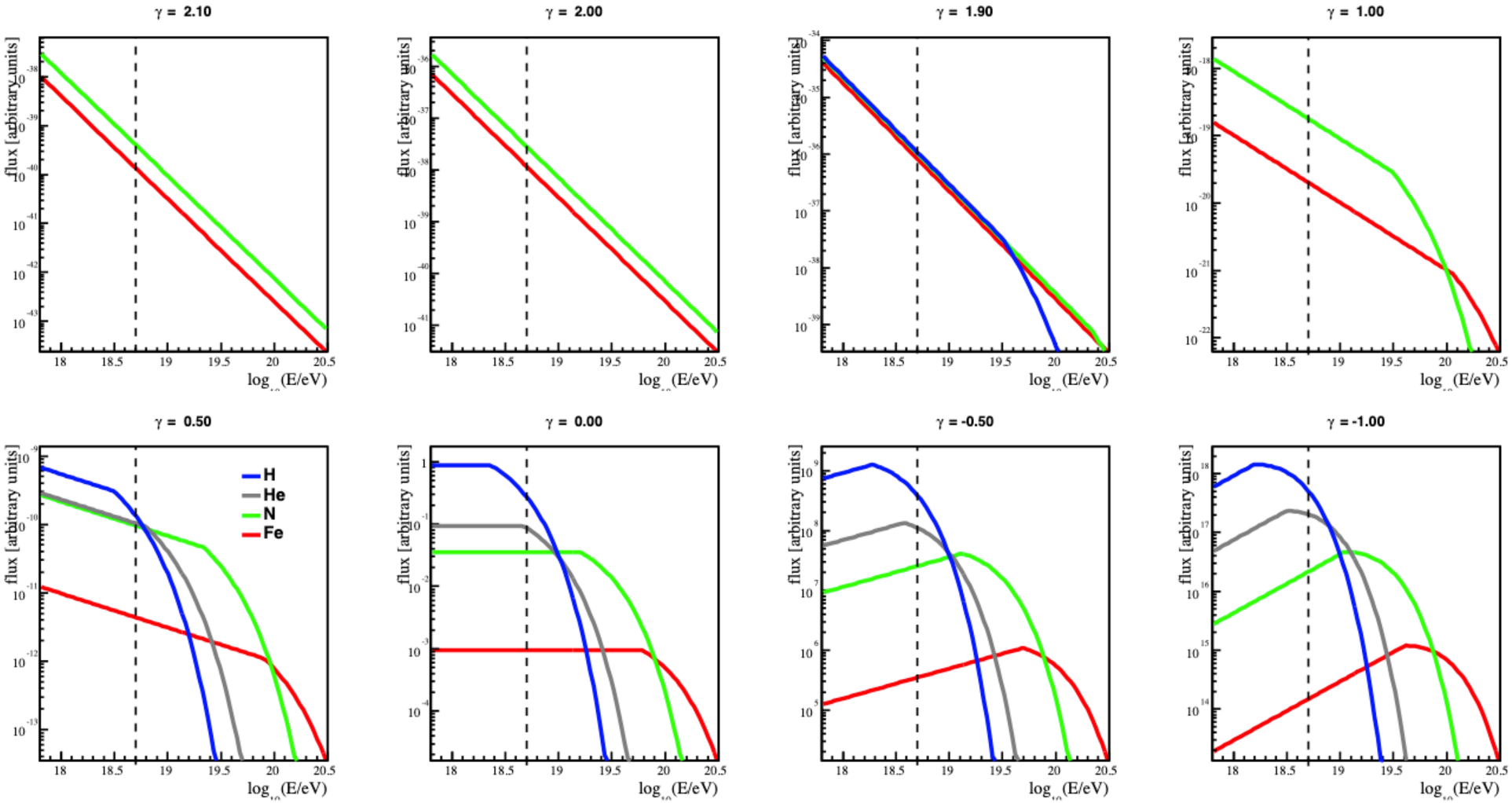

Photo-interaction with nuclei

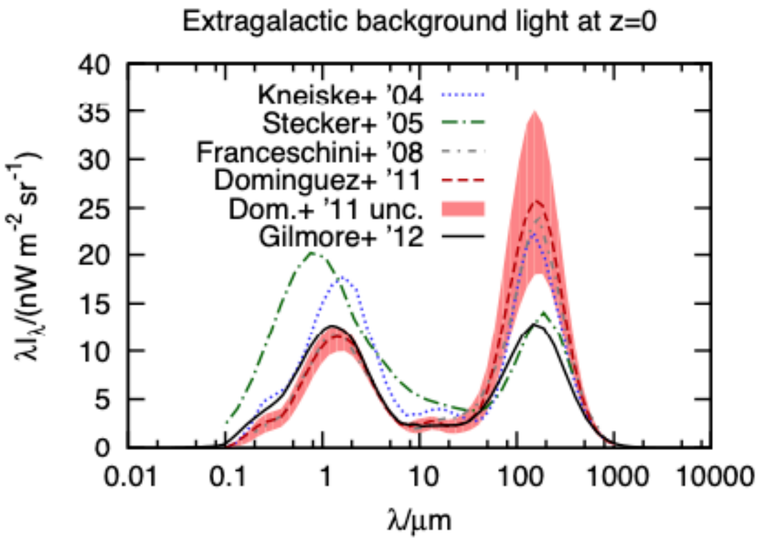

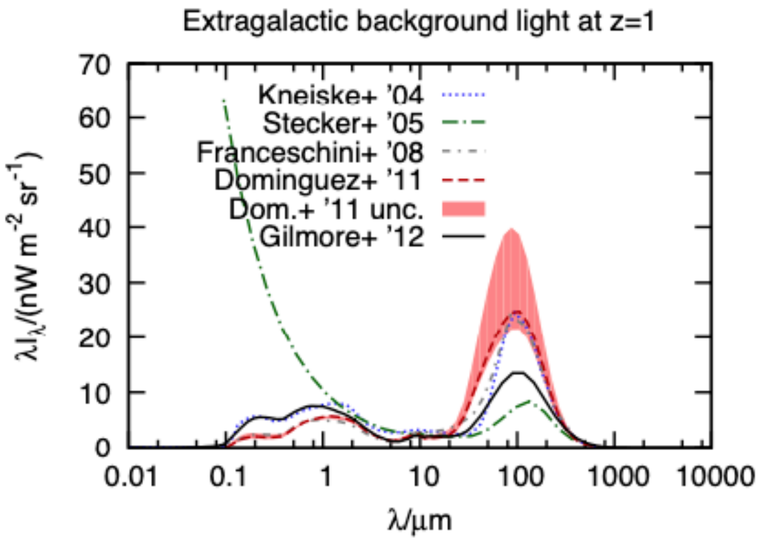

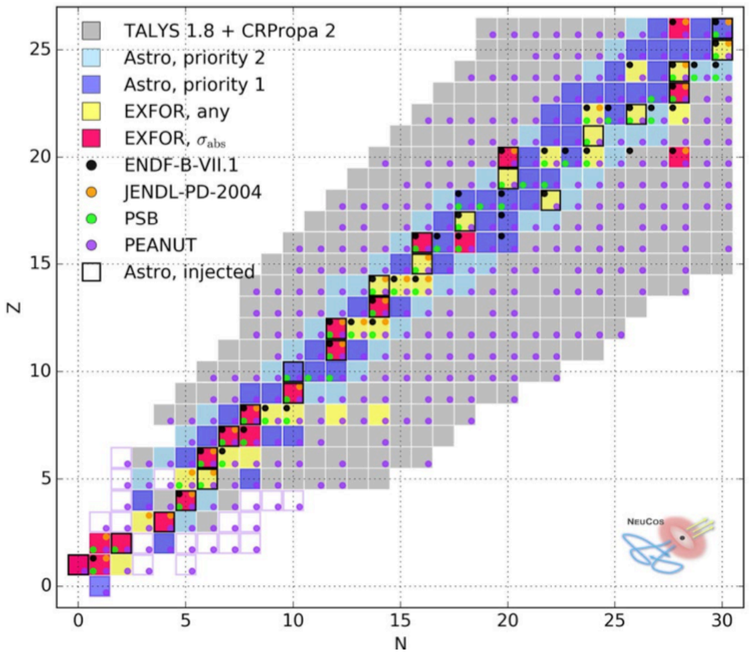

Second minimum

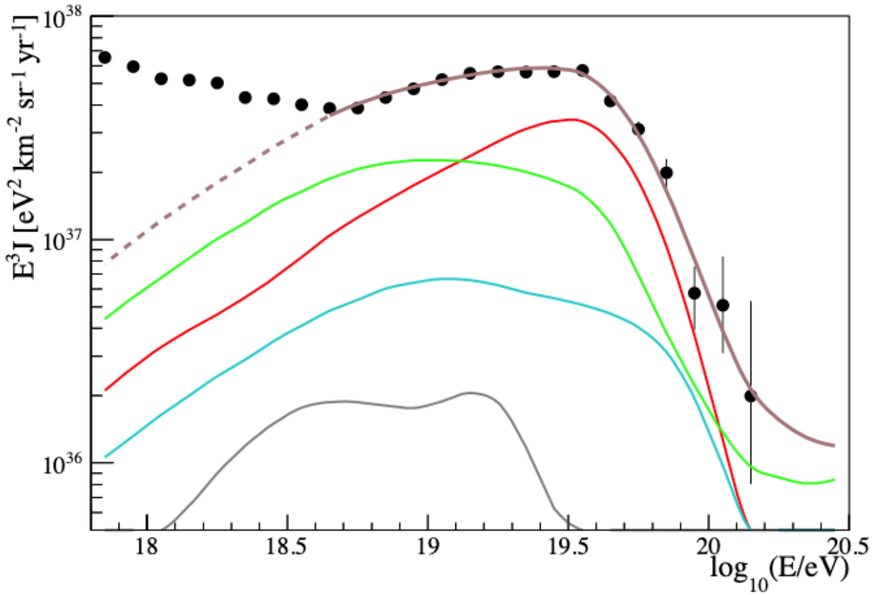

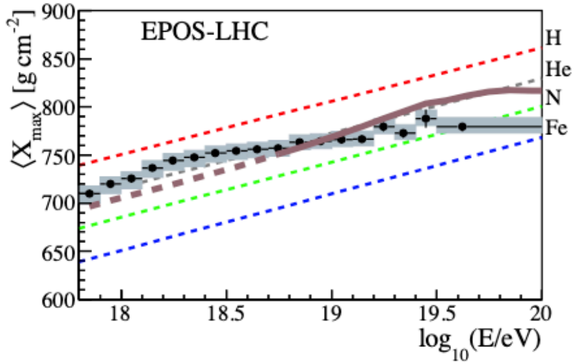

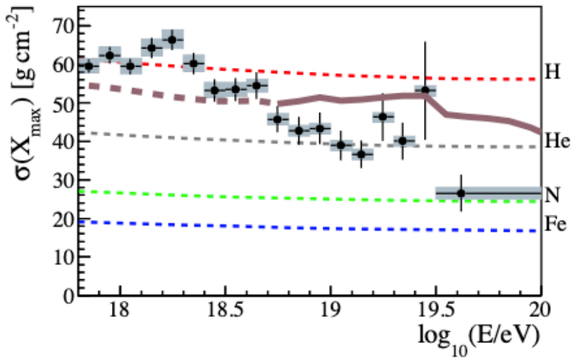

Defining the mass fractions

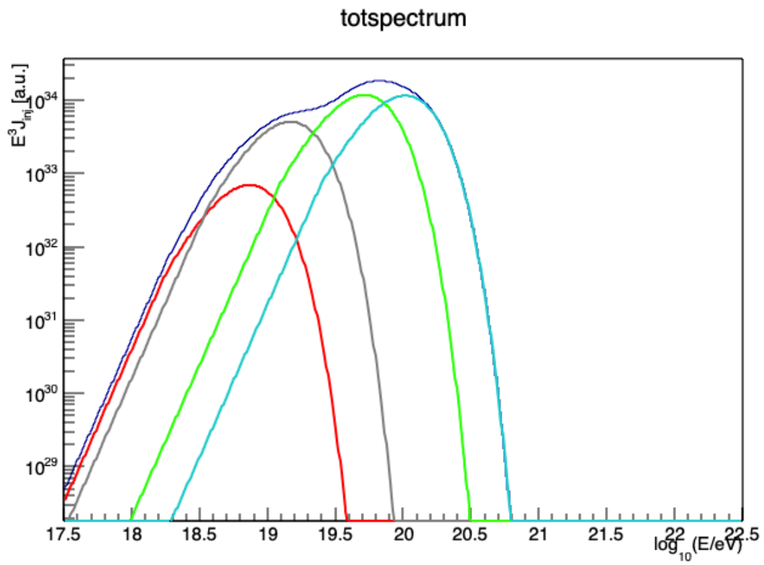

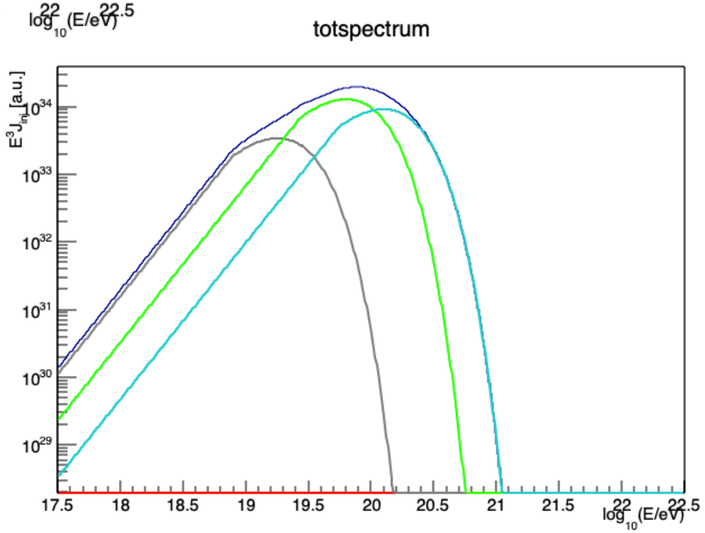

$$\mathcal{L}_0 = \sum_A \mathcal{L}_A = \sum_A \int_{E_{\min}}^{\infty} J_A(E)\ E\ dE$$

$\mathcal{L}_0\ (\mathrm{erg \cdot Mpc^{-3} \cdot yr^{-1}})$	$4.8 \cdot 10^{44}$	$5.37 \cdot 10^{44}$
$I_{\mathrm{H}}(\%)$	$O(10^{-6})$	11.9
$I_{\mathrm{He}}(\%)$	41.4	44.7
$I_{\mathrm{N}}(\%)$	43.3	29.3
$I_{\mathrm{Si}}(\%)$	15.2	14.4
$I_{\mathrm{Fe}}(\%)$	0.00	0.00

$$I_A = \mathcal{L}_A / \mathcal{L}_0$$

Why do you fit distributions and not M and SD?

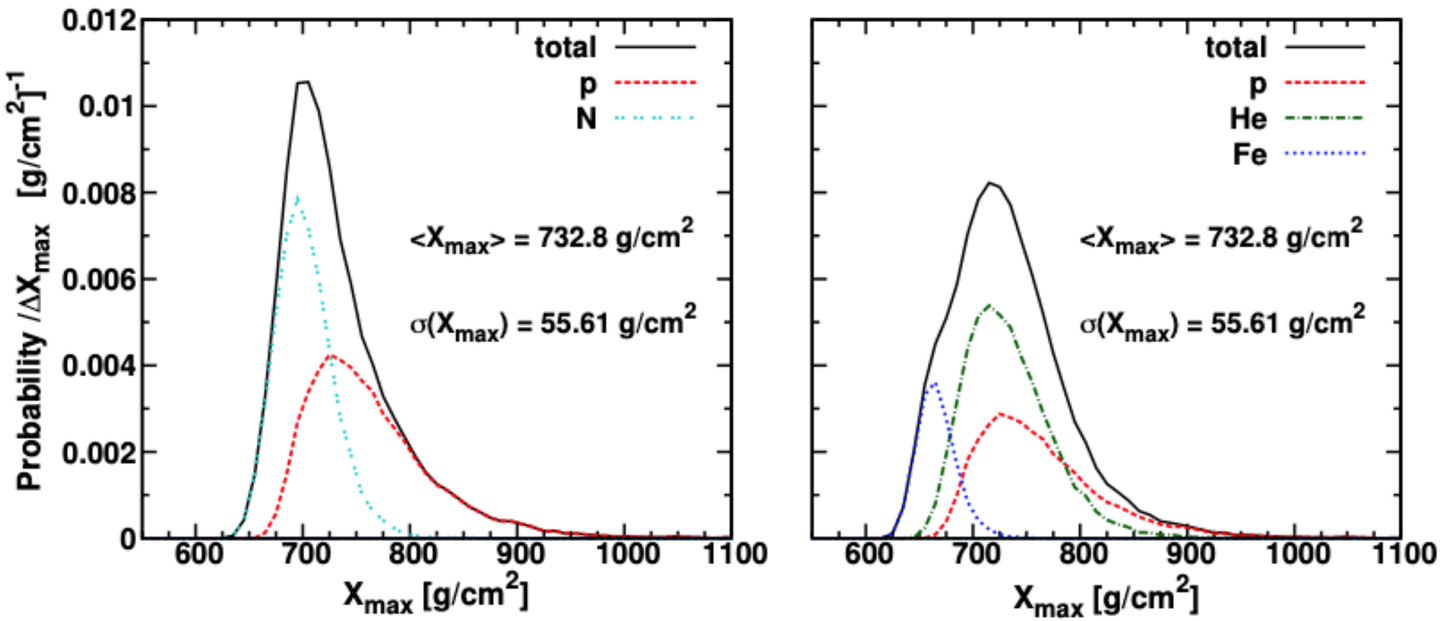

Fit of the distribution

$$g(X_{\max}|\lg E, A) = \frac{\lambda^\lambda}{\sigma\Gamma(\lambda)}\exp\left(-\lambda\frac{X_{\max}-\mu}{\sigma} - \lambda\exp\left(-\frac{X_{\max}-\mu}{\sigma}\right)\right)$$

Including detector effects

$$G_m^{\text{model}}(X_{\max}|\lg E) = \sum_A p_A^{\exp}\cdot\mathcal{G}(X_{\max}|\lg E, A)$$

$$D_{X_{\max}} = \sum_m D_m = \sum_m -2\ln\frac{L_{X_{\max}}}{L^{\text{sat}}_{X_{\max}}} = -2\sum_m\sum_x k_{mx}\left(\ln G_{mx} - \ln\frac{k_{mx}}{N_m}\right)$$

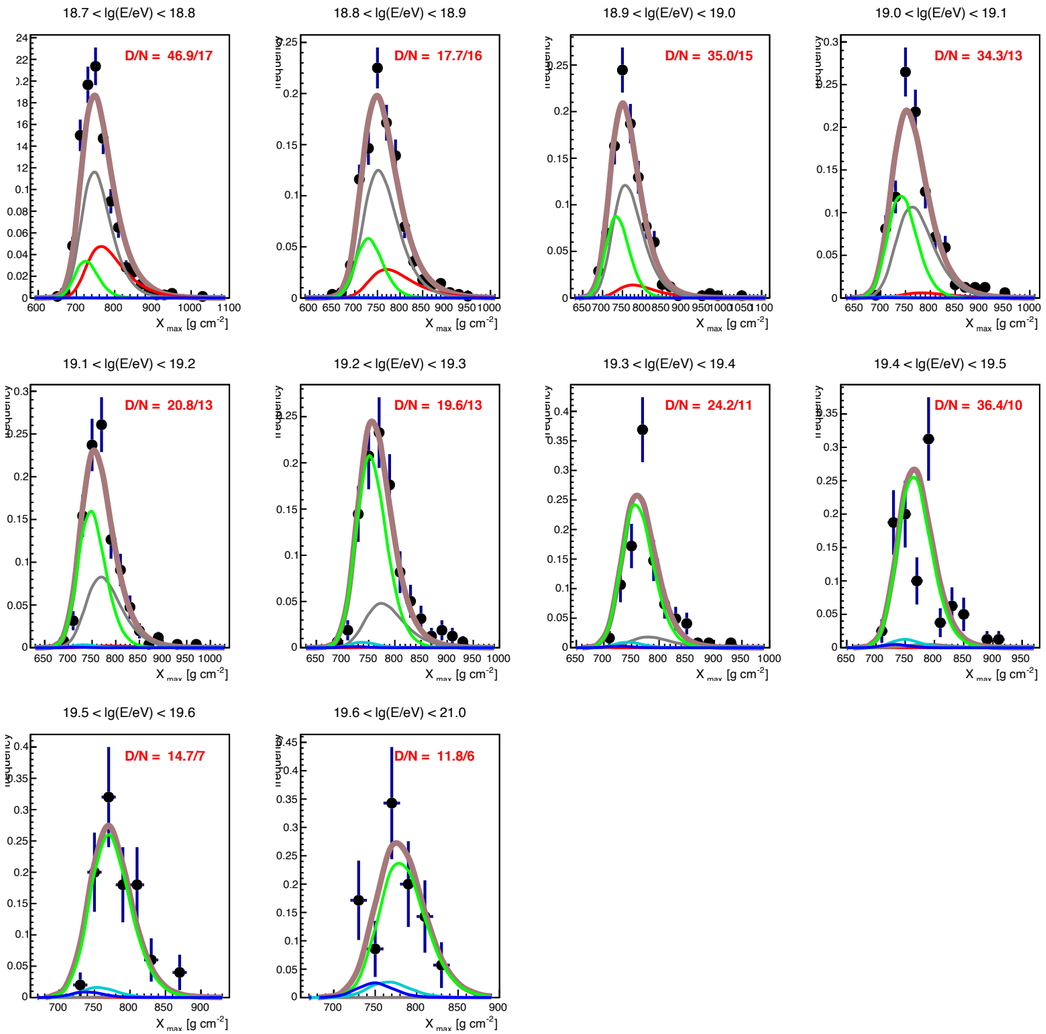

Fraction fit

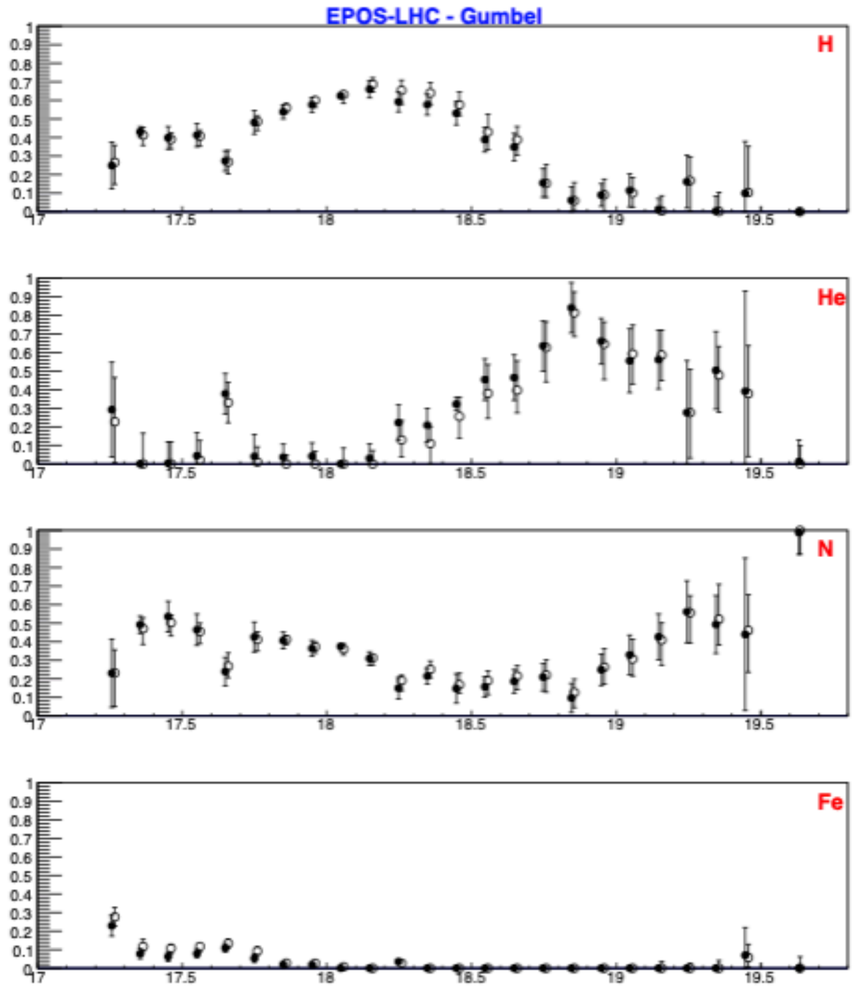

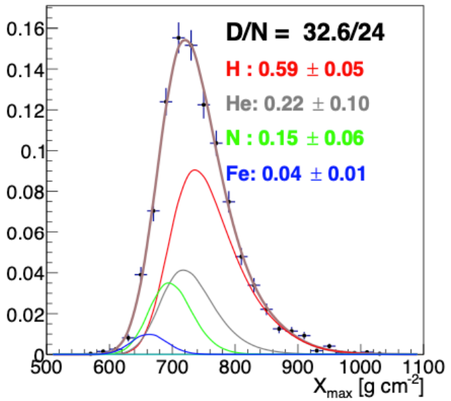

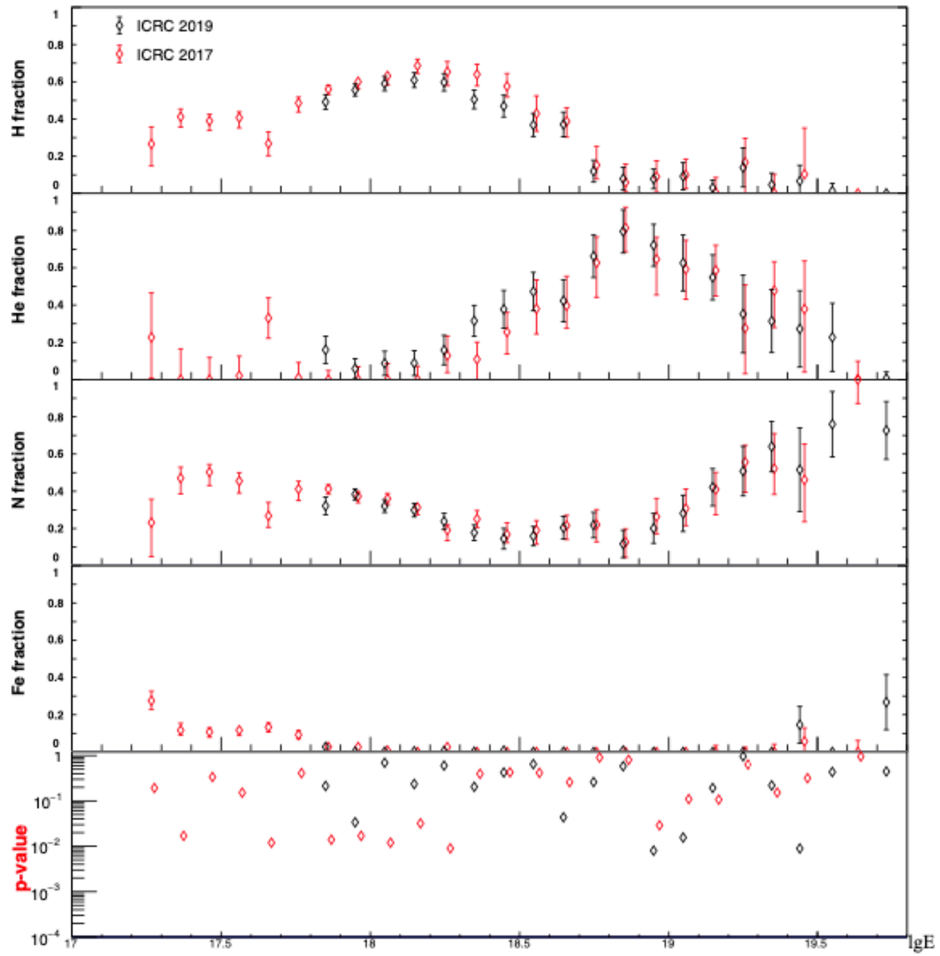

Fraction fit

The fit of the distributions is based on the same log-likelihood minimization method used to fit the $X_{\max}$ distributions in the 'combined fit' paper[2]. Having a total number of events N_m per log-energy bin m, the probability of observing an $X_{\max}$ distribution $\vec{k}_m = (k_{m1}, k_{m2}...)$ follows a multinomial distribution. The goodness-of-fit is assessed with a generalized χ^2, (the *deviance*, D_m), defined as the negative log-likelihood ratio of a given model and the *saturated* model that perfectly describes the data:

$$D_m = -2 \ln \frac{L_{X_{\max}}}{L^{\text{sat}}_{X_{\max}}} = -2 \sum_x k_{mx} \left(\ln G_{mx} - \ln \frac{k_{mx}}{N_m} \right) \tag{3}$$

where G_{mx} is the probability $G_m^{\text{model}}(X_{\max}|f_A)$ calculated at bin x of $X_{\max}$, k_{mx} is the event content of the experimental $X_{\max}$ distribution at $X_{\max}$ bin x and log energy bin m; $N_m = \sum_x k_{mx}$ is the total number events in the log energy bin m.

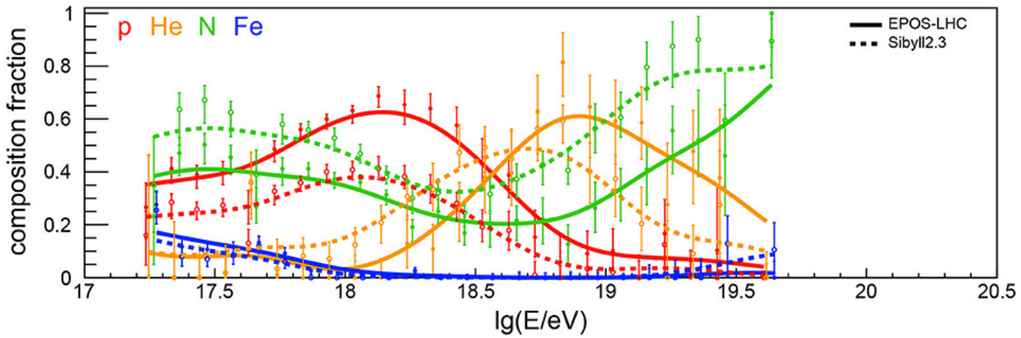

Over-density correction

The peaks at D ≈ 4 Mpc, D ≈ 20 Mpc and D ≈ 70 Mpc correspond to the Council of Giants, the Virgo Cluster, and the Hydra–Centaurus Supercluster, respectively.

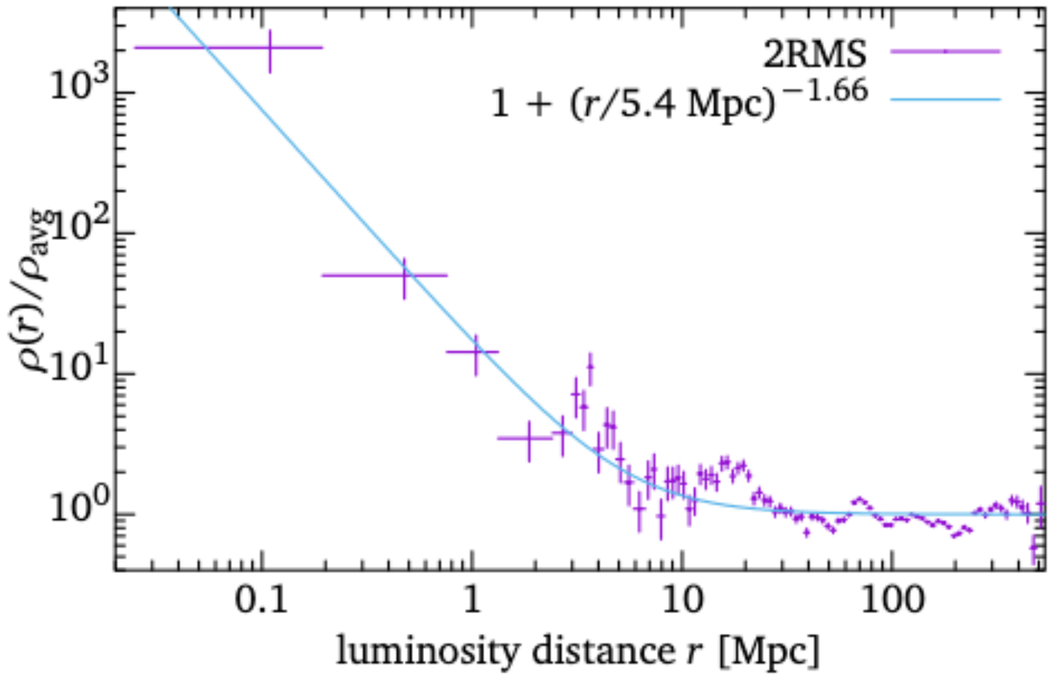

J.J. Condon et al, The Astrophysical Journal, Volume 872, Issue 2, article id. 148, 20 pp. (2019).

Hylke B. J. Koers et al.,*Monthly Notices of the Royal Astronomical Society*, Volume 399, Issue 2, October 2009, Pages 1005–1011

Over-density correction

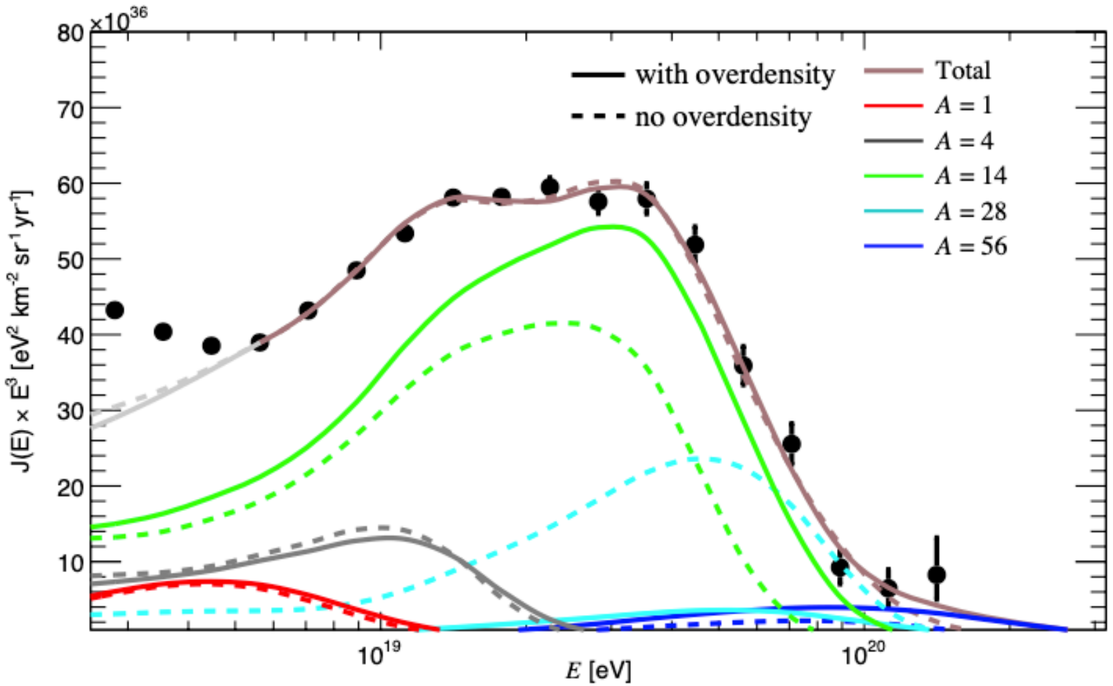

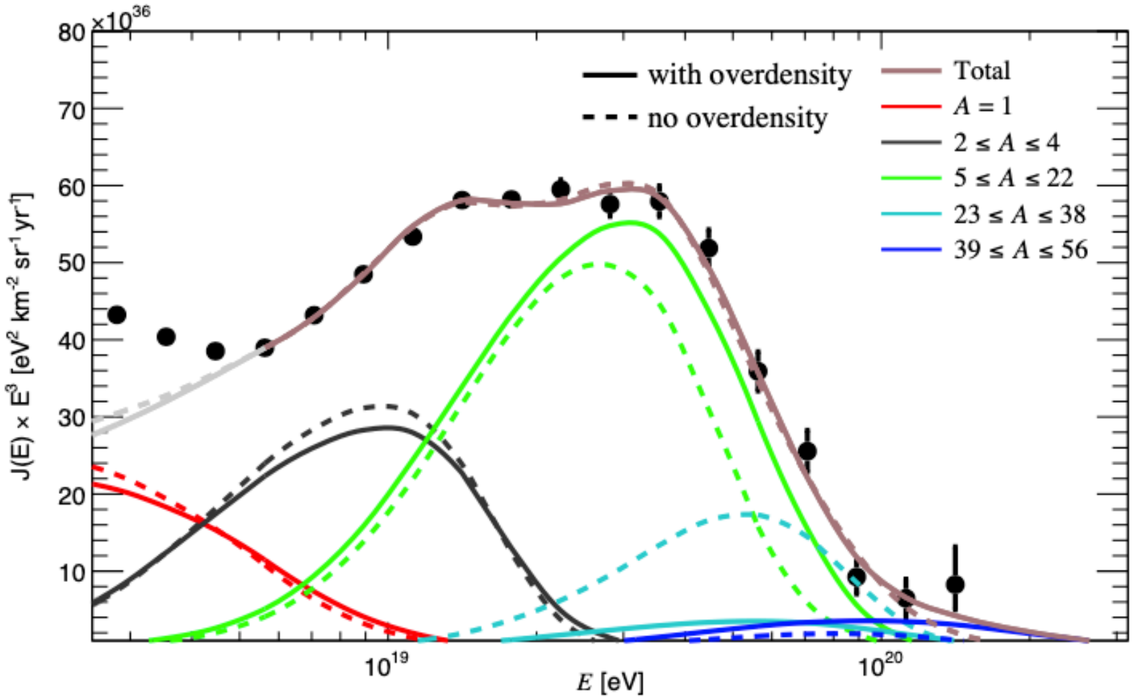

HIM and photo-disintegration cross section model

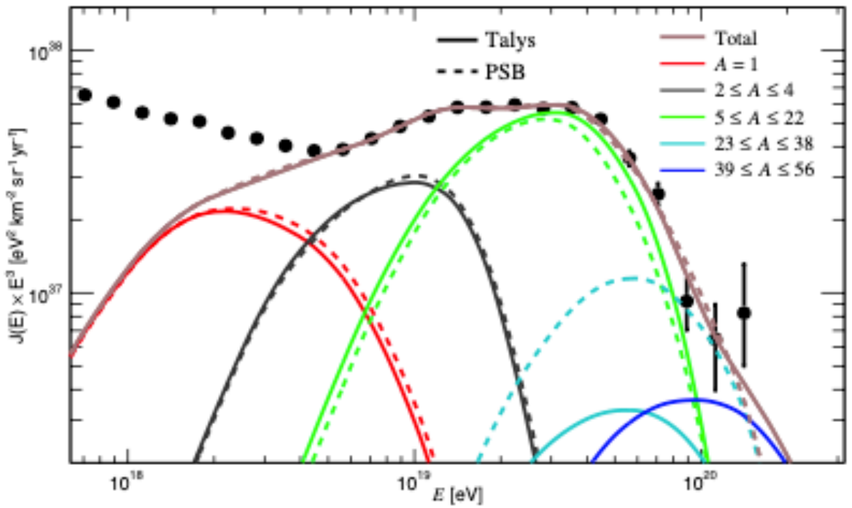

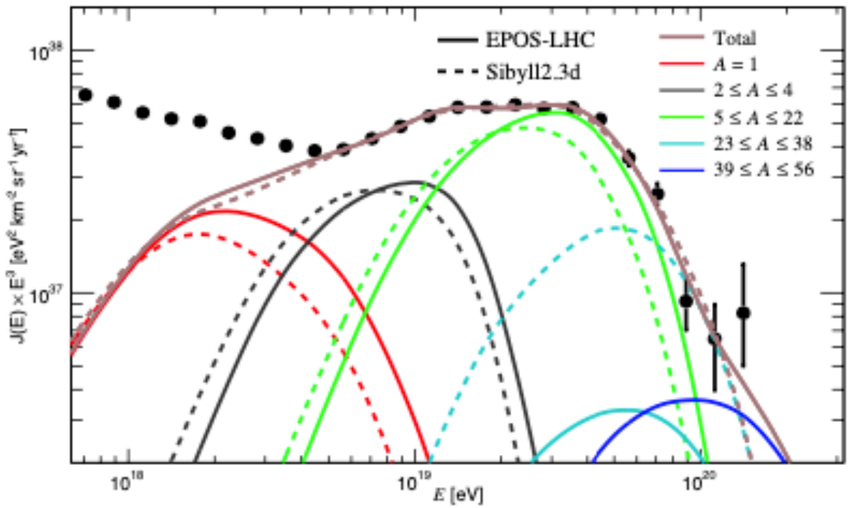

Cap 4

Wolf-Rayet

While most of the supernova explosions take place in the interstellar medium, some of them can also occur in the winds of objects like Wolf-Rayet stars, whose contribution could actually explain an intermediate-mass Galactic contribution

Considering that the estimated number of Wolf-Rayet stars in our Galaxy is ~ 1200 and that 1 Wolf-Rayet star is estimated to explode in the Galaxy in every 7 supernova explosions, it was found in Thoudam et al., that such a Galactic contribution of cosmic rays is expected to be dominant between ~ 10^{17} eV and ~ 10^{18} eV.

More specifically, depending on the compositions of the Wolf-Rayet winds, such explosions may accelerate N nuclei up to an energy cutoff of ~ 10^{18} eV, which would make plausible to observe the tail of this Galactic component in the energy range included in our fit.

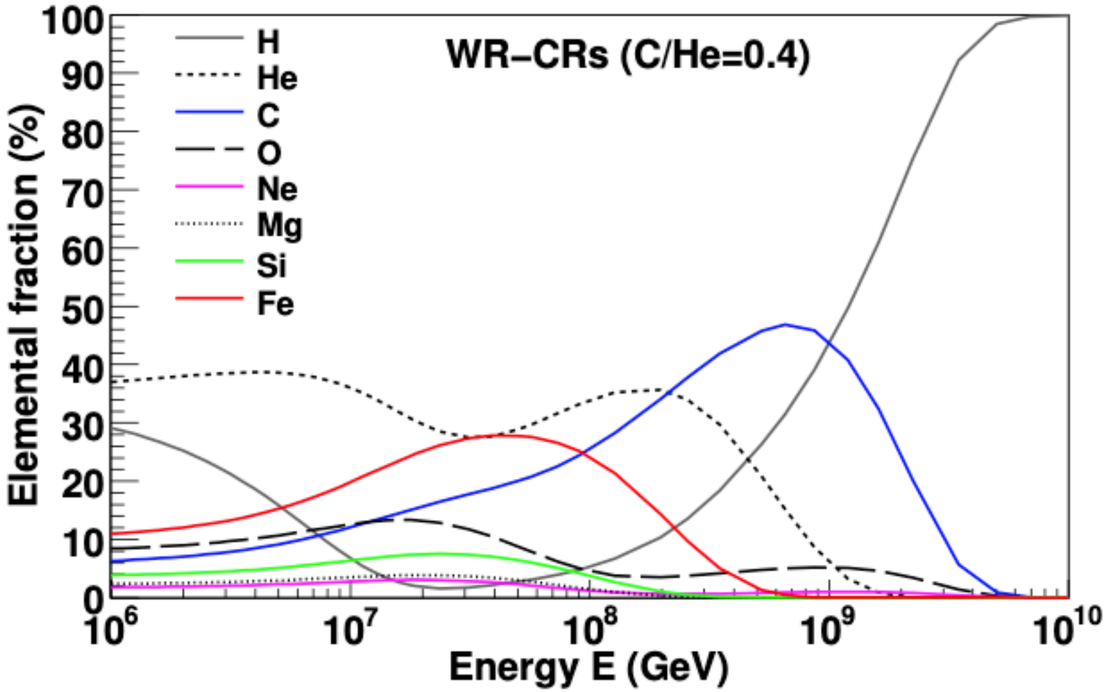

S.Thoudam et al, Astron.Astrophys. 595 (2016) A33

Kascade-GRANDE

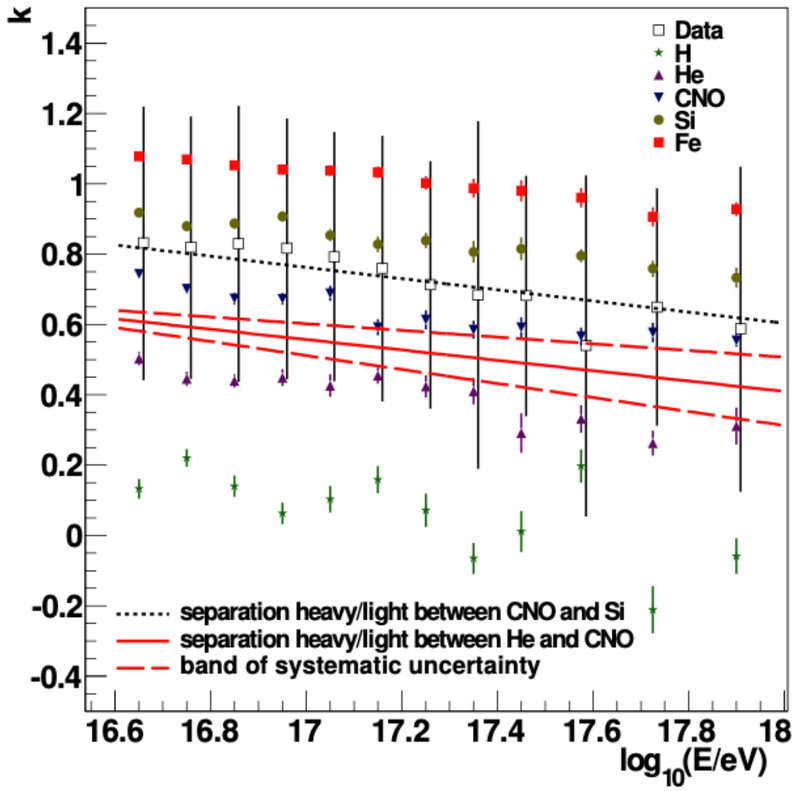

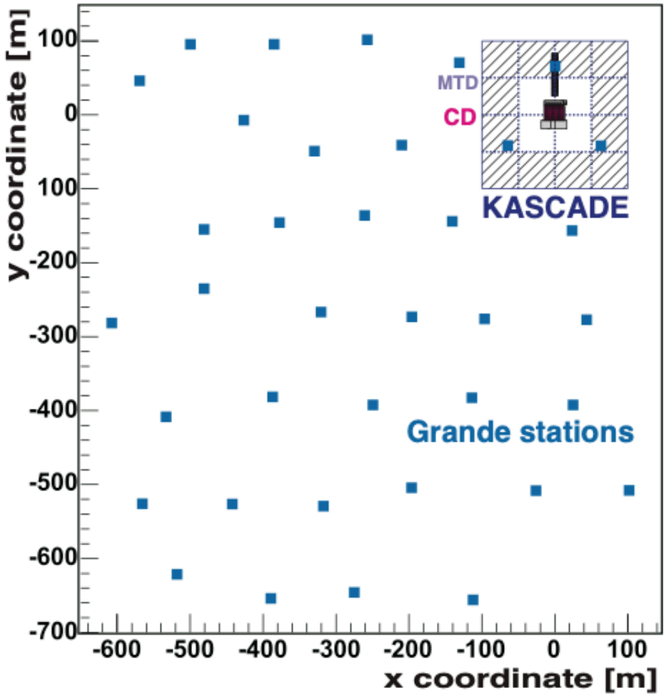

$$k = \frac{\log_{10}(N_{ch}/N_\mu) - \log_{10}(N_{ch}/N_\mu)_H}{\log_{10}(N_{ch}/N_\mu)_{Fe} - \log_{10}(N_{ch}/N_\mu)_H}$$

M. Bertaina [Kascade-Grande coll.], *PoS* ICRC2015 (2016) 359
W.-D. Apel et al. - [KASCADE-Grande Coll.], *Phys. Rev. D* **87** (2013) 081101

KG data

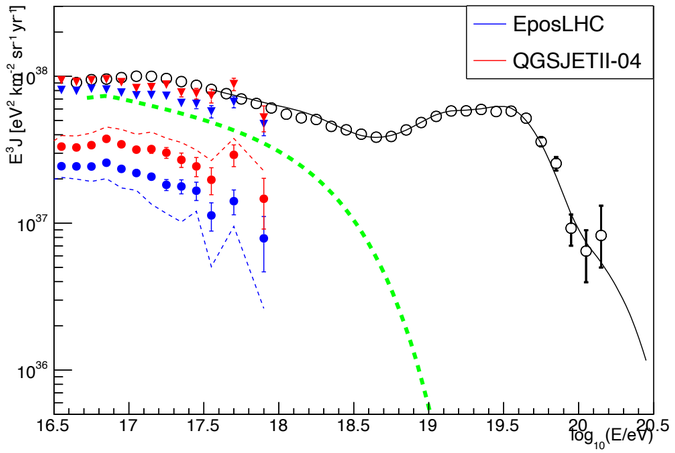

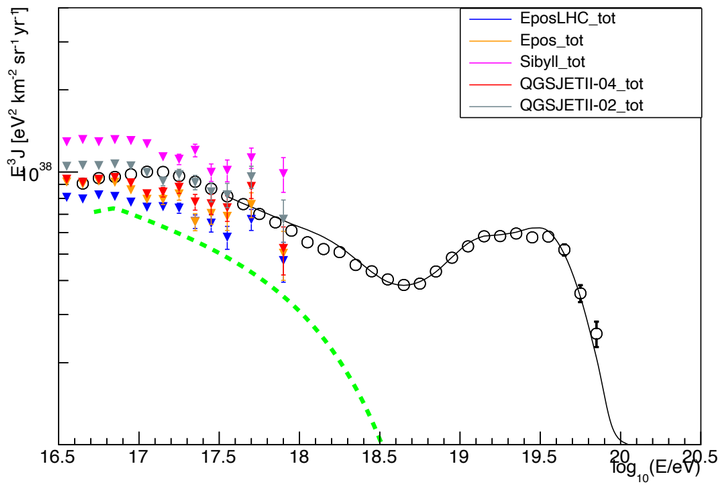

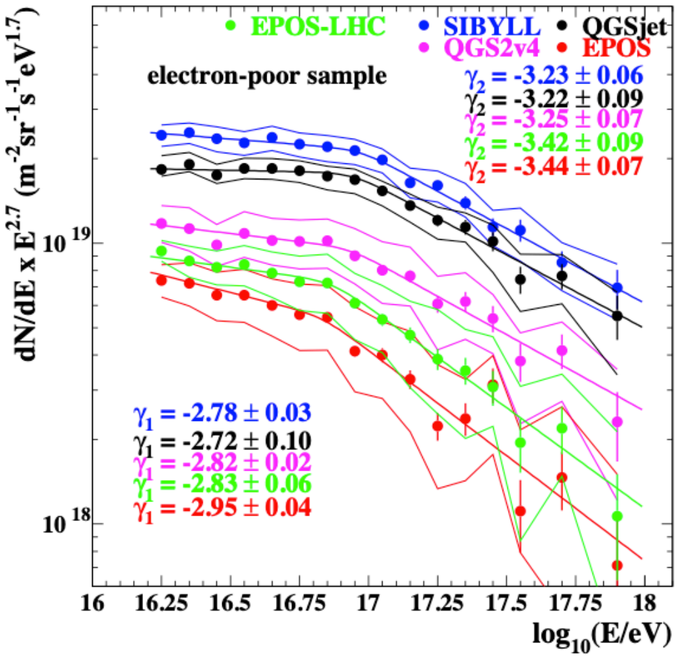

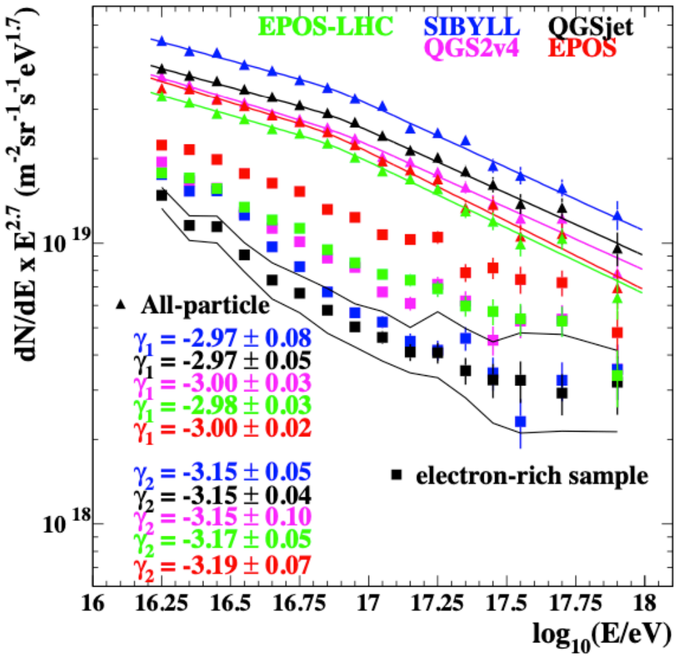

Galactic magnetic field

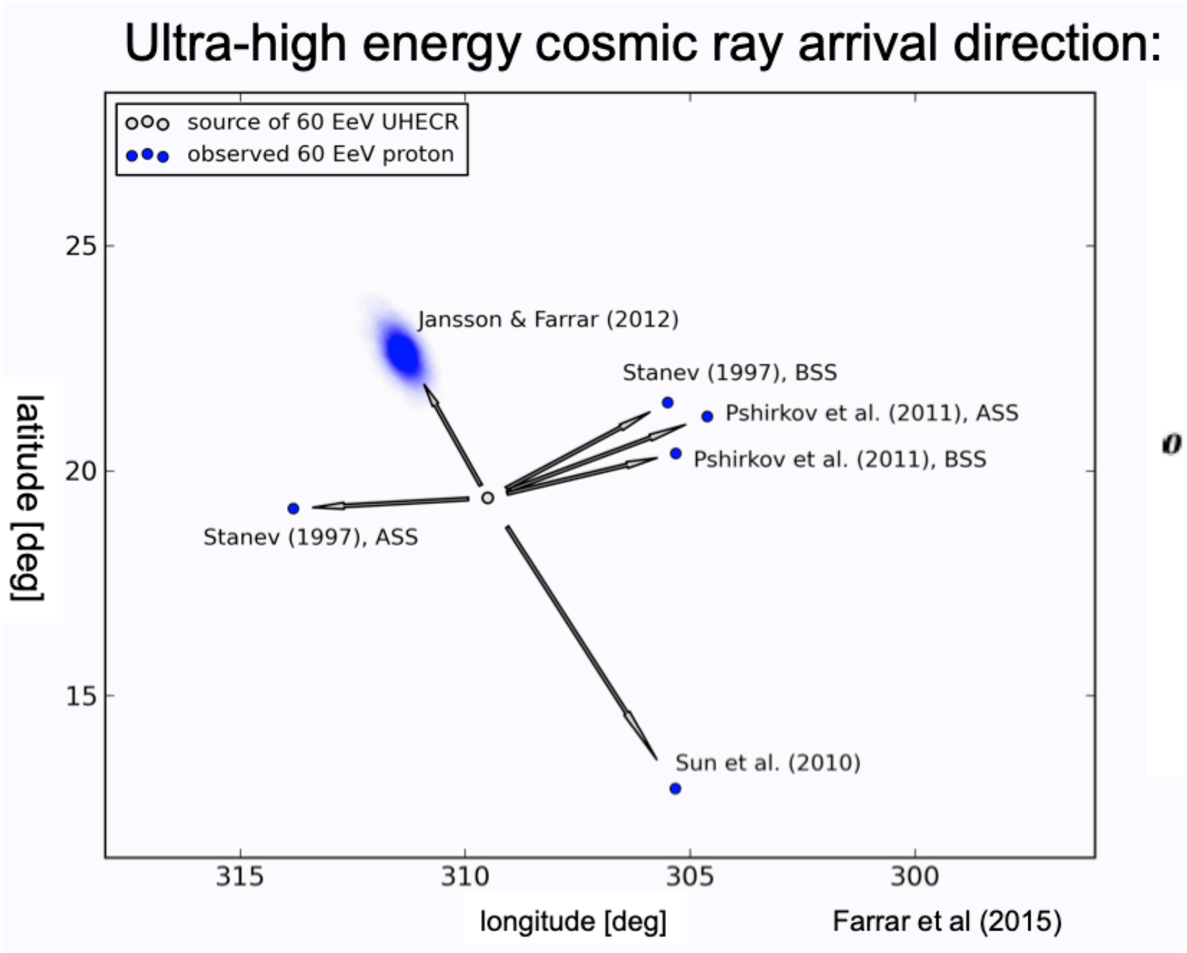

p-values

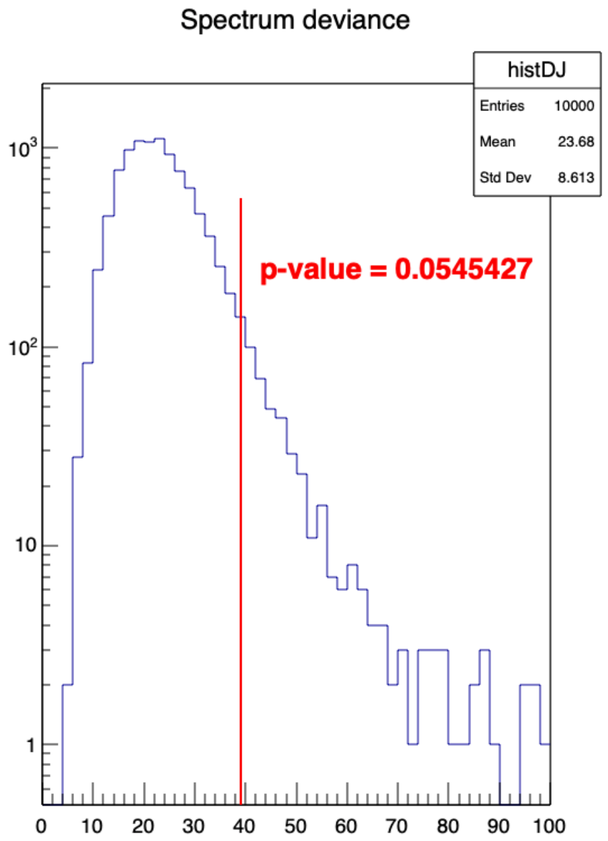

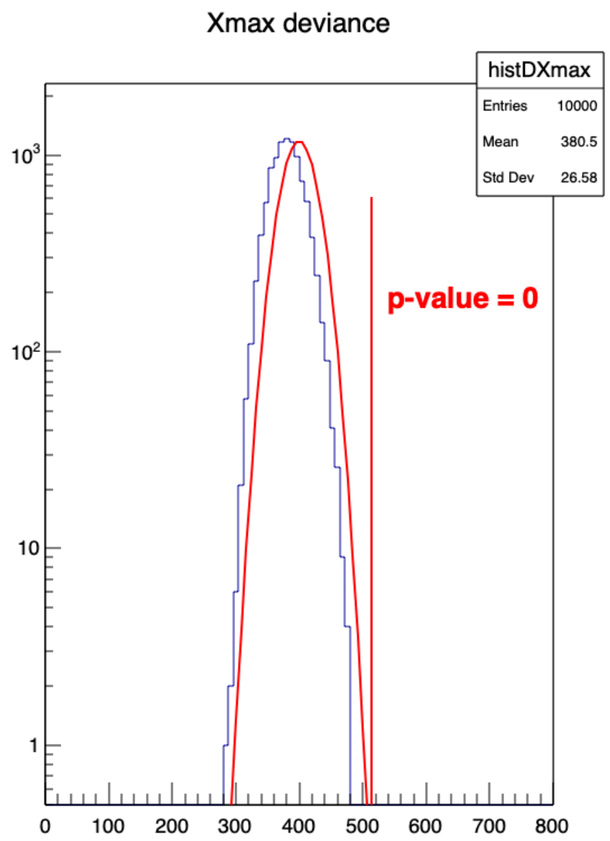

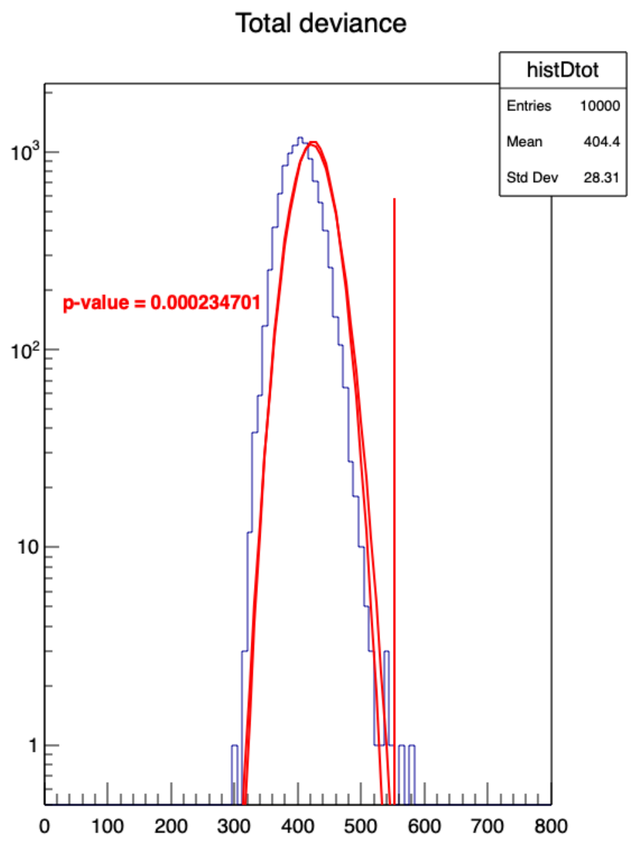

Neutrino single component

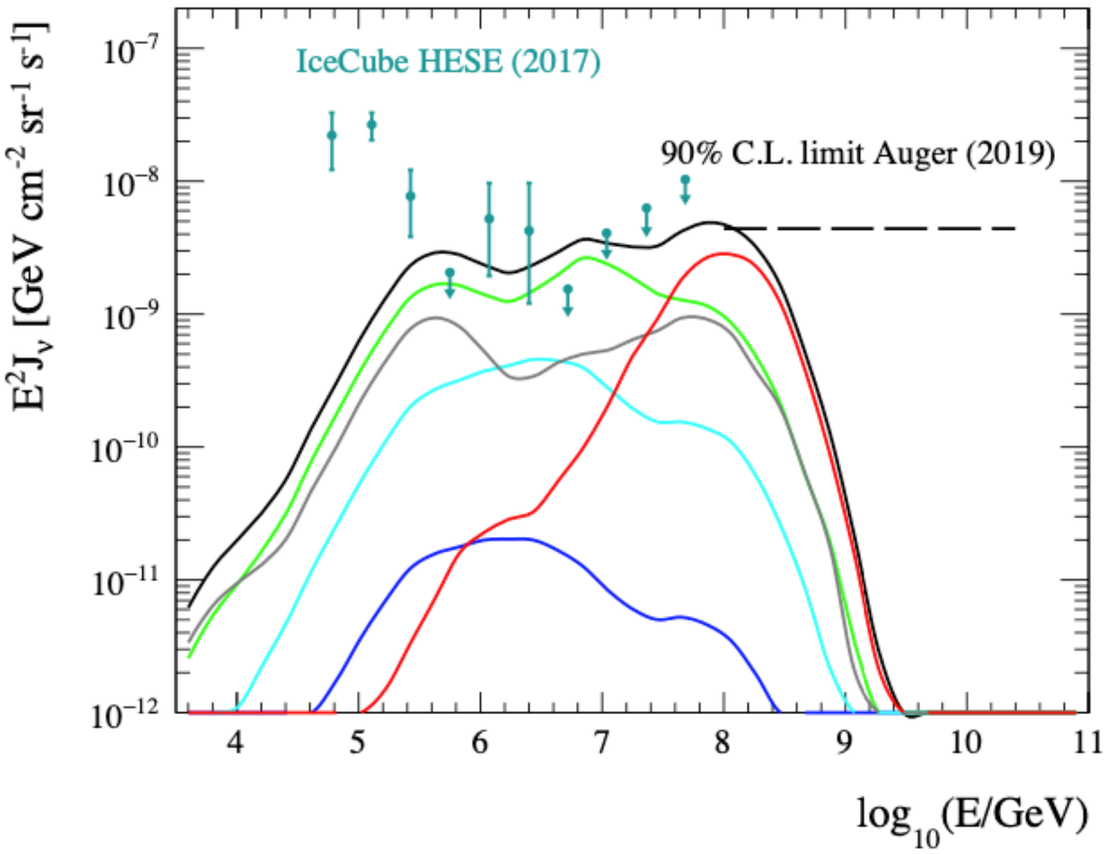

Cap 5

UFA results

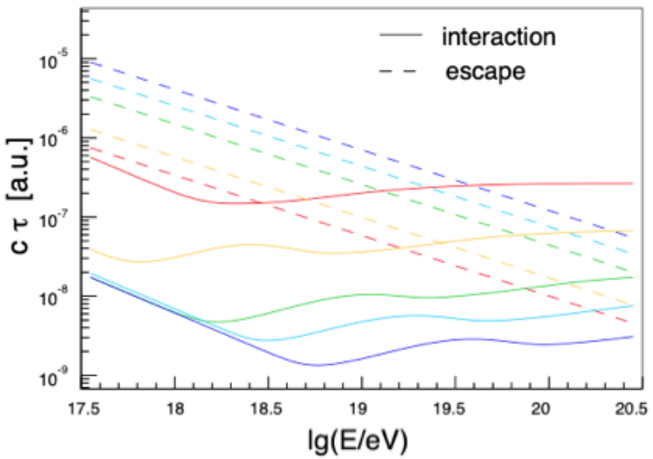

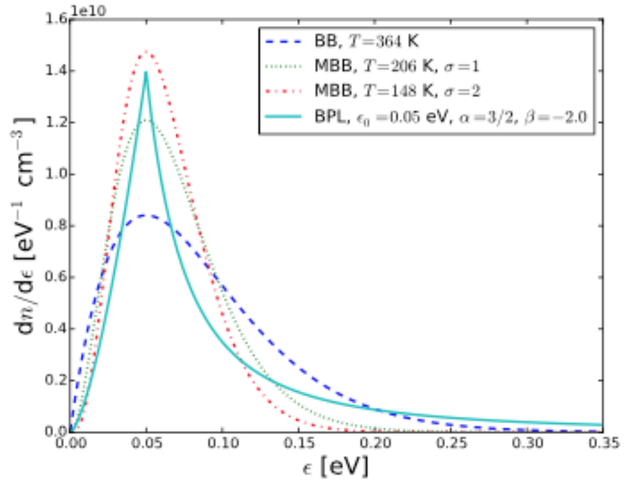

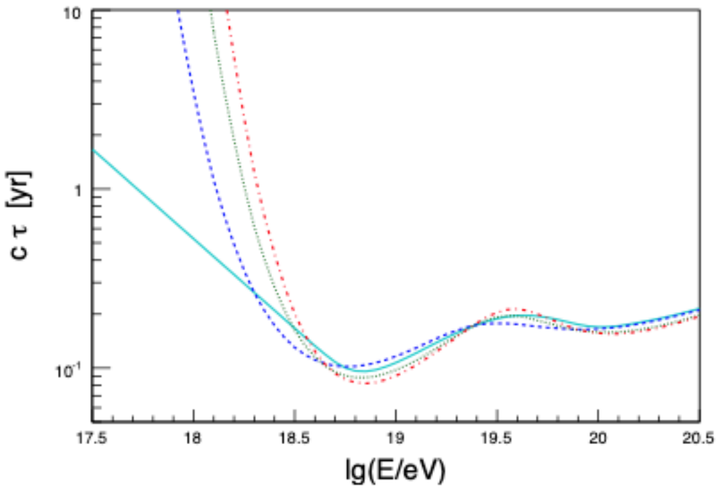

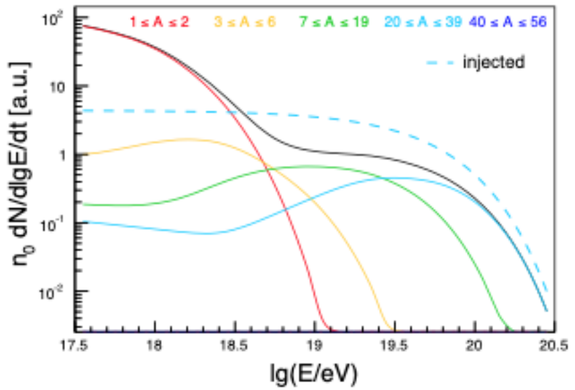

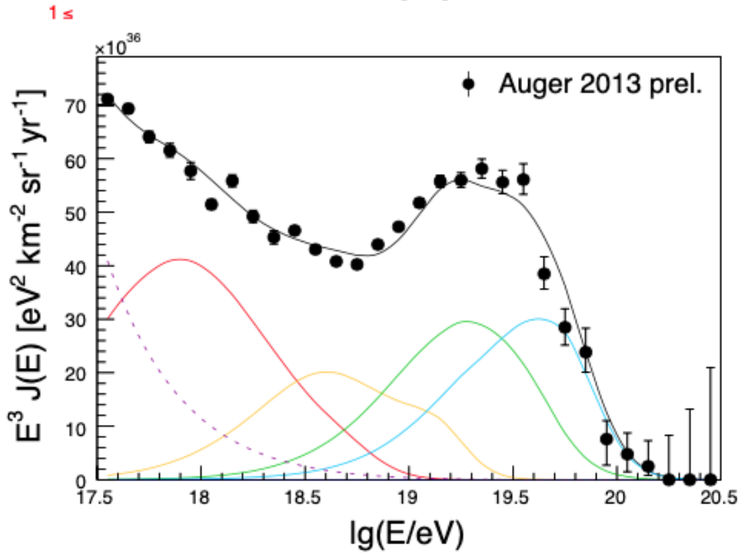

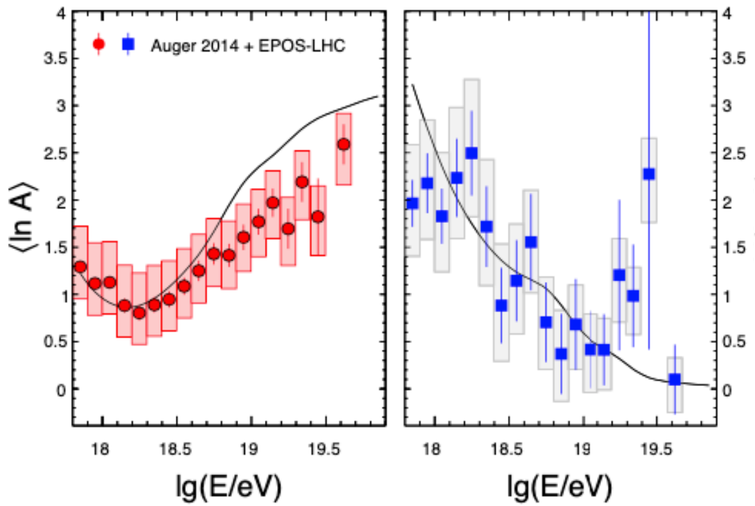

Why SBG?

SBG are unique objects in the Universe characterized by a high rate of supernova explosions and star formation rate which can often be as high as ~ 10^2 $M_\odot yr^{-1}$

In several SBGs, the star forming region is observed to be localized in the central part of the galaxy with typical radial extension of R ~ 0.2−0.5 kpc. These objects are referred to as starburst nuclei (SBNi) and their interstellar medium (ISM) is naturally expected to be highly perturbed with a strong level of turbulence.

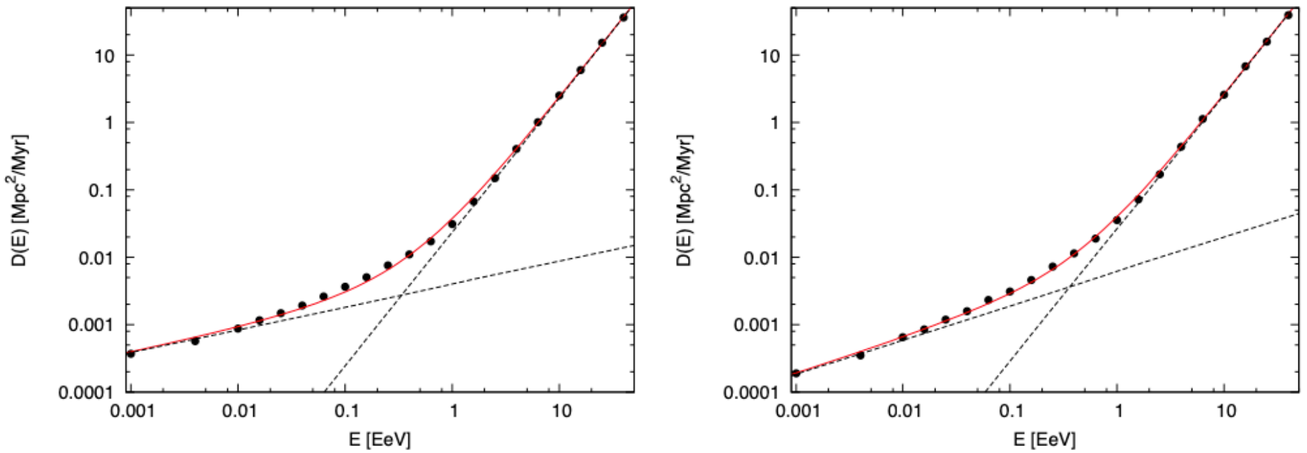

$$D(E) = \frac{c}{3} l_c \left[4 \left(\frac{E}{E_c} \right)^2 + a_I \left(\frac{E}{E_c} \right) + a_L \left(\frac{E}{E_c} \right)^{2-m} \right]$$

For δB/B«1 particles follow helical trajectories around magnetic field lines

For δB/B≈1 particles are confined for longer time

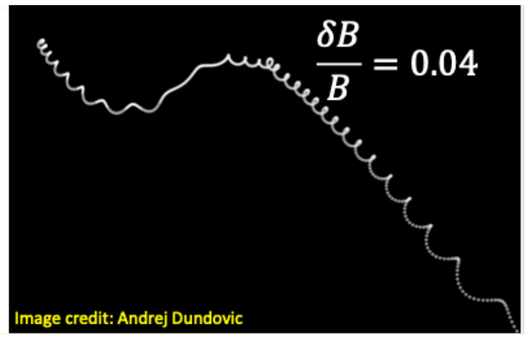

PRD 89, 123001 (2014)

Photons

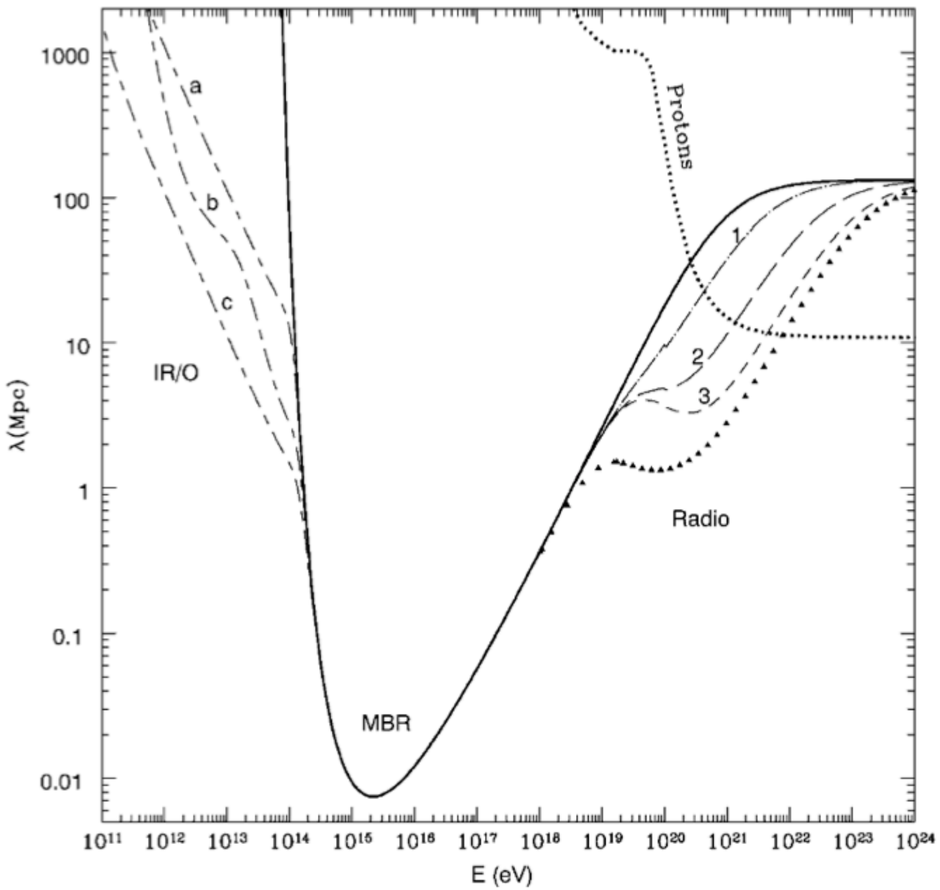

Fi

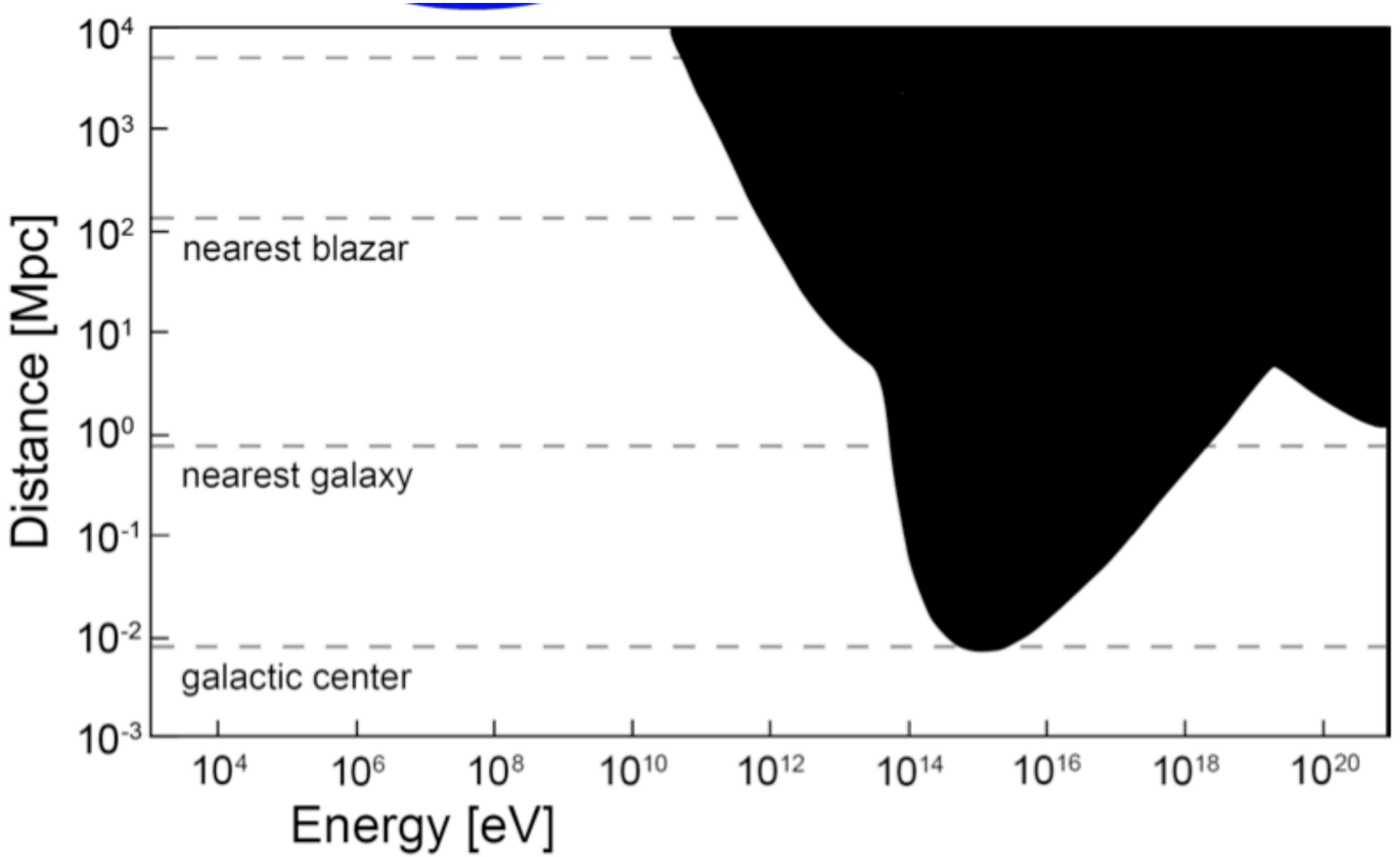

SFR evolution

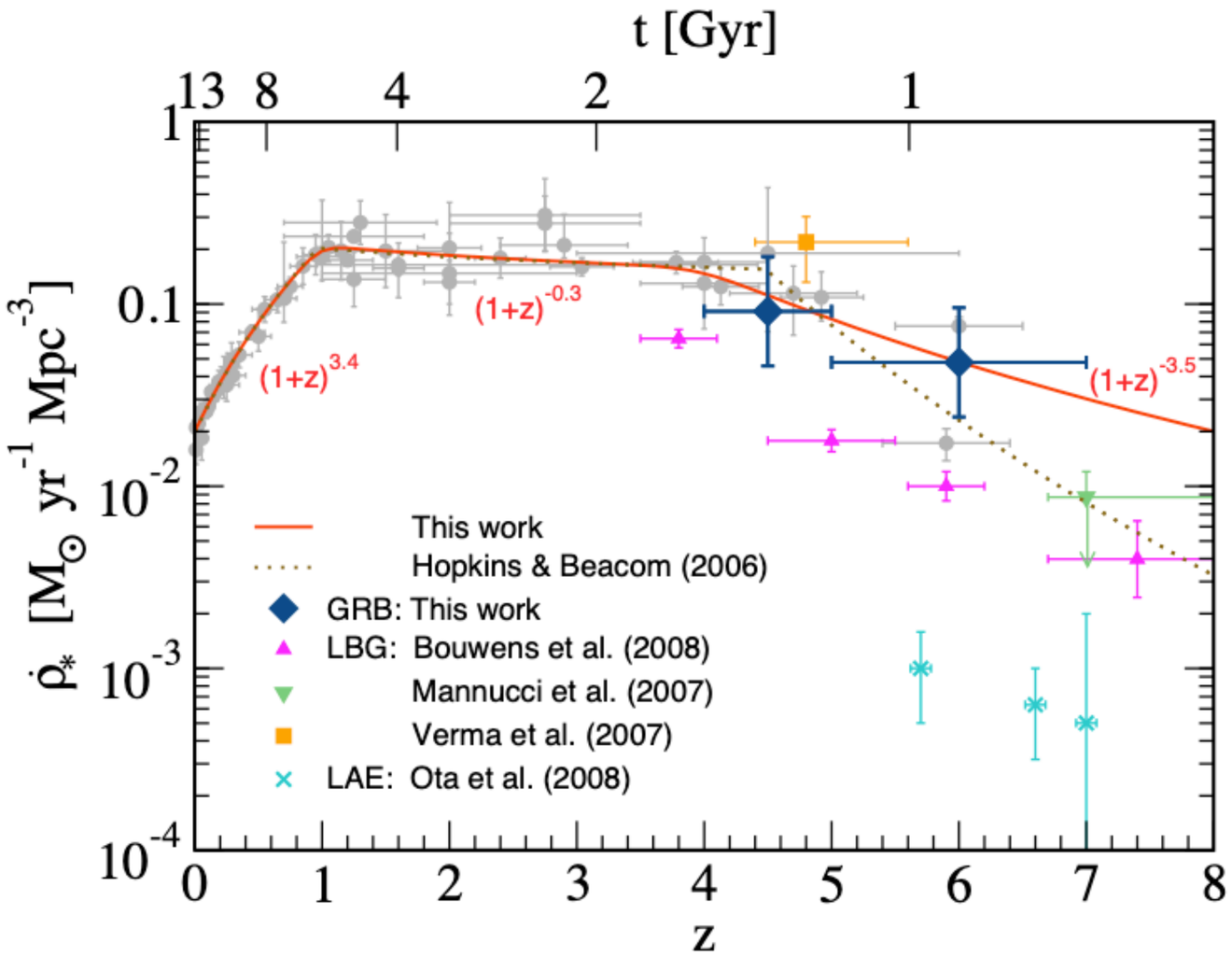

$$S_{\rm SFR}(z) \propto \begin{cases} (1+z)^{3.4} & z \leq 1 \\ 2^{3.7} \cdot (1+z)^{-0.3} & 1 < z \leq 4 \\ 2^{3.7} \cdot 5^{3.2} \cdot (1+z)^{-3.5} & z > 4 \end{cases}$$

$$S_{\rm AGN}(z) \propto \begin{cases} (1+z)^{5} & z \leq 1.7 \\ 2.7^{5} & 1.7 < z \leq 2.7 \\ 2.7^{5} \cdot 10^{2.7-z} & z > 2.7 \end{cases}$$

Hasan Yuksel et al,. Astrophys.J.Lett. 683 (2008) L5-L8

Why these values in the parameter space?

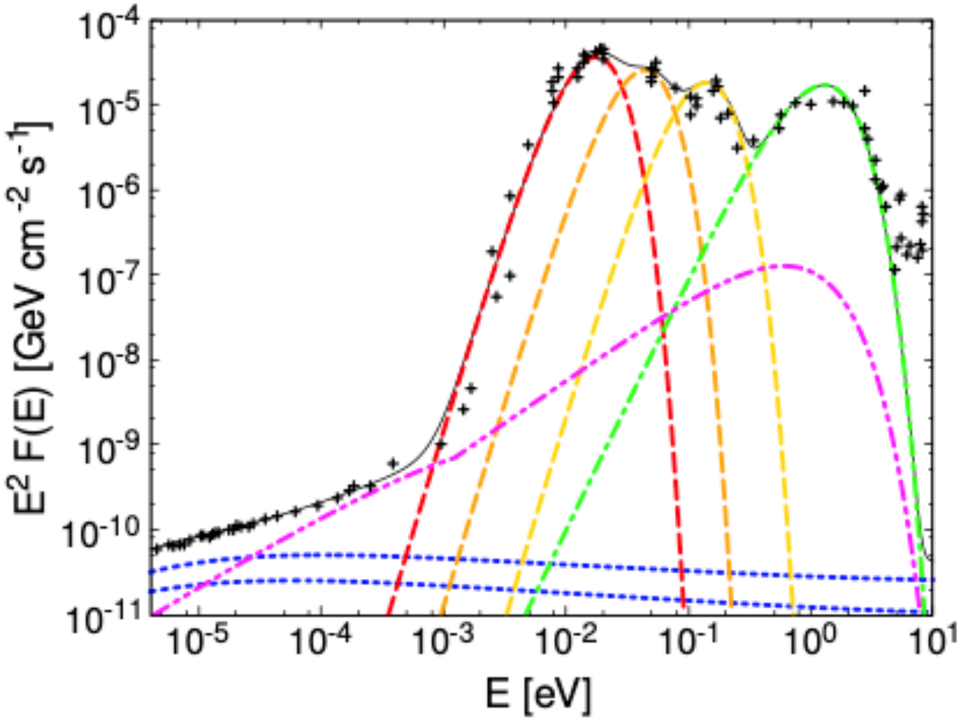

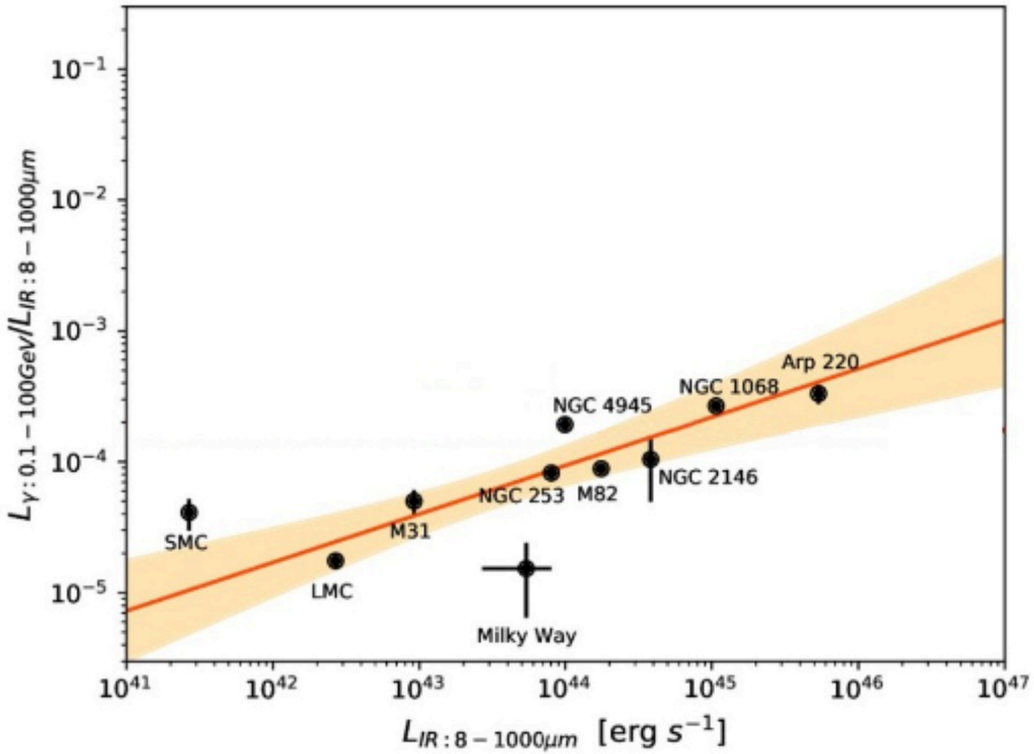

Spallation in detail

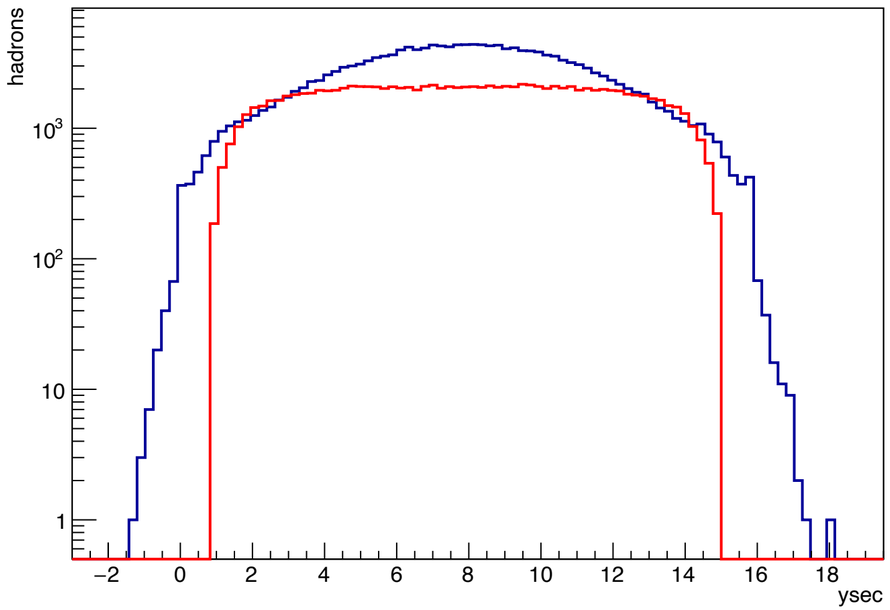

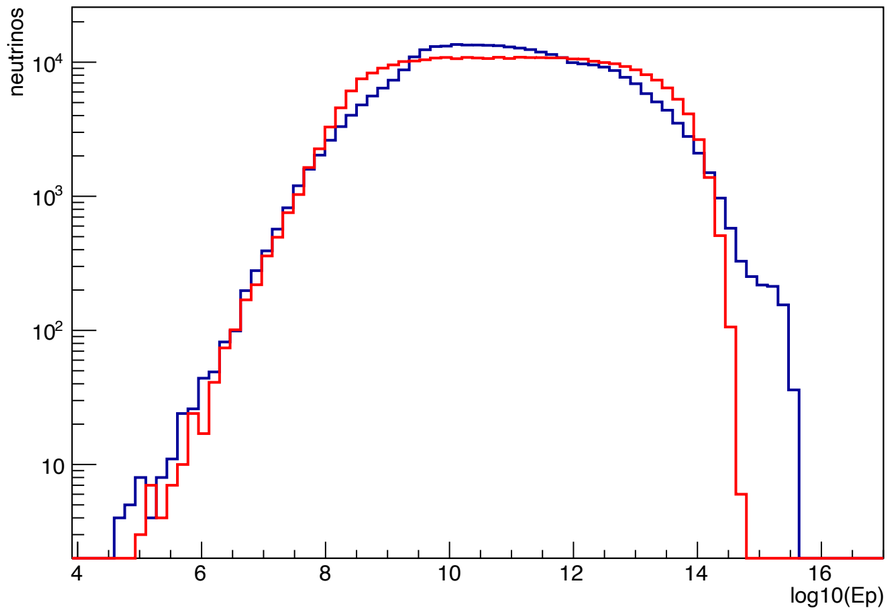

Spallation in detail

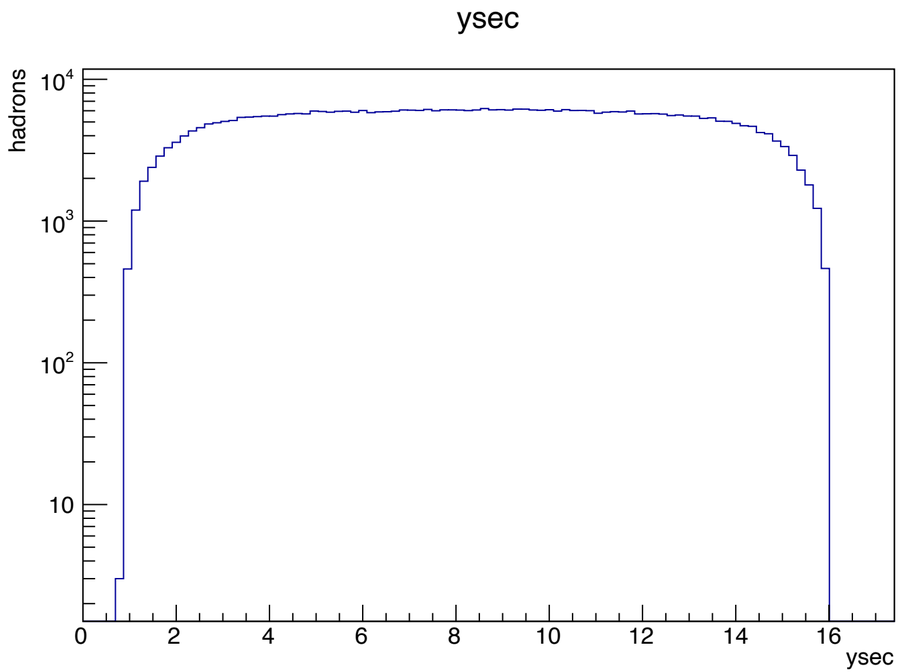

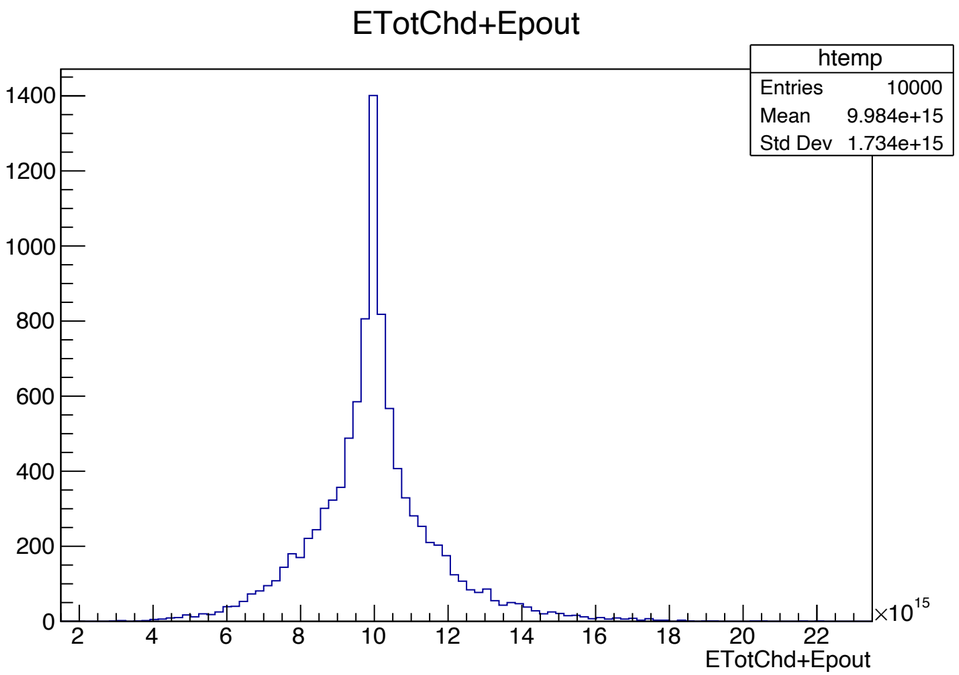

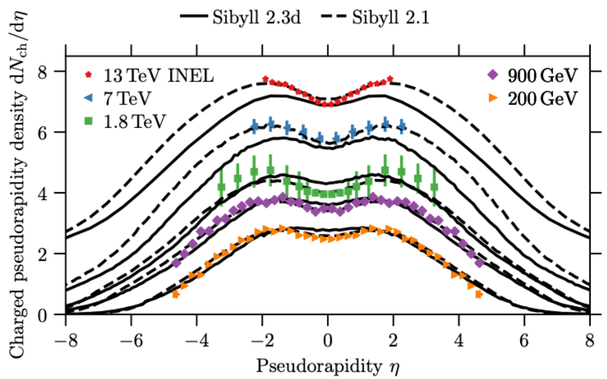

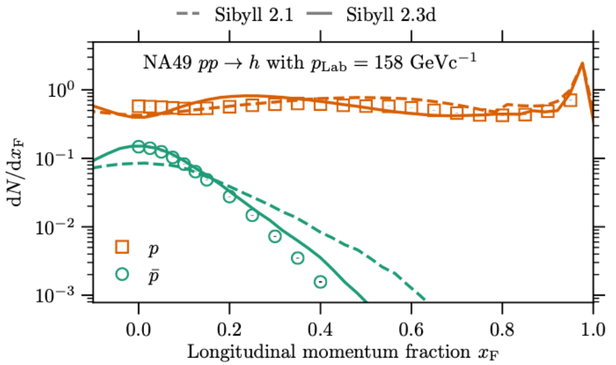

Spallation in detail

$$\log(\sigma/\mathrm{mb}) = a_0 + a_1 \cdot \ln A + (b_0 + b_1 \cdot \ln A) \cdot L + (c_0 + c_1 \cdot \ln A) \cdot L^2$$

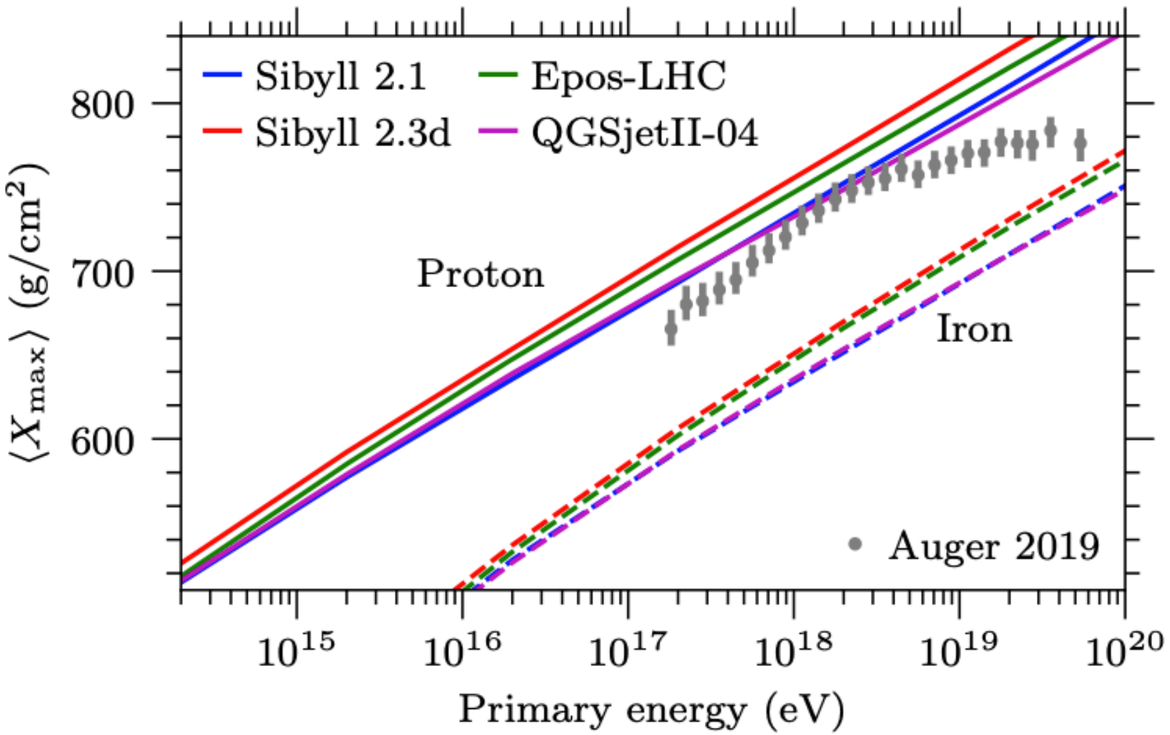

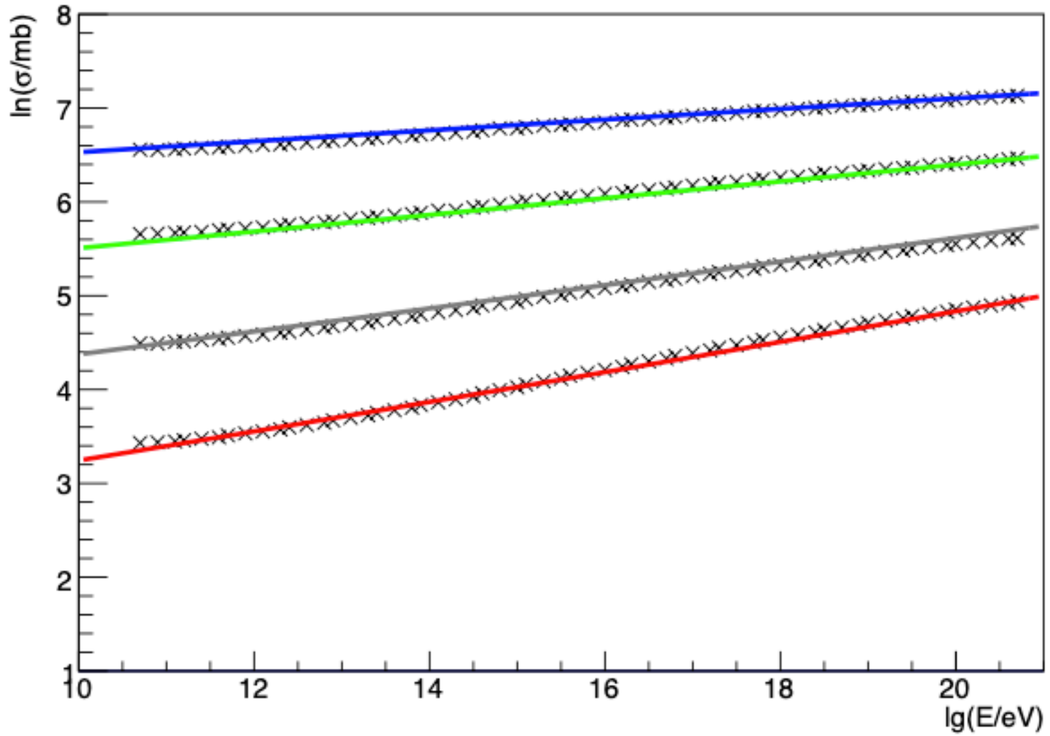

Timescale final

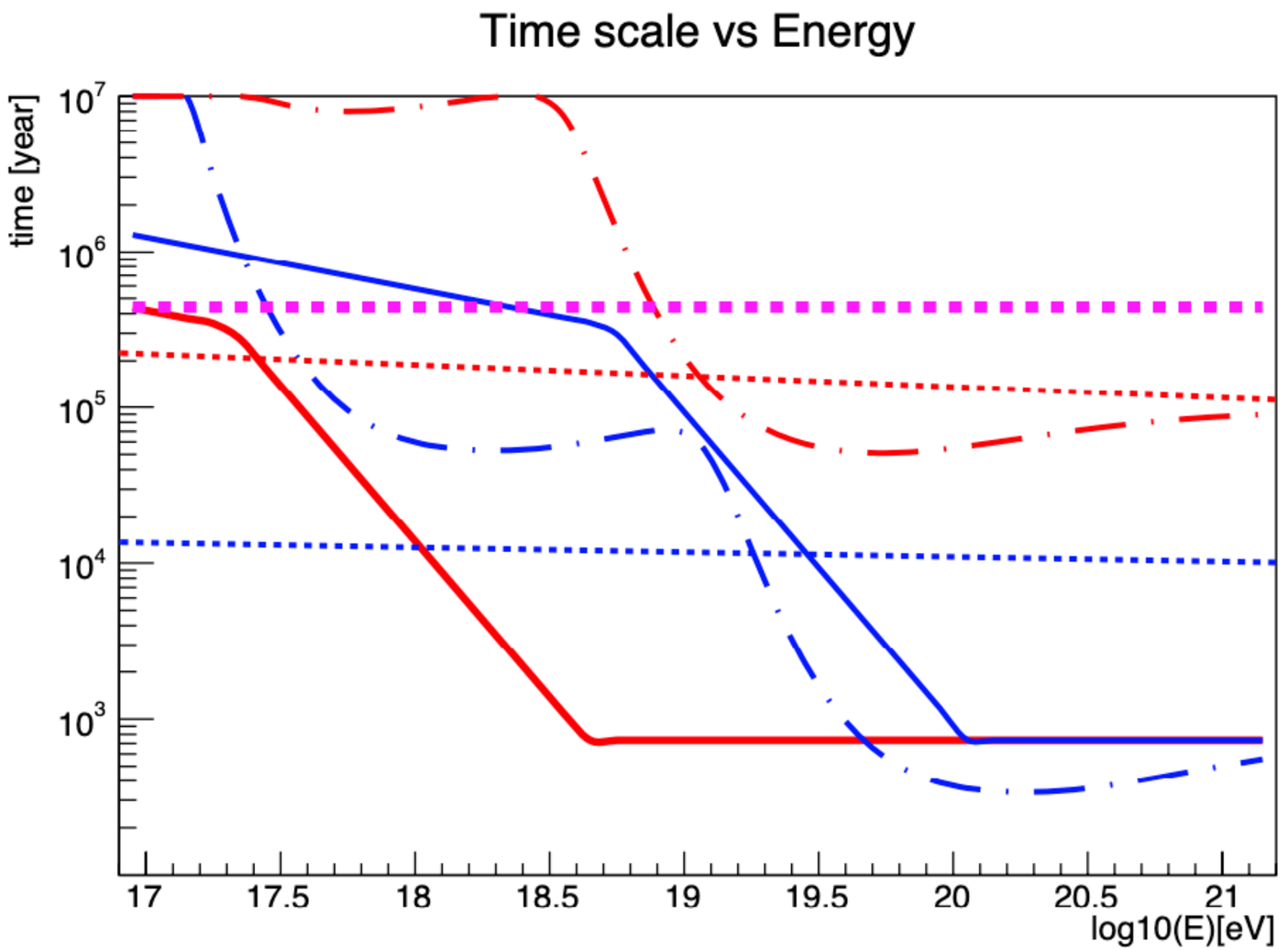

Auger-TA

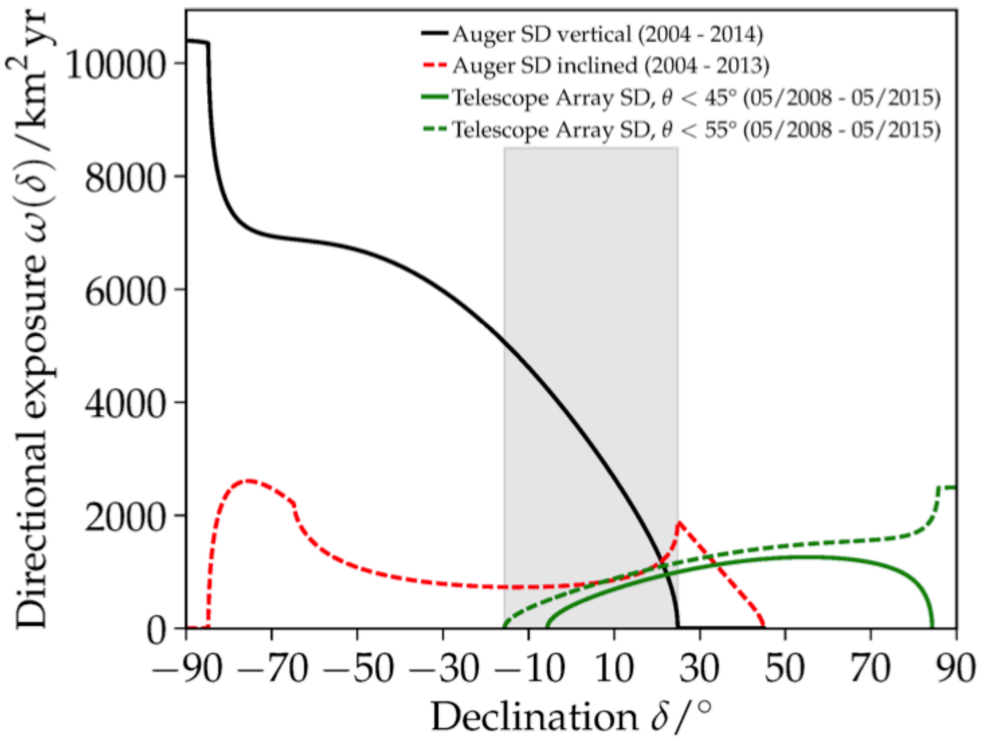

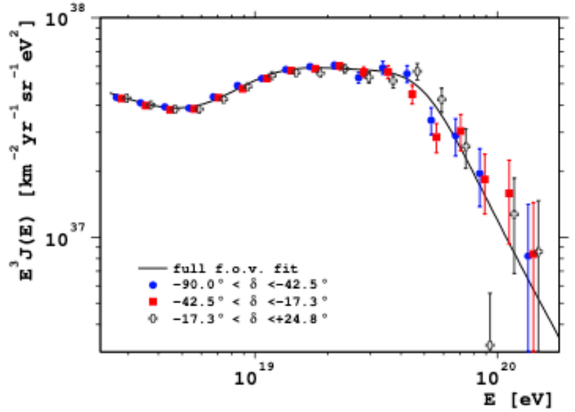

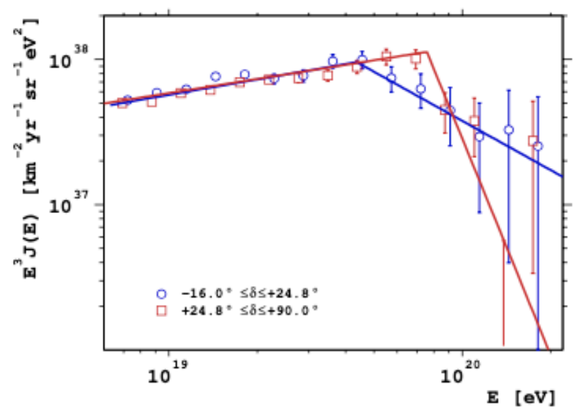

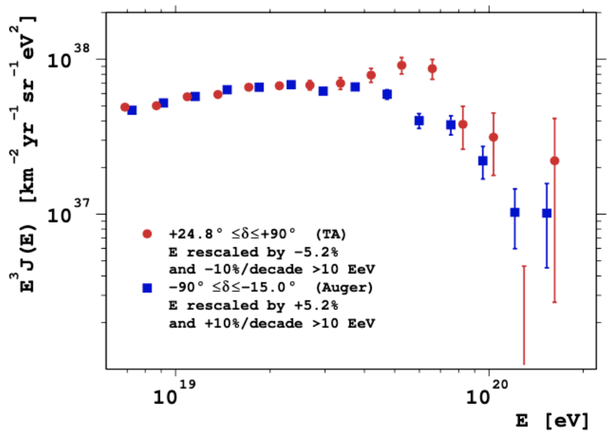

Updated Results on the UHECR Hotspot Observed by the Telescope Array Experiment
T. Abu-Zayyad et al. (Telescope Array and Pierre Auger Collaborations), EPJ Web Conf. 210, 01002 (2019).

Neutrinos

The total exposure $\mathcal{E}_{\rm tot}$ folded with a single-flavor flux of UHE neutrinos per unit energy, area A, solid angle Ω and time, $\phi(E_\nu) = \mathrm{d}^6 N_\nu/(\mathrm{d}E_\nu\ \mathrm{d}\Omega\ \mathrm{d}A\ \mathrm{d}t)$ and integrated in energy gives the expected number of events for that flux:

$$N_{\rm evt} = \int_{E_\nu} \mathcal{E}_{\rm tot}(E_\nu)\ \phi(E_\nu)\ \mathrm{d}E_\nu. \tag{4.1}$$

Assuming a differential neutrino flux $\phi = k \cdot E_\nu^{-2}$, an upper limit to the value of k at 90% C.L. is obtained as

$$k_{90} = \frac{2.39}{\int_{E_\nu} E_\nu^{-2}\ \mathcal{E}_{\rm tot}(E_\nu)\ \mathrm{d}E_\nu}, \tag{4.2}$$

where 2.39 is the Feldman-Cousins factor [52] for non-observation of events in the absence of expected background accounting for systematic uncertainties [28, 53]. The integrated limit represents the value of the normalization of a E_ν^{-2} differential neutrino flux needed to predict $\sim$ 2.39 expected events.

GRB

Gamma-Ray Bursts

Long-standing candidate as UHECR and neutrino source *[Waxmann '95, Vietri '95]*

- Γ^2 mechanism works only first cicle, large escape probability
- emissivity $Q \sim 10^{43}$erg/Mpc^{3}yr – at least a factor 10 too low
- heavy composition?
- no correlation with IceCuve events

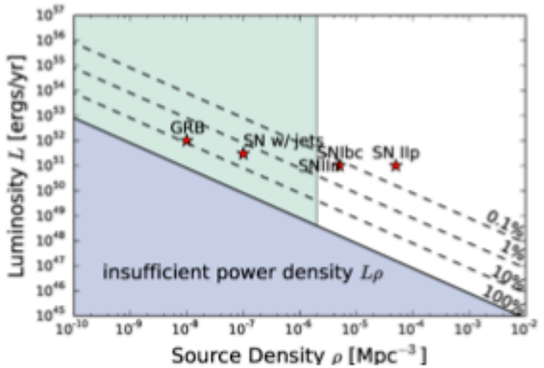

Two classes: High- and low-luminosity GRBs

- HL GRBs, constraints from IceCube require either
  - low $E_{\max}$ or
  - small baryon load

  $\Rightarrow$ excluded as main UHECR source

From M. Kachelriess (ICRC2021)